Electrospray ionization mass spectrometry: from cluster ions to toxic metal ions in biology

by

Nicholas B. Lentz

A dissertation submitted to the graduate faculty

in partial fulfillment of the requirements for the degree of

DOCTOR OF PHILOSOPHY

Major: Analytical Chemistry

Program of Study Committee:
R. S. Houk, Major Professor
Nicola Pohl
Hans Stauffer
Victor Shang-Yi Lin
Klaus Schmidt-Rohr

Iowa State University

Ames, Iowa

2007

TABLE OF CONTENTS

Chapter 1

INTRODUCTION

Historical Background

During the past 25 years, electrospray ionization mass spectrometry (ESI-MS) has become an important analytical tool for inorganic and biological research. Long before electrospray ionization was coupled with mass spectrometry, fundamental studies were conducted on the electrospray process. The first studies were in 1917 when Zeleny studied the electrospray process [1]. Zeleny was the first to observe the electrohydrodynamic pulsation of a charged liquid surface. He concluded that the spray plume was a result of the solvent, high voltage, and pressure of the liquid at the tip of the tube. Zeleny also observed and described different spraying modes such as the dripping, spindle, Taylor cone [2], and multijet modes. In 1994, Cloupeau and Prunet-Foch provided a detailed description of all of the various spraying modes, including the modes first observed by Zeleny [3].

In 1968, Dole et al. used electrospray ionization to determine the molecular weight of a dilute polymer solution [4]. This is the first article where electrospray ionization was used for mass analysis. In lieu of a mass spectrometer, a Faraday cage was used to detect the ionic current and a mass was deduced from this measurement. Polystyrene macroions of 51,000 and 411,000 amu were detected. In a second paper, further measurements with polymer solutions were conducted [5].

The next significant paper using electrospray ionization wasn't published until 1984, when Yamashita and Fenn were the first to couple an electrospray source to a mass spectrometer [6, 7]. For this achievement, Fenn shared the Nobel Prize in Chemistry in

2002. At approximately the same time as Yamashita and Fenn, Aleksandrov et. al. investigated inorganic ions by ESI-MS [8]. This article demonstrated that ESI-MS could be a useful tool in the fields of inorganic and organometallic chemistry.

In 1994, Wilm and Mann developed a micro electrospray source that is now called nanospray or nanoelectrospray [9, 10]. Nanospray sources are typically made out of silica glass rods which have one end pulled down to an inner diameter of 1 to 20 μm. Nanospray sources typically have flow rates in the 10-500 nL/min range, don't require a sheath gas, and can easily spray 100 % water solutions. The signal obtained using a nanospray source is equivalent or greater than that of a traditional ESI source because the ionization efficiency is higher due to the production of smaller droplets at the tip. The main advantage is that very small sample volumes, as small as 0.5 μL, are used. This is advantageous because samples, especially biological samples, are often expensive to buy or synthesize.

Applications of ESI-MS

Biological Applications

In the late 1980's, the biological era of ESI-MS began. Fenn et al. demonstrated that the soft ionization of ESI allowed for intact proteins to be transferred into the gas phase [11]. Since mass spectrometers actually measure m/z, the multiply charged peaks generated by ESI of biomolecules can be analyzed by common mass analyzers such as quadrupoles. For example, equine heart myoglobin has a mass of 16,952 Da. If this protein were only singly charged, this m/z would be much too high for a quadrupole mass analyzer, which has an upper m/z limit of 3000 to 4000 m/z. When equine heart myoglobin is sprayed and mass analyzed, there is a charge distribution present with peaks ranging from +26 to +9. On the

m/z scale, these peaks are present between, m/z 652 and 1883, which is within the useful analytical range of all mass analyzers.

For the first time, ESI-MS also provided accurate mass measurements for large biomolecules. Each multiply charged peak present in a mass spectrum represents an independent measurement of the ion's mass. For example, a 13+ ion of equine heart myoglobin has a mass of 1305.0 m/z. Multiply the 1305.0 by the 13 charges and subtract off the 13 protons that gave myoglobin the 13+ charge; the mass is 16,952 Da. When the same calculation is done on the 14+ ion at m/z 1211.9, a mass of 16,952.6 Da is obtained. The measured mass from each charge state is averaged to provide an accurate mass of the ion. The measured values typically have a mass accuracy within 0.01% of the actual values. At the time of this discovery, the best mass accuracy for large biomolecules via other methods was 5 to 10%.

With biological molecules, the molecular weight is often not enough information for an accurate identification. Two proteins may have the same 50 residues, but a completely different order. On the m/z scale, the two proteins would have the same peak, but they could have completely different biological functions. Protein sequencing using ESI-MS provides structure and sequence information that allows for accurate protein identification. ESI-MS is capable of performing both "bottom-up", and "top-down" sequencing. In bottom-up sequencing, the proteins are first separated with a 2D gel separation. Next, there is either an in-gel digest or a solution-phase digest, which cleaves the protein at specific residues, depending on the enzyme used. Common digest enzymes are trypsin, Lys-C, and chymotrypsin. After the digest, high pressure liquid chromatography (HPLC) is often performed to clean up the sample and to achieve another level of separation. Two peaks may

have the same m/z in the mass spectrum, but their LC retention times may differ. This enables an accurate identification of the two peptide pieces. After the LC separation, the samples are introduced into the ESI-MS. This is commonly done on-line, but the LC fractions can also be collected and analyzed later. Each individual peptide peak in the mass spectrum is subjected to collision induced dissociation (CID) to identify the residues and their locations within the peptide. Since the digest enzymes cleave at specific locations, the order of the peptide pieces can also be reconstructed.

Database searches drastically decrease the data interpretation time. The mass spectral peaks of the peptides and their corresponding CID spectral peaks can be entered into a database. The database uses the spectral information to find the residue sequences and sequence order of the peptides. The database can then piece together the peptide fragments and provide the original protein.

There are some limitations to the bottom-up sequencing method. If a sample contains multiple unknown proteins, there will be many peptide peaks because each protein produces multiple peptide pieces when it is digested. Since peptides often carry more than one charge, there are multiple peaks present for each peptide in the mass spectrum. This often complicates the mass spectrum and can lead to spectral overlap between peaks. CID of all the peptides pieces is time consuming and uses more sample. This is a disadvantage because sample volumes are often only a few hundred microliters. Another limitation to bottom-up sequencing is that the protein digest enzymes don't have 100% efficiency, so the appropriate peptide fragments are not always seen.

Top-down protein sequencing was developed to address some of the drawbacks of the bottom-up approach and to make the sequencing process faster. The initial work for the top-

down approach was done by McLafferty [12]. In top-down sequencing, the intact protein is mass analyzed, followed by CID. A database search is performed on the CID spectrum to get the amino acid sequence for the protein. This method is much faster and requires little sample preparation. Since the whole protein is subjected to CID, post-translational modifications can be identified and their locations determined. These are huge advantages relative to the bottom-up approach.

One of the main drawbacks to the top-down approach is that it requires instrumentation with high mass resolution, accuracy, and the ability to fragment large ions. Until recently, these requirements limited the top-down sequencing method to expensive FT-ICR mass analyzers. Recently, the orbitrap mass analyzer has shown promise as an alternative mass analyzer capable of top-down sequencing [13]. Also, current research is being done to use ion traps for top-down sequencing [14]. Other disadvantages include data interpretation/library searching limitations and charge state effects within the mass analyzer.

Cluster Ions

Clusters or cluster ions are ions that are composed of a group of individual molecules or ions. The most well known cluster is the buckminsterfullerene or "Bucky Ball" [15]. This cluster resembles a soccer ball and has a formula of C_{60}. This cluster was made via laser ablation of graphite. Cluster ions with different elements are commonly made by ablating two solids and having the resulting plumes interact.

ESI-MS has also proven to be very useful in cluster ion research. The soft ionization of ESI-MS allows ions to interact within the shrinking droplets of the ESI plume. If the

interactions between the individual ions are strong enough, the cluster ion will traverse the mass spectrometer and be detected.

Cluster ions have also been very useful for ESI-MS research. Cluster ions like $Na_xI_y^-$ have been used to calibrate the m/z scale in ESI-MS. These clusters can span a range from m/z 150 to 4,000 or higher, which covers the m/z range of most mass analyzers [16, 17]. Cluster ions have also been used to gain insight into the ionization process of ESI [18-20].

Dissertation Objective and Organization

This dissertation is organized into chapters and focuses on novel applications of ESI-MS on cluster ions and toxic metals in biology. Chapter 2 is a manuscript published in the *Journal of the American Society for Mass Spectrometry*. This manuscript uses negative ion mode ESI-MS to examine the clusters of protonated amine salt solutions with chloride counter ions. CID measurements and CID threshold measurements were performed to provide insight into ion structure and bond strengths. Chapters 3 and 4 are manuscripts, ready to be submitted to the *Journal of the American Society for Mass Spectrometry* for publication. In Chapter 3 highly negatively charged alkali metal sulfated cluster ions are examined using ESI-MS. Ions with charges up to 7- and ions as large as $Na_{131}(SO_4)_{69}^-$ were present in the mass spectra. Two different ESI-MS interface geometries, source conditions, and solvent ratios were examined to determine their effect on the cluster ion distributions present in the mass spectra. Chapter 4 utilizes negative ion mode ESI-MS to study mixed metal cluster ions. Metal clusters of $M_xCl_z^-$ ($M = Ce^{3+}$, Co^{2+}, Zn^{2+} or Ho^{3+}) or $Ce_xM_yCl_z^-$ ($M = Co^{2+}$, Zn^{2+} or Ho^{3+}) were present in the mass spectra. Heated capillary temperature, source

conditions and solvent ratios were examined to determine their effect on the mixed metal cluster ions present and their distribution in the mass spectra.

In Chapter 5, the interaction of toxic metals with the [Gln^{11}]-amyloid β-protein fragment (1-16) was studied by ESI-MS. This chapter looks at the binding location of Cd, Pb and Hg to the amyloid protein fragment (1-16). Competition studies found that Cd and Pb have a higher affinity for the binding site than Zn. Cd and Pb were also able to displace bound Zn, but an excess of Zn did not remove the bound toxic metals. This manuscript has been submitted to the *Journal of Biological Inorganic Chemistry*. General conclusions and future research directions are summarized in Chapter 6.

References

1. Zeleny, J. Electric Discharge from Points. *Phys. Rev.* **1917**, *9*, 562-563.
2. Taylor, G. Disintegration of Water Droplets in an Electric Field. *Proc. R. Soc. London* **1964**, *280*, 383-397.
3. Cloupeau, M; Prunet-Foch, B. Electrohydrodynamic Spraying Functioning Modes: A Critical Review. *J. Aerosol Sci.* **1994**, *25*, 1021-1036.
4. Dole, M.; Mack, L. L.; Hines, R. L.; Mobley, R. C.; Ferguson, L. D.; Alice, M. B. Molecular Beams of Macroions. *J. Chem. Phys.* **1968**, *49*, 2240-2249.
5. Mack, L. L.; Kralik, P.; Rheude, A.; Dole, M. Molecular Beams of Macroions. II. *J. Chem. Phys.* **1970**, *52*, 4977-4986.
6. Yamashita, M.; Fenn, J. B. Electrospray Ion Source. Another Variation on the Free-Jet Theme. *J. Phys. Chem.* **1984**, *88*, 4451-4459.

7. Yamashita, M.; Fenn, J. B. Negative Ion Production with the Electrospray Ion Source. *J. Phys. Chem.* **1984**, *88*, 4671-4675.

8. Aleksandrov, M. L.; Gall, L. N.; Krasnov, N. V.; Nikolaev, V. I.; Shkurov, V. A. Mass Spectrometric Analysis of Low-Volatility Thermally Unstable Substances Based on Extraction of Ions from Solution at Atmospheric Pressure. *Zh. Anal. Khim.* **1985**, *40*, 1570-1580.

9. Wilm, M.; Mann, M. Electrospray and Taylor-Cone Theory, Dole's Beam of Macromolecules at Last? *Int. J. Mass Spectrom. Ion Processes* **1994**, *136*, 167-180.

10. Wilm, M.; Mann, M. Analytical Properties of the Nanoelectrospray Ion Source. *Anal. Chem.* **1996**, *68*, 1-8.

11. Fenn, J. B.; Mann, M.; Meng, C. K.; Wong, S. F.; Whitehouse, C. M. Electrospray Ionization for Mass Spectrometry of Large Biomolecules. *Science* **1989**, *246*, 64-71.

12. Ge, Y.; Lawhorn, B. G.; ElNaggar, M.; Strauss, E.; Park, J. H.; Begley, T. P.; McLafferty, F. W. Top Down Characterization of Larger Proteins (45 kDa) by Electron Capture Dissociation Mass Spectrometry. *J. Am. Chem. Soc.* **2002**, *124*, 672-678.

13. Macek, B.; Waanders, L. F.; Olsen, J. V.; Mann, M. Top-down Protein Sequencing and MS^3 on a Hybrid Linear Quadrupole Ion Trap-Orbitrap Mass Spectrometer. *Mol. Cell. Proteomics* **2006**, *5*, 949-958.

14. Coon, J. J.; Ueberheide, B.; Syka, J. E.; Dryhurst, D. D.; Ausio, J.; Shabanowitz, J.; Hunt, D. F. Protein Identification using Sequential Ion/Ion Reactions and Tandem Mass Spectrometry. *Proc. Natl. Acad. Sci U. S. A.* **2005**, *102*, 9463-9468.

15. Kroto, H. W.; Heath, J. R.; O'Brien, S. C.; Curl, R. F.; Smalley, R. E. C_{60}: Buckminsterfullerene. *Nature* **1985**, *318*, 162-163.

16. Anacleto, J. F.; Pleasance, S.; Boyd, R.K. Calibration of Ion Spray Mass Spectra using Cluster Ions. *Org. Mass Spectrom.* **1992**, *27*, 660-666.

17. Moini, M.; Jones, B.L.; Rogers, R. M.; Jiang, L. Sodium Trifluoroacetate as a Tune/Calibration Compound for Positive- and Negative-Ion Electrospray Ionization Mass Spectrometry in the Mass Range of 100-4000 Da. *J. Am. Soc. Mass Spectrom.* **1998**, *9*, 977-980.

18. Kebarle, P; Tang, L. From Ions in Solution to Ion in the Gas Phase - the Mechanism of Electrospray Mass Spectrometry. *Anal. Chem.* **1993**, *65*, 972A-986A.

19. Tang, L; Kebarle, P. Dependence on Ion Intensity in Electrospray Mass Spectrometry on the Concentration of the Analytes in the Electrosprayed Solution. *Anal. Chem.* **1993**, *65*, 3654-3668.

20. Zhou, S.; Hamburger, M. Formation of Sodium Cluster Ions in Electrospray Mass Spectrometry. *Rapid Commun. Mass Spectrom.* **1996**, *10*, 797-800.

CHAPTER 2. NEGATIVE ION MODE ELECTROSPRAY IONIZATION MASS SPECTROMETRY STUDY OF AMMONIUM-COUNTER ION CLUSTERS

A paper published in the *Journal of the American Society for Mass Spectrometry*

N. B. Lentz and R. S. Houk

Abstract

Electrospray ionization mass spectrometry (ESI-MS) was used to examine clusters of protonated amine salt solutions with chloride counter ions in the negative ion mode. These ions have the general formula $[(RNH_3)_xCl_{x+1}]^-$. Primary amines generate a wide cluster distribution with clusters up to 14 mers for methylamine hydrochloride clusters. Secondary and quaternary amines only generate the monomer ion under identical conditions. Collision induced dissociation (CID) of the cluster ions generates cluster ions of lower m/z with the next lower cluster being the most abundant. The product ions from $MeNH_3Cl_2^-$, $Me_2NH_2Cl_2^-$ and $(MeNH_3)_2Cl_3^-$ have low threshold appearance energies of 1.24 to 2.22 eV center-of-mass frame. Secondary amine monomer ions have lower threshold CID energies than primary amine monomer ions. The amine threshold CID energy decreases as the carbon chain length increases. As an electrospray solvent, isopropyl alcohol (IPA) promotes the formation of counter ions and clustering.

Introduction

ESI-MS is a rapid and sensitive tool for the determination of molecules in solution [1]. Usually, the electrospray interface attempts to desolvate and remove all counter ion

complexes and clusters before the ions enter the mass spectrometer. Cluster ions usually lower analyte signals, complicate mass spectra, and hinder quantification. However, there are times when cluster ions are beneficial in ESI-MS. They can be used to calibrate the m/z scale and to study ionization mechanisms and solvent effects on the ESI process [2-6]. Cluster distributions for species such as $Na_xCl_{x-1}^+$ exhibit "magic numbers" and are of interest in their own right [7, 8]. If a molecule is poorly ionized in electrospray, counter ions can be added to increase the ionization yield [9, 10]. The counter ions can also provide a net charge for a neutral molecule so that it can be detected in a mass spectrometer. The counter ions change the ionization properties of the molecule by changing the charge state of the molecule. If the ion originally has a net positive charge, the addition of counter ions will reduce the charge state of the ion or even convert it to the opposite polarity. If the overall charge of the ion is changed from positive to negative, negative ion mode ESI must be used. Negative ion mode has the added benefit of fewer background ions in the mass spectrum.

Clusters can also lock in the charge state of a given ion in solution. Counter ions can interact with the ion of interest, and keep the ion in a specific charge state. Halides are commonly used due to their charge affinity and ability to coordinate around an ion [11, 12]. This charge state can be preserved by adjusting the ionization conditions at the electrospray interface.

In order to observe cluster ions, softer ion extraction conditions are sometimes required. This often means a lower capillary temperature and/or lower extraction voltages in the atmospheric sampling region [8].

Previous studies in our group have shown that anions like nitrate can stabilize the oxidation state of highly charged, reactive metal ions in solution [13, 14]. In this paper,

complex and cluster ions from various amine salts are investigated by ESI-MS. CID spectra show the fragmentation pattern of the cluster ions. Threshold dissociation energies are determined for primary and secondary monomer ions as well as for a methylamine cluster ion. The threshold reactions provide valuable information regarding differences in cluster ion formation and the strength of the interaction between the cations and anions comprising the cluster.

Experimental

Samples and Sample Preparation

The amine salts and IPA were purchased from Sigma (St. Louis, MO) and used without further purification. Table 1 shows the structures of the amine salts and the molecule abbreviations used in this paper. The amine salts were dissolved in a 99% isopropyl alcohol (IPA) 1% deionized water (Millipore 18.2 MΩ) solution. The final concentration of the amine salt was 1 mM. Only a stoichiometric amount of chloride was present. No extra chloride anions were added to the solution.

ESI-MS (Figures 1, 2, 5 and 6)

A triple quadrupole (QoQ) MS (TSQ-7000, Thermo Finnigan, San Jose, CA) with an on-axis electrospray source, was used. Samples were infused continuously at 5 μL/min with a syringe pump (Model 22, Harvard Apparatus, Southnatic, MA). Nitrogen (80 psi) and high-purity argon were used as the nebulizing gas and collision gas, respectively. The electrospray needle voltage was set to -2.5 kV, and the heated capillary was kept at 250 °C,

-39.9 V. The ring electrode and first octopole voltage were -37.4 and +3.0 V, respectively. The skimmer is at ground on this instrument.

CID Spectra (Figures 3 and 4)

The collision gas pressure was 0.13 Pa for these experiments. The collision energies (skimmer to collision cell potential offset) were 10 to 21 eV (lab frame). The resolution of the first quadrupole was reduced to obtain higher signals in CID experiments.

CID Threshold Measurements (Figures 7 and 8)

For threshold experiments, the collision gas pressure was reduced to 0.0267 Pa. At this pressure, the mean free path was about 25 cm, which was longer than the octopole (18.2 cm). Thus, most ions passing through the collision cell experienced only one collision. The collision energy was increased from 2.5 to 26.5 eV (lab frame) in increments of 0.2, 0.3 or 0.5 eV. Each ion of interest was monitored for 1 second in selected reaction monitoring (SRM) mode. Data were collected for 3 to 4 minutes at each collision energy and averaged.

The signal intensities were converted to collision cross sections, and the collision energy was converted to the center-of-mass frame. These conversions allow for accurate comparisons of the threshold energies for different ions [15-17]. Armentrout provides detailed discussions on how to convert intensities to collision cross sections, and why the center-of-mass frame must be used for threshold energy data [16]. The same methods were used in our previous paper on metal nitrate complex ions [13].

The instrument used for this experiment is not intended for accurate thermochemical measurements. For example, the kinetic energy spread of the ion beam is greater than

desirable. Most analytical mass spectrometers are designed for maximum sensitivity, not accurate thermochemical measurements. However, approximate thresholds can be measured and used for general or qualitative purposes. In a previous paper, the relationship between the measured and true collision energy was evaluated by using the reaction listed below:

$NO_3^- \rightarrow NO_2^- + O$ (1)

The instrument was found to under-estimate the collision energy by 0.76 eV [13].

We performed an additional threshold measurement to confirm the ion beam kinetic energy offset previously found [13]. Sodium dichloride ions ($NaCl_2^-$) were chosen because of their similarity to the amine chloride ions investigated in this study. The $NaCl_2^-$ ion is comprised of only ionic interactions, like the amine clusters. NO_3^- is held together by covalent bonds, and the energy offset could be different for an ion comprised of only ionic interactions. The reaction

$NaCl_2^- \rightarrow NaCl + Cl^-$ (2)

was used to determine the kinetic energy offset of the ion beam. Cl^- is the only measurable ion produced from this fragmentation reaction. The results from the threshold measurement for the dissociation of $NaCl_2^-$ gave a threshold energy of 1.65 eV (center of mass, data not shown). This measured value is 0.63 eV lower than the computational value of 2.277 eV [18]. This offset value is similar to the 0.76 eV offset obtained from the previous NO_3^- threshold measurement [13] and confirms that the offset is not strongly dependent on the ion selected. We are more confident in the experimentally-measured thermochemical data used previously, so 0.76 eV has been added to all the voltage thresholds reported below to generate "corrected" thresholds. Even if this offset is inaccurate, it is the same for all ions, and trends in the thresholds can still be compared.

Results and Discussion

MS and CID of Primary Amines

A mass spectrum of a methylamine hydrochloride solution is shown in Figure 1. As m/z increases the cluster ion abundances decay in an exponential fashion, without any obvious "magic numbers," unlike those observed for alkali metal halide clusters [2, 7, 8]. Three different cluster patterns are evident. The first is of the form $[(MeNH_3)_xCl_{x+1}]^-$. This pattern is the most intense, and cluster ions can be seen up to x = 14.

The second cluster pattern includes one contaminant sodium ion and is of the form $[(MeNH_3)_yNaCl_{y+2}]^-$. The third pattern is similar to the second, except a proton replaces the sodium ion $[(MeNH_3)_zHCl_{z+2}]^-$. The $[(MeNH_3)_yNaCl_{y+2}]^-$ pattern is more prevalent, and is seen for larger clusters, than the $[(MeNH_3)_zHCl_{z+2}]^-$ pattern. These patterns are also present in ethylamine (not shown) and propylamine, Figure 2. There are few or no cluster ions with more than one Na^+ or H^+ ion, unlike the numerous $[(MeNH_3)_xCl_{x+1}]^-$ ions. As seen in Figures 1 and 2, larger clusters become less abundant as the size of the alkyl group increases.

The inset to Figure 2 compares the calculated and measured isotope distributions for $(EtNH_3)_3Cl_4^-$. In general, the observed isotope peaks agree with the calculated values to within 2% for all the ions identified in this study. When the mass range is set to include ions down to m/z 30, Cl^- ions are seen. This observation suggests that Cl^- ions are not the limiting factor in determining cluster ion formation.

A typical CID product ion spectrum is shown for $[(PrNH_3)_3Cl_4]^-$ in Figure 3. A collision cell offset voltage of 21 eV was used to fragment the parent ion. The parent cluster ion fragments into smaller cluster ions. The next smaller cluster ion is the most intense product ion. Despite the low resolution of the first quadrupole, it does not transmit the

various isotopomers equally, especially for large clusters with multiple Cl atoms. Therefore, the product ions in Figures 3 and 4 often do not have the expected natural isotope distributions.

The observed CID products from Figure 3 are as follows:

$[(PrNH_3)_3Cl_4]^- \rightarrow [(PrNH_3)_2Cl_3]^- + \textit{PrNH}_3\textit{Cl (or PrNH}_2 + \textit{HCl)}$

$\rightarrow [(PrNH_3)HCl_3]^- + \textit{PrNH}_3\textit{Cl} + \textit{PrNH}_2$

$\rightarrow PrNH_3Cl_2^- + 2\textit{PrNH}_3\textit{Cl}$

The species in italics are the inferred neutral products from the CID reactions. They cannot be observed due to their lack of overall charge. The reactions shown above are not meant to imply an actual mechanism, i.e., unimolecular decay of the excited parent ion. Stepwise reactions are also likely, especially because these spectra are not measured under single-collision conditions.

It is interesting to note the lack of Cl^- fragment ions in Figure 3. Cl^- fragment ions are not seen when clusters larger than the monomer are fragmented. This means that not all of the Cl^-/NH_3^+ ionic bonds are broken during CID.

Figure 4 shows a CID spectrum of the $MeNH_3Cl_2^-$ monomer taken with a collision energy of 15 eV (lab); HCl_2^- and Cl^- are the only product ions present in the spectrum. $MeNH_2$ leaves as a neutral fragment and is not seen in the mass spectrum. It is clear that the monomer ions behave differently than the larger cluster ions since the monomers are the only ions that yield Cl^- fragment ions on CID.

MS of Secondary and Quaternary Amines

Under the same ESI conditions, higher order amines do not generate a wide cluster distribution like the primary amines. The mass spectrum for diethylamine hydrochloride is given in Figure 5. The ions at m/z 71 and m/z 95 are HCl_2^- and the chloride adduct of IPA, respectively. The only ion arising from the diethylamine is the monomer ion $Et_2NH_2Cl_2^-$ at m/z 144. Chloride solutions of dimethylamine and quarternary amines also yield only monomer peaks (data not shown).

Other halide anions yield similar spectra, as shown for tetrabutylammonium iodide in Figure 6. Again, some free I^- is observed, even though the solution contains stoichiometrically equivalent amounts of the tetrabutylammonium and iodide ions. Thus, the anion concentration is not the limiting factor in cluster ion formation for the secondary and higher amines, as noted above for the primary amines.

Our previous studies of counter anion complexes from methanol-water solutions used a large excess of nitrate to drive complex ion formation [13]. In our experience, large clusters are much more prevalent at lower anion concentrations in the isopropanol solvent used in the present work.

Figure 6 has an interesting peak at m/z 381, which is ascribed to $^{127}I_3^-$. Apparently, some of the I^- is oxidized to I_2 and/or I_3^-. The high negative voltage applied to the ESI needle would drive reduction, not oxidation, so the I_3^- is not made by electrolysis at the needle.

CID Threshold Measurements

In order to investigate the interaction strength of the different amine clusters, threshold measurements were performed. As mentioned earlier, the threshold results should

be considered merely as approximate values, partly because of uncertainty in the correction term of 0.76 eV added to all the measured voltages. Nevertheless trends and general conclusions can be drawn from the measurements.

The threshold energies for the monomer ions of different primary and secondary amine clusters were examined to see if the size or number of hydrocarbon chains affected the stability of the ion. The threshold appearance energies for HCl_2^- and Cl^- from the monomer ions of methylamine ($MeNH_3Cl_2^-$), dimethylamine ($Me_2NH_2Cl_2^-$) , and diethylamine ($Et_2NH_2Cl_2^-$) were monitored under the same experimental conditions. Figure 7 shows typical results for the threshold measurement for $MeNH_3Cl_2^-$ at m/z 102. The corrected threshold energies are 2.06 and 2.22 eV (center-of-mass) for HCl_2^-, and Cl^-, respectively.

In the inset to Figure 7, the same experiment is performed with the methylamine monomer ion, but without any collision gas. The cross section initially decreases, then levels off at a low value. This observation confirms that the initial signal decrease is due to instrumental conditions, and is not related to the threshold measurement of the ion. The initial decrease can be ignored, and the increase from the minimum is called the threshold energy.

All the measured CID thresholds are compared in Table 2. For CID of the $Me_2NH_2Cl_2^-$ monomer ion, measured threshold energies are 1.94 and 2.14 eV (CM) for formation of HCl_2^- and Cl^-, respectively. These values are slightly lower than those for $MeNH_3Cl_2^-$. The addition of the second methyl group decreases the threshold energy, which means that the ion is less stable and requires less energy to dissociate than the cluster of the analogous primary amine. This trend is further supported by threshold measurements for $Et_2NH_2Cl_2^-$, which produces HCl_2^- and Cl^- at 1.63 and 1.93 eV (CM, Table 2). The monomer

ions with the larger alkyl groups and more alkyl groups are less stable based upon the lower threshold energies. According to this pattern, larger cluster ions will have even lower threshold energies.

In order to test this theory, a threshold measurement was performed on the methylamine dimer ion $(MeNH_3)_2Cl_3^-$, m/z 169. The products monitored are $[(MeNH_3)HCl_3]^-$, $MeNH_3Cl_2^-$, and HCl_2^- at m/z 138, 102, and 71, respectively. Figure 8 shows the threshold energies for all of the product ions of $(MeNH_3)_2Cl_3^-$. The corrected threshold energies for $[(MeNH_3)HCl_3]^-$, $MeNH_3Cl_2^-$, and HCl_2^- are very low: 1.47, 1.41, and 1.24 eV (CM). This dimer ion is larger and more complex than the monomer ions, so the dimer dissociates at even lower threshold energies. The threshold energy for the production of HCl_2^- from the dimer is much lower than the values recorded for the monomer ions. Even though the hydrocarbon chain and saturation are the same, the dimer ion is less stable.

The corrected threshold energies range from 1.24 to 2.22 eV (CM). These values are reasonable for ions held together by electrostatic interactions. According to Gutsev et al. [18], CID of $NaCl_2^-$ to Cl^- takes 2.28 eV, similar to that found for the more stable ions studied in the present work. Figures 7 and 8 show that the instrument can distinguish the CID threshold energies for the various ions, although there could be a systematic error in the measured values if the instrumental offset (see end of Experimental section) is incorrect.

Conclusions

Electrospray ionization mass spectrometry was used to evaluate the cluster ion formation capabilities of amine salts. Primary amines form many clusters which decay off in an exponential fashion. Secondary and higher order amines produce only intense monomer

peaks. This is attributed to the steric hindrance of the additional carbon chains around the charged amine. When activated by CID, the parent ion fragments into the next smaller clusters in the pattern with the next smaller cluster being the most intense. The amine molecule leaves as a neutral fragment when CID is performed on the monomer ions.

The threshold energies are low (1.2 to 2.2 eV), which is a further indication that counter ion complexation can stabilize fragile species and allow them to survive the ESI extraction process [13, 14]. The CID thresholds depend on several properties of the ionic clusters. Larger alkyl groups decrease the dissociation energy. Increasing the degree of substitution from primary to secondary amines also lowers the CID threshold energy of the ion. Increasing the degree of substitution from primary to secondary amines also lowers the CID threshold energy of the ion. Perhaps the larger or more numerous carbon chains increase the distance between the opposing charges and thus weaken the electrostatic attraction. Dimer ions also exhibit lower threshold CID energies than the monomer ions. Even though the threshold energies are low, the electrostatic forces keeping the ion together are strong enough for the molecule to survive the ion extraction process and traverse through the mass spectrometer, and allow the ion to be detected. Currently, studies are underway to explore other interesting applications of counter ion complexes and cluster ions and their ability to provide new information regarding molecular interactions in ESI-MS.

Acknowledgements

Ames Laboratory is operated by Iowa State University for the U.S. Department of Energy, contract no. W-7405-Eng-82. This work was supported by the Chemical and Biological Sciences Program, Office of Basic Energy Sciences, Division of Chemical

Sciences. The authors thank L. Huang and Bayer Company for donating the triple quadrupole instrument.

References

1. Yamashita, M.; Fenn J. B. Electrospray ion source. Another variation on the free-jet theme. *J. Phys. Chem.* **1984**, *88*, 4451-4459.
2. Zhou, S.; Hamburger, M. Formation of sodium cluster ions in electrospray mass spectrometry. *Rapid Commun. Mass Spectrom.* **1996**, *10*, 797-800.
3. Wang, G.; Cole, R. B. Charged residue versus ion evaporation for formation of alkali metal halide cluster ions in ESI. *Anal. Chim. Acta.* **2000**, *406*, 53-65.
4. Gamero-Castaño, M.; Fernandez de la Mora, J. Modulations in the abundance of salt clusters in electrosprays. *Anal. Chem.* **2000**, *72*, 1426-1429.
5. Gamero-Castaño, M.; Fernandez de la Mora, J. Mechanisms of electrospray ionization of singly and multiply charged salt clusters. *Anal. Chim. Acta.* **2000**, *406*, 67-91.
6. Charles, L.; Pépin, D.; Gonnet, F.; Tabet, J. Effects of liquid phase composition on salt cluster formation in positive ion mode electrospray mass spectrometry: implications for clustering mechanism in electrospray. *J. Am. Soc. Mass Spectrom.* **2001**, *12*, 1077-1084.
7. Zhang, D.; Cooks, R. G.; Doubly charged cluster ions $[(NaCl)_m(Na)_2]^{2+}$: magic numbers, dissociation, and structure. *Int. J. Mass Spectrom.* **2000**, *195/196*, 667-684.
8. Hao, C.; March, R. E.; Croley, T. R.; Smith, J. C.; Rafferty, S. P. Electrospray ionization tandem mass spectrometric study of salt cluster ions. Part 1- Investigations

of alkali metal chloride and sodium salt cluster ions. *J. Mass Spectrom.* **2001**, *36*, 79-96.

9. Cai, Y.; Cole, R. B. Stabilization of anionic adducts in negative ion electrospray mass spectrometry. *Anal. Chem.* **2002**, *74*, 985-991.
10. Cech, N. B.; Enke, C. G. Practical implications of some recent studies in electrospray ionization fundamentals. *Mass Spectrom. Rev.* **2001**, *20*, 362-387.
11. Barnett, D.; Horlick, G. Quantative electrospray mass spectrometry of halides and halogenic anions. *J. Anal. At. Spectrom.* **1997**, *12*, 497-501.
12. Charles, L.; Chiron, J.; Galy, J. Characterization of ammonium chloride derivatives by salt clustering in electrospray ionization mass spectrometry. *Rapid Commun. Mass Spectrom.* **2003**, *17*, 2471-2474.
13. Li, F.; Beyers, M. A.; Houk, R. S. Tandem mass spectrometry of metal nitrate negative ions produced by electrospray ionization. *J. Am. Soc. Mass Spectrom.* **2003**, *14*, 671-679.
14. Mollah, S.; Pris, A. D.; Johnson, S. K.; Gwizdala, A. B., III; Houk, R. S. Identification of metal cations, metal complexes, and anions by electrospray mass spectrometry in the negative ion mode. *Anal. Chem.* **2000**, *72*, 985-991.
15. Armentrout, P. B. Mass spectrometry-not just a structural tool: the use of guided ion beam mass spectrometry to determine thermochemistry. *J. Am. Soc. Mass Spectrom.* **2002**, *13*, 419-434.
16. Armentrout, P. B. Fundamentals of ion-molecule chemistry. *J. Anal. At. Spectrom.* **2004**, *19*, 571-580.

17. Armentrout, P. B. Kinetic energy dependence of ion-molecule reactions: guided ion beams and threshold measurements. *Int. J. Mass Spectrom.* **2000**, *200*, 219-241.

18. Gutsev, G. L.; Bartlett, R. J.; Boldyrev, A. I.; Simmons, J. Adiabatic electron affinities of small superhalogens: LiF_2, $LiCl_2$, NaF_2, and $NaCl_2$. *J. Chem. Phys.* **1997**, *107*, 3867-3875.

Table 1. Chemicals, formulas, and abbreviations.

Compound name	Formula	Abbreviation
Methylamine hydrochloride	$CH_3NH_3^+Cl^-$	$MeNH_3Cl$
Ethylamine hydrochloride	$CH_3CH_2NH_3^+Cl^-$	$Et\ NH_3Cl$
Propylamine hydrochloride	$CH_3CH_2CH_2NH_3^+Cl^-$	$Pr\ NH_3Cl$
Dimethylamine hydrochloride	$(CH_3)_2NH_2^+Cl^-$	Me_2NH_2Cl
Diethylamine hydrochloride	$(CH_3CH_2)_2NH_2^+Cl^-$	Et_2NH_2Cl
Tetraethylammonium chloride	$(CH_3CH_2)_4N^+Cl^-$	Et_4NCl
Tetrabutylammonium chloride	$(CH_3CH_2CH_2CH_2)_4N^+Cl^-$	Bu_4NCl
Tetrabutylammonium iodide	$(CH_3CH_2CH_2CH_2)_4N^+I^-$	Bu_4NI

Table 2. Threshold appearance energies for CID product ions

Precursor	Corrected[a] appearance energy (eV) of indicated product ion	
	HCl_2^-	Cl^-
$MeNH_3Cl_2^-$	2.06	2.22
$Me_2NH_2Cl_2^-$	1.94	2.14
$Et_2NH_2Cl_2^-$	1.63	1.93

Precursor	HCl_2^-	$MeNH_3Cl_2^-$	$(MeNH_3)HCl_3^-$
$(MeNH_3)_2Cl_3^-$	1.24	1.41	1.47

[a]"Corrected" means the listed values are the measured thresholds plus the 0.76 eV instrumental offset. See ref. 13 and Experimental section.

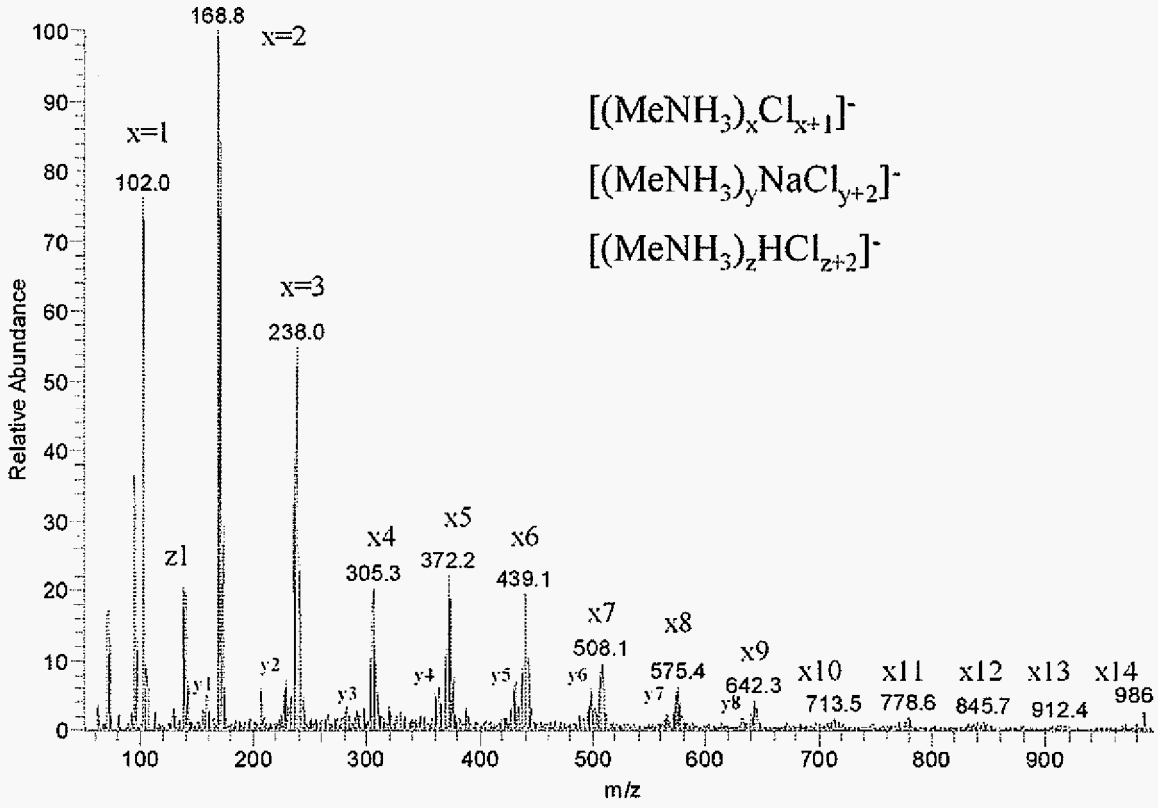

Figure 1. Mass spectrum of 1 mM methylamine hydrochloride in 99 % IPA, 1% H_2O. The subscripts x, y and z indicate three different cluster patterns. Clusters can be seen up to x = 14 for the main cluster pattern.

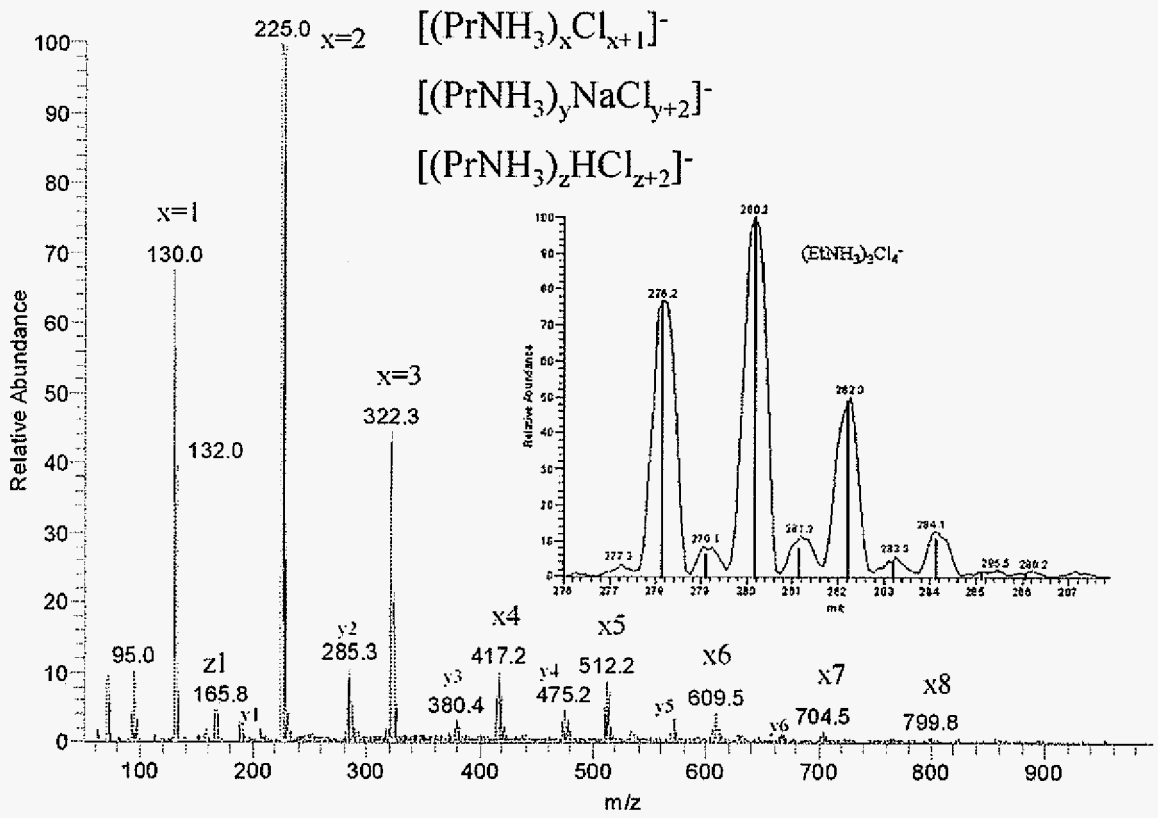

Figure 2. Mass spectrum of 1 mM propylamine hydrochloride in 99 % IPA, 1% H_2O. The cluster distribution is present up to x = 8 for the main cluster pattern. Inset shows isotope peaks for $(EtNH_3)_3Cl_4^-$. The black bars indicate the calculated isotope distribution for this cluster ion.

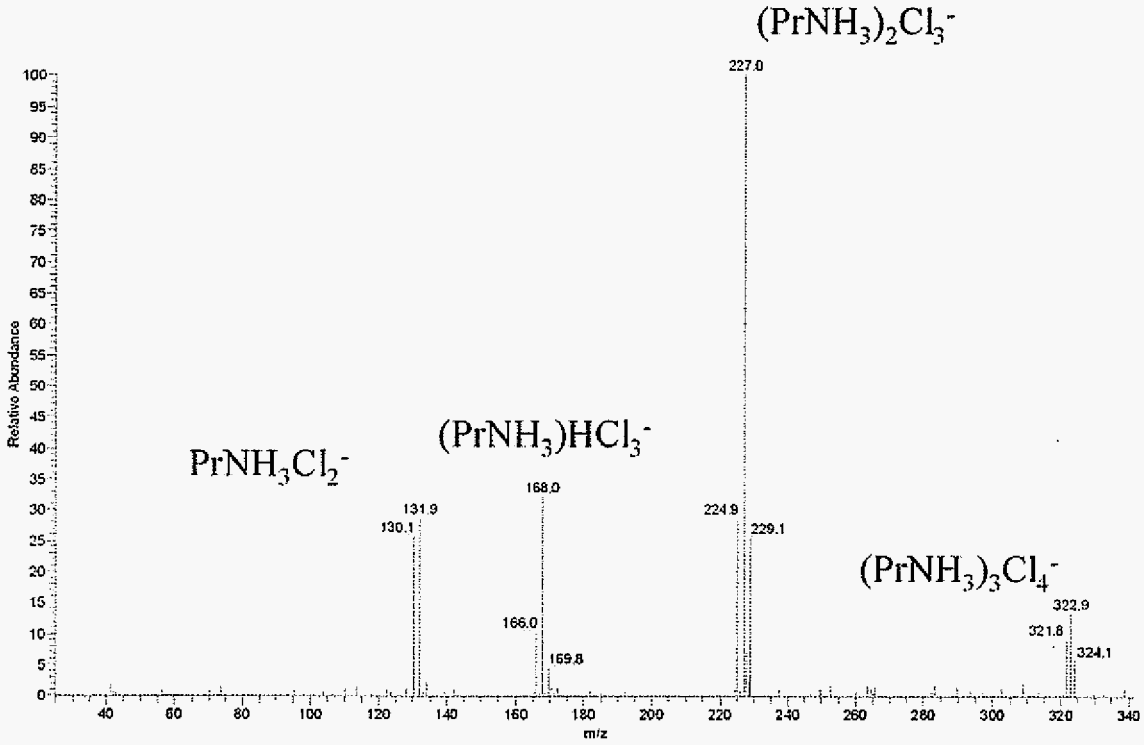

Figure 3. CID product spectrum of the $(PrNH_3)_3Cl_4^-$ ion. The parent ion fragments into smaller cluster ions with the next smaller cluster being the most intense. Note that no Cl^- ions are observed in the mass spectrum. The first mass analyzer does not transmit all the isotopomers of the parent ion equally, so the product ions do not have the expected natural isotope distribution.

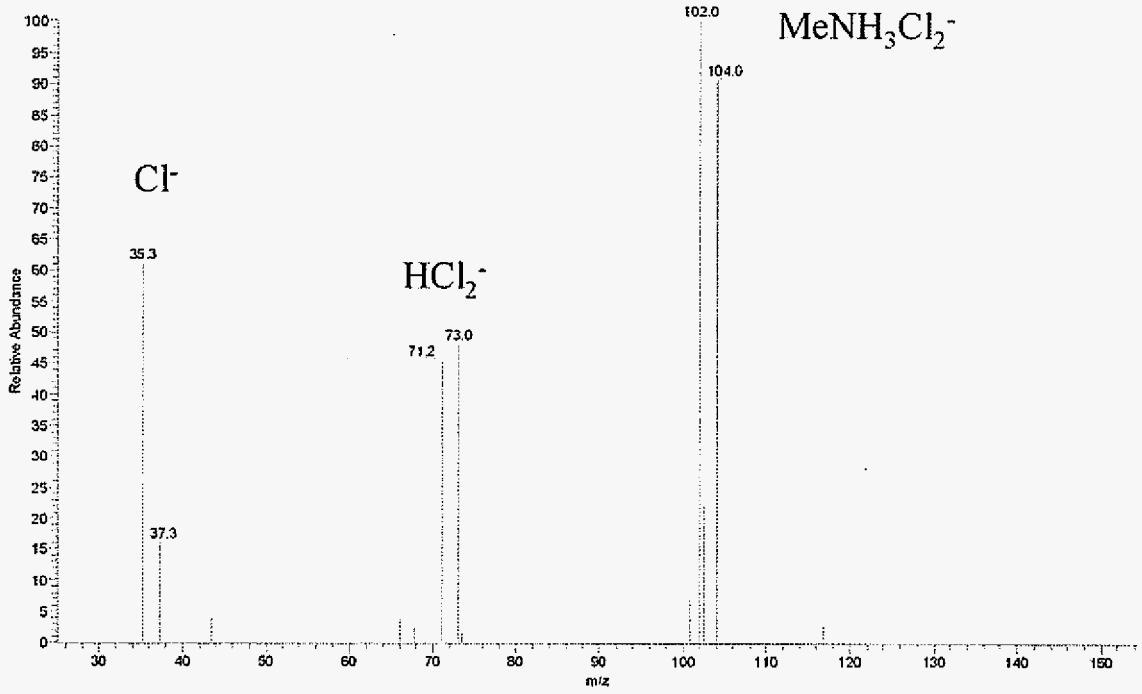

Figure 4. CID product spectrum of the $MeNH_3Cl_2^-$ monomer ion, which fragments into HCl_2^- and Cl^-.

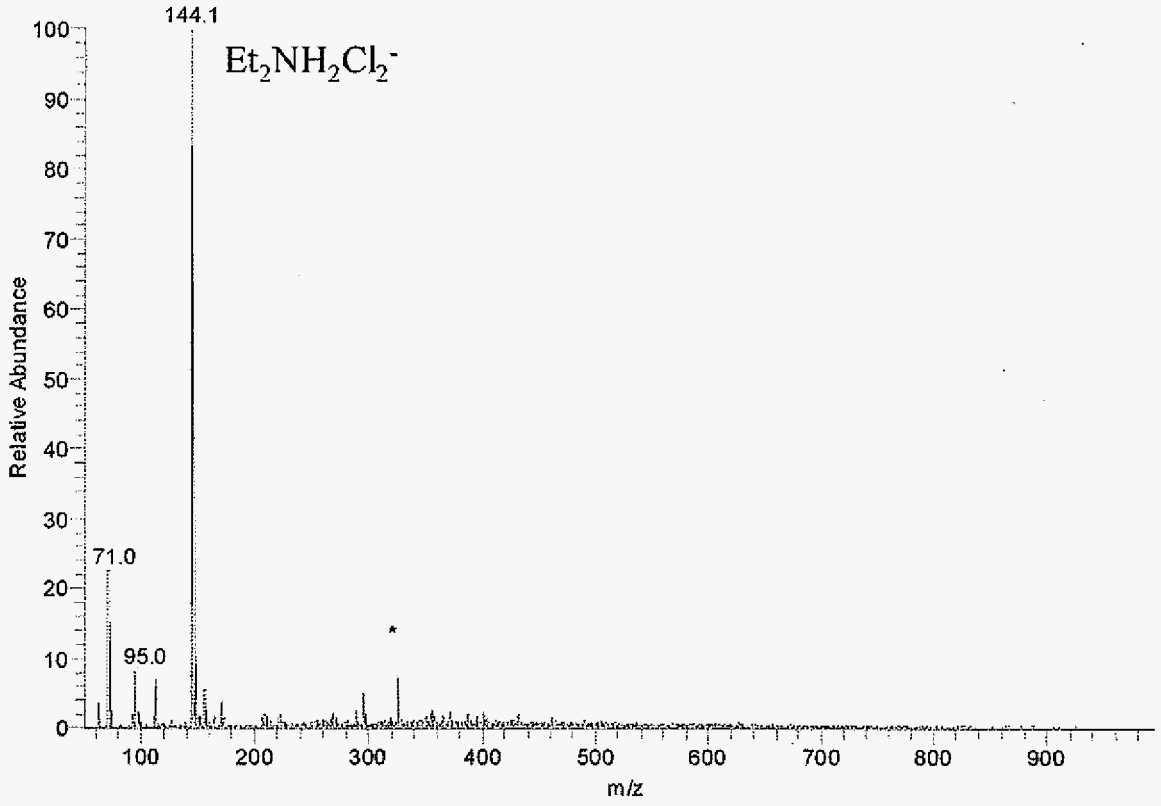

Figure 5. Mass spectrum of 1 mM diethylamine hydrochloride in 99 % IPA, 1 % H_2O. The only analyte ion present is the monomer ion of $Et_2NH_2Cl_2^-$ (m/z = 144). The peak labeled with an asterisk is a noise spike.

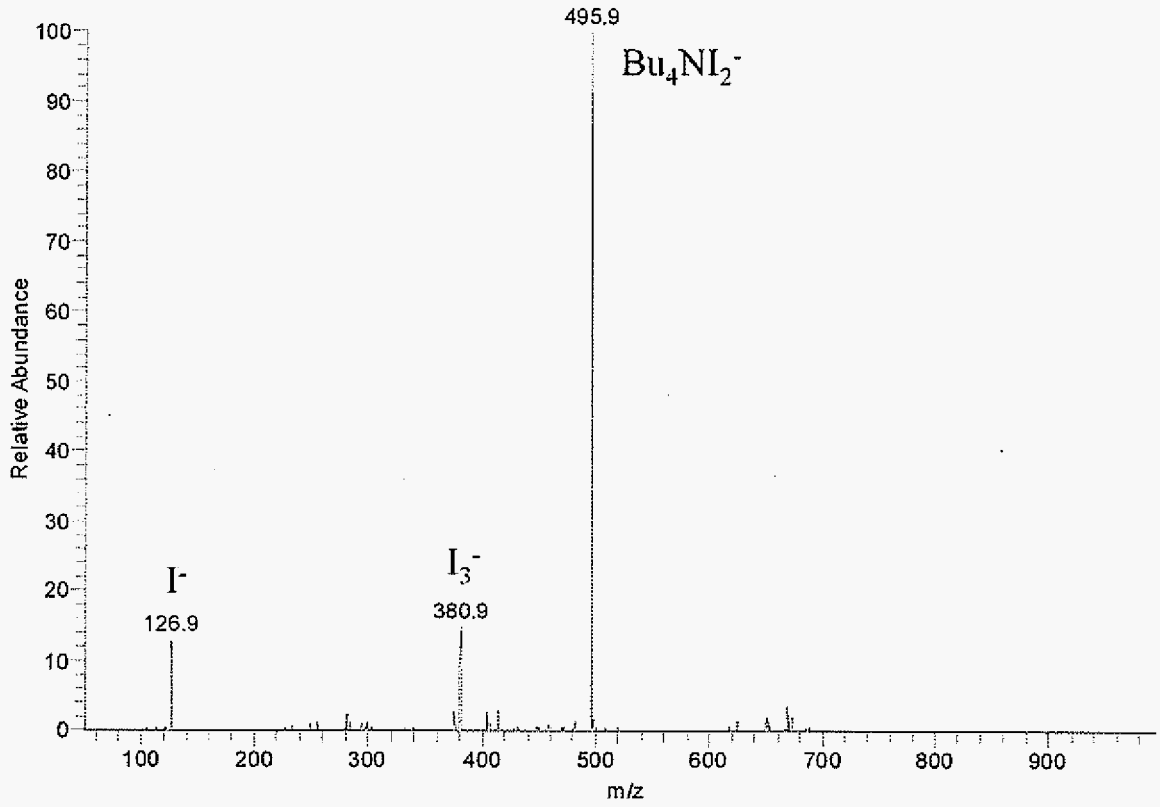

Figure 6. Mass spectrum of 1 mM tetrabutylammonium iodide. The three ions present are I^-, I_3^-, and $Bu_4NI_2^-$.

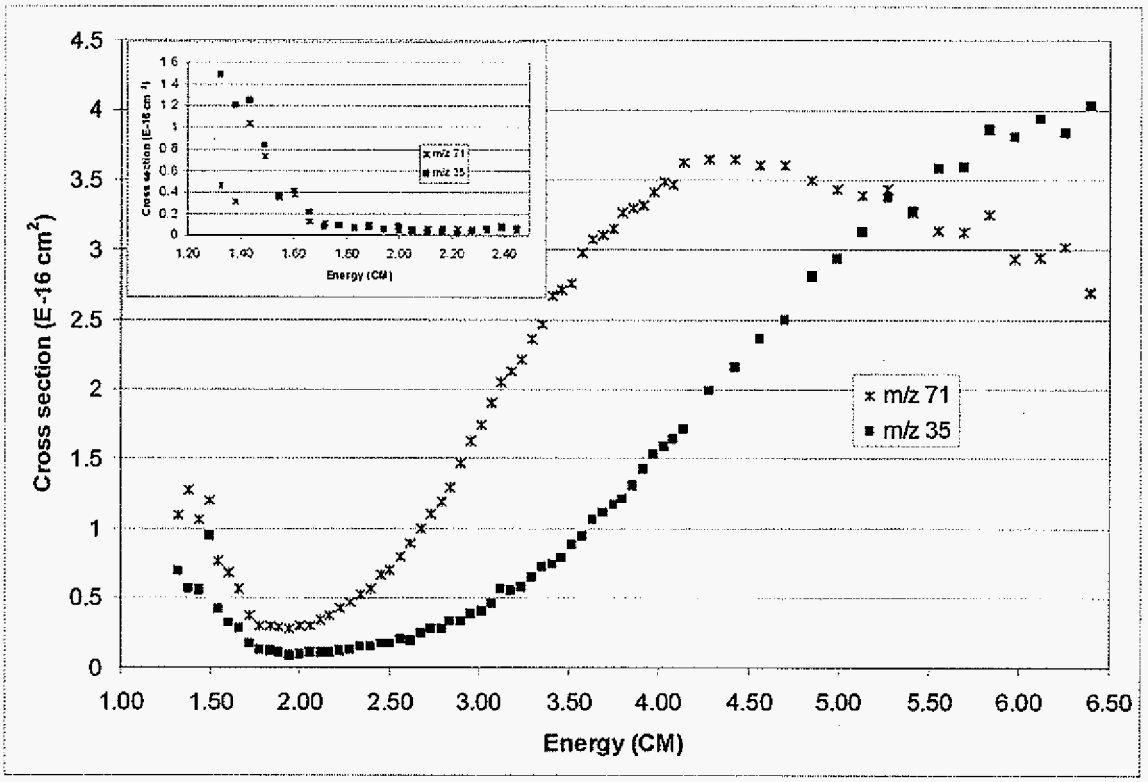

Figure 7. Measured cross sections for the production of HCl_2^- and Cl^- from $MeNH_3Cl_2^-$ versus collision energy in center of mass frame. The threshold energies are 2.06 and 2.22 eV, respectively. The collision gas pressure was 0.0267 Pa and the data were collected in SRM mode. The threshold energies have been corrected by addition of the 0.76 eV instrumental offset, as described in the Experimental section. Inset shows measured cross sections for HCl_2^- and Cl^- from $MeNH_3Cl_2^-$ without any collision gas present in the collision cell. No apparent cross section is measured. The initial decrease is attributed to instrumental effects.

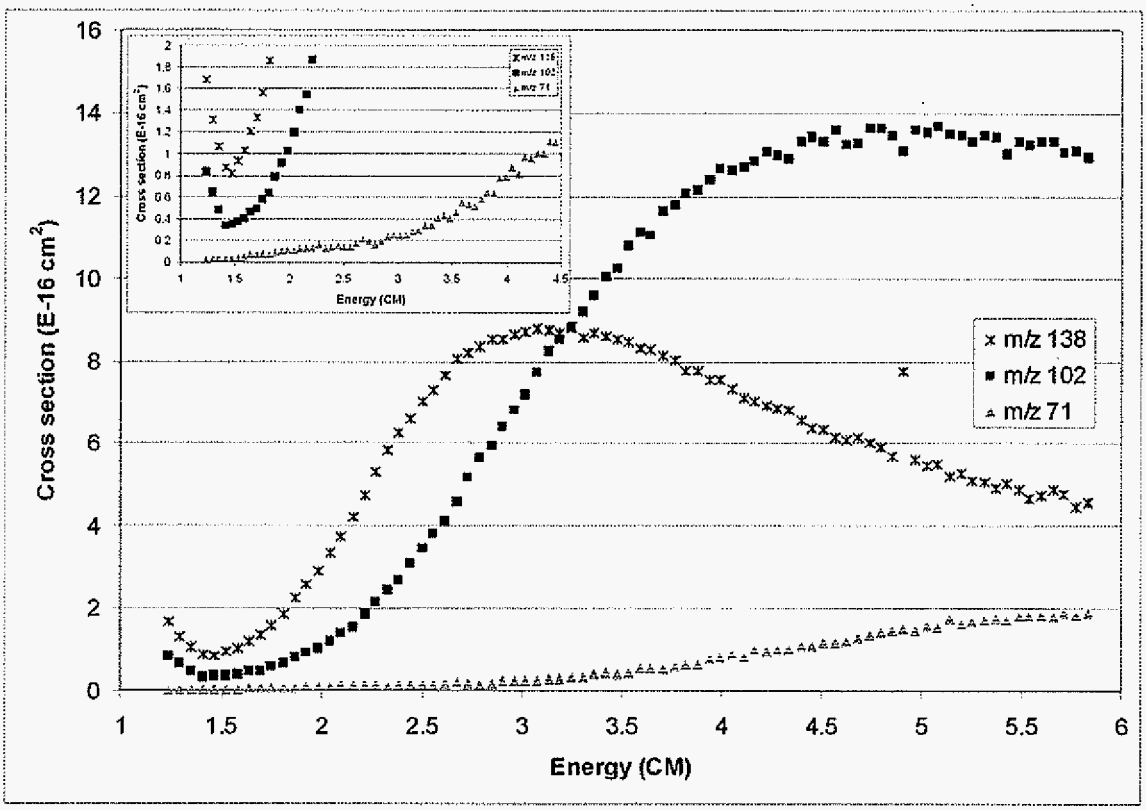

Figure 8. Measured cross sections for the production of $(MeNH_3)HCl_2^-$, $MeNH_3Cl_2^-$, and HCl_2^- from $(MeNH_3)_2Cl_3^-$. The threshold energies are 1.47, 1.41 and 1.24 eV, respectively. Inset shows an expanded view of the threshold region.

CHAPTER 3. ELECTROSPRAY IONIZATION MASS SPECTROMETRY OF HIGHLY NEGATIVELY CHARGED ALKALI METAL SULFATE CLUSTER IONS

A paper to be submitted to the *Journal of the American Society for Mass Spectrometry*

N. B. Lentz, T. C. Hutcheson, and R. S. Houk

Abstract

Salt cluster ions of alkali metal sulfates $M_x(SO_4)_y^{z-}$ (M = Li, Na, and Cs) were studied by electrospray ionization mass spectrometry. Ions with charges up to z = -7, i.e., $Na_{131}(SO_4)_{69}^{7-}$ were present in the mass spectra. The effects of capillary temperature, capillary voltage, tube lens voltage, fragmentor voltage, and various solvents were investigated. Collision induced dissociation of the clusters showed that there was an overlap of singly and multiply charged ions at the same m/z. Two different types of instrument interfaces, heated capillary and fragmentor, were utilized in this study. The different cations produced different cluster distributions with lithium sulfate clusters generating the most multiply charged cluster ions. The capillary voltage altered the cluster ion intensity and distribution more than any other parameter on the instrument with the heated capillary interface. The fragmentor voltage produced the largest variation in the cluster ion distribution. Overall, the heated capillary interface produced smaller changes to the cluster ion distribution than the fragmentor interface.

Introduction

Electrospray ionization [1-4] has proved to be a significant advance in the field of mass spectrometry. Over the past 15 to 20 years, cluster ions have been utilized for many electrospray applications. Anacleto et al. found that protonated water clusters and salt clusters could be used for mass calibration in both positive and negative ion modes of electrospray ionization mass spectrometry (ESI-MS) [5]. Later, sodium trifluoroacetate cluster ions were also found to be a useful calibration standard for ESI-MS [6].

Clusters are useful calibration standards for ESI-MS because they cover the mass to charge scale from around 50 m/z to 4000+ m/z. This covers the range of quadrupole, quadrupole ion trap, and most linear trap mass analyzers. This also covers a significant portion of a time of flight (TOF) mass analyzer's m/z range. Cluster ions are also closely spaced throughout the entire mass range, but far enough apart to allow for the identification of the correct peak. These characteristics allow for an excellent mass calibration throughout the entire m/z range.

Cluster ions have been used to study the electrospray ionization process. Currently, there are two proposed mechanisms that explain the ESI process: the ion evaporation model (IEM) and the charge residue model (CRM). The IEM was proposed by Iribarne and Thompson [7, 8] in the 1970's, and the CRM initiated with the research done by Dole et al. [1] and further developed by Röllgen and coworkers [9, 10]. More recent research by Wang and Cole focused on weakly solvated ions and led to a proposed extended form CRM model [11, 12]. For low m/z cluster ions, Kebarle and Peschke were unable to distinguish the IEM and CRM models because ions supporting both models were present in the mass spectra [13].

Several other interesting studies utilizing cluster ions have been done to try and explain the IEM and CRM models [14-16].

Even though a lot of cluster ion research has been conducted, very little research has been done on multiply charged cluster ions and other fundamental areas. In this paper, multiply charged cluster ions are defined as cluster ions that have two or more charges. In addition, very little research has been done on collision induced dissociation of cluster ions. Also the effects of solvents, ESI source conditions, and the mass spectrometer interface have not been rigorously studied.

A few years ago, two papers by March and coworkers sought to address many of the issues stated above [17, 18]. These papers looked at multiply charged clusters, solvent conditions, pH, and CID. This paper expands on the cluster ions studied by March and coworkers by analyzing clusters in which cations and anions have different fundamental charges as well as using mass spectrometers with different source designs.

Experimental

Samples and Sample Preparation

The sulfate salts ($LiSO_4$, $NaSO_4$, $CsSO_4$) and organic solvents were purchased from Sigma (St. Louis, MO) and used without further purification. The samples were dissolved at 1 mM in either a H_2O/MeOH or isopropanol (IPA)/H_2O (Millipore 18.2 MΩ, Bedford, MA) solution. The percent composition of each solvent was altered during some experiments, but a 50/50 H_2O/MeOH solution was used unless otherwise noted.

ESI-MS

A triple quadrupole (QoQ) MS (TSQ-7000, Thermo Finnigan, San Jose, CA) with an on-axis ESI source and heated capillary interface (stainless steel, 400 μM i.d. 114 mm long), was used for the majority of the experiments. Samples were continuously infused at 5 μL/min with a syringe pump (Model 22, Harvard Apparatus, Southnatic, MA). Nitrogen (60 psi) and high purity argon were used as the nebulizing gas and collision gas, respectively. The electrospray needle voltage was set to -3.2 to -4.0 kV, and the heated capillary was kept at 200 °C, -136 V. The voltages on the ring electrode and first octopole were -85 and +3.0 V, respectively. The skimmer is at ground on this instrument. The parameters were adjusted to obtain a stable signal with maximum intensity over the mass range investigated. The scan range was 50 to 2000 m/z. Data were collected for 2 to 5 minutes at 2 seconds per scan. For CID studies, the collision pressure was 1.0-1.5 mtorr, and the collision voltage was 20-25 eV (lab frame). The resolution of the first quadrupole was reduced to increase ion transmission into the collision cell.

A single quadrupole MS (6130A, Agilent Technologies, Santa Clara, CA) with an orthogonal ESI source was also used for some experiments as noted. The interface geometry of this instrument employs a heated nitrogen counter-current gas flow, a stainless steel capped glass transfer capillary (600 μM i.d. 180 mm long), and a skimmer with an adjustable voltage. The skimmer voltage is referred to as the fragmentor voltage. The electrospray needle voltage was set to -3.5 kV, and the drying gas temperature was set to 250 °C. Nitrogen was used for the nebulizing gas (35 psi) and drying gas. The scan range was 50 to 3000 m/z. The 1 mM samples were introduced via a high pressure liquid chromatography (HPLC) system (model 1200, Agilent Technologies, Santa Clara, CA) at a flow rate of 50

μL/min. No column was used during the experiments. The amount of sample injected was either 50 or 100 μL, which allowed for 1 or 2 minutes of data to be averaged for each mass spectrum.

Results and Discussion

Effect of Cation Size

Solutions of Li_2SO_4, Na_2SO_4, and Cs_2SO_4 were sprayed to see if the size of the cation affects the cluster ion distribution in the mass spectra. The Pauling crystal radii of Li^+, Na^+, and Cs^+ are 60, 95, and 169 pm, respectively [19]. The Yatsimirskii thermochemical radius of SO_4^{2-} anion is 230 pm [20]. Figure 1a-c shows the mass spectra of $LiSO_4$, $NaSO_4$, and $CsSO_4$ cluster ion distributions. All of the instrument conditions were kept constant between the three different samples.

The Li and Na cations (Figures 1a and 1b) have similar cluster ion distributions which decay off in an exponential fashion with many clusters present. In these figures, the number refers to the number of cations in the cluster ion, and the superscript number indicates the charge state. For example the ion labeled as 7^- in Figure 1b is $Na_7(SO_4)_4^-$. The same notation is used for the rest of the figures in this paper. In Figure 1a, there are a lot of "background" peaks present above m/z 1100. These are not background ions. The ions are low intensity multiply charged lithium sulfate clusters. This pattern is present in Figure 1b, but the peaks are further apart due to the larger mass of sodium compared to lithium. This spreads out the ions in the mass spectrum and allows for an accurate mass assignment. The Cs clusters, Figure 1c, also decay off in an exponential fashion, but with few higher charge states present.

Even though there are fewer Cs clusters due to the larger mass of Cs, there are few doubly charged ions present in the mass spectrum. For Li and Na, there is a doubly charged ion present between 3^- and 5^- but this peak is absent in the Cs spectrum. This shows that cation size plays a role in cluster ion formation. It is surprising to note that the smaller cations form more clusters with the larger sulfate anion than the Cs cation, which is similar in size to sulfate anion. It is possible that the smaller cations can fit into holes and spaces into which the larger Cs cation cannot.

At higher m/z values, clusters representing multiple charge states are present for Li and Na clusters. Figure 2a shows that charge states are present up to 5- for sodium sulfate cluster ions acquired on the TSQ-7000 instrument. At higher m/z some 6- ions are also present. In Figure 2b, the Agilent instrument was used to collect a mass spectrum over the same m/z range as in Figure 2a. The spectra have a similar cluster ion distribution, and the same cluster ions are present. Figure 2c shows the m/z 1250-1400 region of a sodium sulfate solution collected on the Agilent instrument. Cluster ions with charges up to 7- are observed. The ion labeled as 131^{7-} is $Na_{131}(SO_4)_{69}^{7-}$. There are 200 total ions stabilized by ionic interactions in this cluster ion.

The ions described above were identified by comparing calculated mass to charge ratios to the mass to charge ratios present in the mass spectrum. These comparisons show excellent agreement, within 0.5 m/z, and allow for the correct identification of the ions. The presence of many different charge states indicates that there is a strong interaction between the sulfate anion and the Li and Na cations. The ions must be reasonably stable in order to traverse the mass spectrometer, and reach the detector.

Effects of Instrumental Conditions on the Masses and Charge States of Cluster Ions

TSQ-7000

It has been shown elsewhere that the cone voltage can drastically alter the appearance of cluster ions in mass spectra [15]. The TSQ-7000 instrument used in this study employs a heated capillary and a tube lens to direct ions into the mass spectrometer instead of a sampler cone. The effects of changing the heated capillary voltage and tube lens voltage are discussed below. The spectra are compared to spectra taken on an instrument that utilizes a sampling cone where the cone voltage is varied.

Figures 3a-f show the spectra at three different capillary voltages (a-c), and three different tube lens voltages (d-f). The voltages cover the normal operating ranges for these components. The three capillary voltages shown are 50, 137, and 150 volts. The three tube lens voltages shown are 5, 60, and 100 volts. As seen in Figures 3a-c, changing the capillary voltage has a significant effect on the cluster ion distribution. At low capillary voltages, the spectrum has a higher number of low m/z multiply charged ions and very few ions present at a m/z greater than 700. At normal to high capillary voltages (Figures 3b and 3c), some of the low m/z multiply charged ions are lost, but many more cluster ions with a higher m/z are observed. Multiply charged clusters are present, but they have less charge so their m/z has shifted to a higher value. The overall intensity of the cluster ion distribution is greater at higher capillary voltages. The greatest number of singly charged clusters occurs at the highest capillary voltages.

The tube lens voltage had little effect on the cluster distribution and location of the multiply charged clusters. The spectra in figures 3d-f have very similar cluster ion distributions, even though the tube lens is changed from 5 to 150 V. This shows that the tube

lens does not cause collision induced dissociation for the ions investigated. The intensity of the cluster ions does change though, with the higher tube lens voltage generating a slightly more intense mass spectrum. The overall function of the tube lens is to focus ions, and not cause ion fragmentation.

The capillary and tube lens voltages were also changed for lithium sulfate and cesium sulfate clusters. When the capillary voltage was changed from 25 to 150 volts for lithium sulfate clusters, more cluster ions were present at higher m/z (data not shown). The low m/z multiply charged cluster ions were present until the capillary voltage reached 150 V. The intensity of the cluster ions increased as the capillary voltage increased. This effect was also seen when the tube lens voltage was changed for the lithium sulfate clusters. Increasing the tube lens voltage allowed for the identification of higher m/z clusters, which could not be seen at low tube lens voltages.

The results for cesium sulfate clusters were more difficult to compare since many fewer cluster ions are present. As with lithium and sodium, the higher capillary voltages produced a more intense spectrum, but the intensity reached a maximum at 100 V (data not shown). The tube lens voltage didn't significantly affect the cesium sulfate cluster ion spectra. The intensities and overall appearance of the spectra remained consistent.

The effect of the heated capillary temperature on the cluster ion distributions was also studied. The results were similar for the different cations studied. At low capillary temperatures, 125 ^{o}C, the ion transmission was very low, and few ions were seen. The middle range of capillary temperatures, 150-200 ^{o}C, provided the best ion transmission and a wide distribution of cluster ions. At 250 ^{o}C, the highest capillary temperature studied, the ion intensity remained high but the cluster ion distribution decreased in the higher m/z range

compared to the spectra taken at 200 °C. Apparently the higher capillary temperature caused fragmentation of the large, highly charged clusters.

Agilent 6130A

The sodium sulfate cluster ions were also analyzed using an Agilent 6130A single quadrupole instrument with a different interface. As stated in the experimental section, this instrument interface uses a heated nitrogen counter-current gas flow, a transfer capillary, and a skimmer with an adjustable voltage. The adjustable voltage on the skimmer is referred to as the fragmentor voltage on this instrument and is comparable to the cone voltage on other instruments. The fragmentor has an adjustable range from 0 to 400 V. The sodium sulfate cluster ion distribution was examined using fragmentor voltages of 50, 100, 150, 200, 250, 300, 350, and 400 V. This covers the entire range of the fragmentor voltage.

When a 1 mM sodium sulfate solution is sprayed at the different fragmentor voltages, significant changes in the cluster ion distribution are observed. Figures 4a-d show the sodium sulfate mass spectrum at 50, 150, 250, and 400 V, respectively. In Figure 4a, multiply charged cluster ions are present in the mass spectrum up to around m/z 1600. There are many multiply charged cluster ions present at low m/z. The overall abundance of the mass spectrum is low, and the ions are all on the low side of the m/z range. In Figure 4b, the overall abundance is more than double that of Figure 4a. The multiply charged ions have shifted to higher m/z values, in the range of 900-2000 m/z. The mass range of the cluster ions has been extended with cluster ions present out to ~2400 m/z.

This trend continues in Figure 4c where the multiply charged ions once again shift to a higher m/z range. The multiply charged cluster ions are in the 1100-2400 m/z range. The

overall abundance is three times higher than in Figure 4a. In the lower m/z range, singly charged sodium sulfate cluster ions are the main ions present. Low intensity doubly charged ions begin to appear at m/z 615. This can be verified by looking at the isotope distribution of the low mass ions. For example, the m/z 261 peak does not have any isotope peaks present at m/z 262 (data not shown). If there was a doubly charged cluster present at the same m/z, the ^{34}S isotope peak would be one m/z higher than the initial peak instead of the 2 m/z higher observed for a singly charged cluster. The resolution on both instruments is sufficient to observe a ^{34}S isotope peak one m/z higher than the initial peak.

In Figure 4d, there is another change in the cluster ion distribution. There are doubly and triply charge cluster ions present from ~ 900-2700 m/z, but the higher multiply charged cluster ions are present from ~ 1700-2700 m/z. The multiply charged ions are weak in intensity, and the singly charged ions are the main ions present. Singly charged cluster ions are present out to 2959.5 m/z. The intensity in Figure 4d is similar to the intensity in Figure 4c.

Effects of Solvent Conditions

Solvent composition also affected cluster ion distributions. Na_2SO_4 was dissolved at 1 mM in 50/50, 75/25, 25/75, and 1/99 H_2O/MeOH. A 50/50 H_2O/IPA solvent mixture was also used. Figures 5a-e show the cluster ion distribution effects as the solvents and solvent ratios are changed. Figure 5c, 25/75 H_2O/MeOH, produced the most intense cluster ion signal with both singly and multiply charged ions present in the mass spectrum. The multiply charged clusters present below m/z 500 are much more intense than in the 50/50 H_2O/MeOH spectrum in Figure 5a. The solvents with a higher proportion of methanol will

evaporate faster than the water based solvents in the atmospheric region of the ion source. This favors cluster ion formation for the analytes investigated. The 75/25 H_2O/MeOH solution produced the least intense mass spectrum (Figure 5b).

The 50/50 H_2O/IPA solution (Figure 5e) generated a mass spectrum with multiply charged clusters present throughout the whole mass spectrum. The multiply charged clusters are low in intensity, but they are present at both low and high m/z. This ion distribution is not present with the H_2O/MeOH solutions, and thus the 50/50 H_2O/IPA solution generated the most diverse distribution of clusters. Under these conditions, the m/z 283 peak is the most intense ion in the mass spectrum. This shows that the cluster properties change when IPA is used as a solvent.

CID of Cluster Ions

CID is a powerful fragmentation tool that gives structural information, fragmentation pathways, as well as bond strengths within ions. CID mass spectra were obtained on the TSQ-7000 instrument for some sodium sulfate cluster ions of various charge states. The resolution of the first quadrupole was decreased in order to obtain better ion transmission through the collision cell. The resolution was not decreased enough to transmit the ^{34}S isotope of the singly charged cluster ions. For multiply charged parent ions, both ^{32}S and ^{34}S isotopes were transmitted through Q1. The ^{32}S and ^{34}S isotopes of the multiply charged cluster ions were both transmitted, being at least one m/z closer to the parent ion than the singly charged cluster ion.

Figure 6 shows a CID spectrum for the m/z 402.7, $Na_5(SO_4)_3^-$, cluster ion. The presence of the peak at m/z 544.6 indicates the presence of a doubly or multiply charged ion

in the peak at m/z 402.7. The possible multiply charged ions that may be present at m/z 402.7 are $Na_{10}(SO_4)_6^{2-}$, $Na_{15}(SO_4)_9^{3-}$, and $Na_{20}(SO_4)_{12}^{4-}$. These ions were present in the low m/z range of the original mass spectrum, and those with the same isotopes (e.g. all ^{32}S and ^{16}O) cannot be distinguished because they have exactly the same m/z values, discounting the energy mass equivalent to the energy in their chemical bonds. A high resolution instrument may be able to separate the isotope peaks to give insight as to which ions are present.

A closer look at the m/z 544.6 peak shows ^{34}S isotope peaks only two m/z from the base peak. This indicates that there are not any doubly charged product ions at this m/z. In order to make a doubly charged ion at 544.6, a 3- or 4- ion at m/z 402.7 would have to undergo CID. This indicates that the peak at 402.7 is comprised mainly of singly and doubly charged ions. The peak at m/z 260.8 also does not show any doubly charged ions present based on the location of the ^{34}S isotope peak.

Figure 7 shows the CID spectrum of the sulfate clusters at m/z 544.6. Here the singly and doubly charged cluster ions are $Na_7(SO_4)_4^-$ and $Na_{14}(SO_4)_8^{2-}$, respectively; other possible cluster ions are $Na_{21}(SO_4)_{12}^{3-}$ and $Na_{28}(SO_4)_{16}^{4-}$. The product ions at m/z 686.7 and m/z 828.7 indicate that there is at least a doubly charged ion, and possibly a triply charged ion present at m/z 544.6. These ions are of very low intensity, but the m/z is the same as the ions seen in the original scan (see Figure 1b). It is possible that a triply charged ion is present because there were triply charged ions identified on either side of m/z 544.6 in the scan mode mass spectrum. Triply charged ions cannot be directly identified at m/z 544.6 because the instrument does not have sufficient resolution to separate the 3- isotope peaks from the 2- and 1- isotope peaks.

The ions at m/z 686.7 and m/z 828.7 are from the fragmentation of a doubly charged parent ion. When the singly charged m/z 828.7 ion is produced, a singly charged ion at m/z 260.7 is also produced. This accounts for all of the sodium and sulfate ions in the doubly charged m/z 544.6 ion. The m/z 686.7 ion and some of the 402.6 ion are also produced from the fragmentation of a doubly charged ion at m/z 544.6. When the singly charged ions at m/z 544.6 undergo CID, m/z 260.7 and m/z 402.6 ions are present.

Figure 8 shows the CID mass spectrum of the doubly charged sodium sulfate cluster at m/z 331.8. At m/z 331.8, there cannot be any singly charged cluster ions present because m/z 331.8 is in between the singly charged cluster ions of $Na_3(SO_4)_2^-$ (m/z 260.8) and $Na_5(SO_4)_3^-$ (m/z 402.8). Few, if any, 4- ions are present based on the lack of 4- ions at surrounding m/z. The formula for the m/z 331.8 cluster is $Na_8(SO_4)_5^{2-}$. Two product ions are seen at m/z 260.7 and m/z 402.6. The product ions are singly charged because the ^{34}S isotope is 2 m/z units away from the ^{32}S isotope peak. These two ions account for all of the sodium and sulfate ions in the doubly charged peak at m/z 331.8. Since no other product ions are observed, it is likely that the peak at m/z 331.8 only contains the doubly charged cluster ion and is not a combination of 2- and 4- cluster ions. If a 4- cluster ion was present, multiply charged product ions would have been present in the CID spectrum of the m/z 331.8 ion.

Conclusions

Instrument interface geometry has a significant influence on the appearance of sulfate cluster spectra. The heated capillary/tube lens interface provides the most consistent spectra at different conditions for the cluster ions studied. As seen in previous work, changing the

voltage on the cone/fragmentor can completely change the cluster ion distribution in the mass spectrum [17].

Based on this information, instrument geometry plays a critical role in cluster ion analysis. If a wide variety of cluster ions are being analyzed, the heated capillary/tube lens interface offers fewer spectral changes than other instrument interface geometries. It may be possible to use a general set of tune conditions and compare a wide variety of cluster ions, which could be useful when looking for a cluster ion to bind an ion of interest.

On the other hand, if a specific cluster ion needs to be studied, the cone/fragmentor voltage could be optimized to maximize the intensity for the desired cluster ion. This could be useful if a cluster ion is going to be isolated from a cluster ion distribution and used for another purpose, such as gas phase reactions in an ion trap or ion mobility studies.

Acknowledgements

Ames Laboratory is operated by Iowa State University for the U.S. Department of Energy, contract no. W-7405-Eng-82. This work was supported by the Chemical and Biological Sciences Program, Office of Basic Energy Sciences, Division of Chemical Sciences. The authors thank L. Huang and Bayer Company for donating the triple quadrupole instrument and Agilent Technologies for the loan of their instrument.

References

1. Dole, M.; Mack L. L.; Hines, R. L.; Mobley, R. C.; Ferguson, L. D.; Alice, M. B. Molecular Beams of Macroions. *J. Chem. Phys.* **1968**, *49*, 2240-2249.

2. Yamashita, M; Fenn, J. B. Electrospray Ion Source. Another Variation on the Free-Jet Theme. *J. Phys. Chem.* **1984**, *88*, 4451-4459.

3. Yamashita, M; Fenn, J. B. Negative Ion Production with the Electrospray Ion Source. *J. Phys. Chem.* **1984**, *88*, 4671-4675.

4. Whitehouse, C. M.; Dreyer, R. N.; Yamashita, M; Fenn, J. B. Electrospray Interface for Liquid Chromatographs and Mass Spectrometers. *Anal. Chem.* **1985**, *57*, 675-679.

5. Anacleto, J. F.; Pleasance, S.; Boyd, R. K. Calibration of Ion Spray Mass Spectra using Cluster Ions. *Org. Mass Spectrom.* **1992**, *27*, 660-666.

6. Moini, M.; Jones, B. L.; Rogers, R. M.; Jiang, L. Sodium Trifluoroacetate as a Tune/Calibration Compound for Positive- and Negative-Ion Electrospray Ionization Mass Spectrometry in the Mass Range of 100-4000 Da. *J. Am. Soc. Mass Spectrom.* **1998**, *9*, 977-980.

7. Iribarne, J. V.; Thomson, B. A. On the Evaporation of Small Ions from Charged Droplets. *J. Chem. Phys.* **1976**, *64*, 2287-2294.

8. Thomson, B. A.; Iribarne, J. V. Field Induced Ion Evaporation from Liquid Surfaces at Atmospheric Pressure. *J. Chem. Phys.* **1979**, *71*, 4451-4463.

9. Röllgen, F. W.; Bramer-Wegner, E.; Bütfering, L. *J. Phys. Colloq.* **1984**, *45*(Suppl. 12): C9.

10. Schmelzeisen-Redeker, G; Bütfering, L.; Röllgen, F. W. Desolvation of Ions and Molecules in Thermospray Mass Spectrometry. *Int. J. Mass Spectrom. Ion Proc.* **1989**, *90*, 139-150.

11. Wang, G.; Cole, R. B. Solvation Energy and Gas-Phase Stability Influences on Alkali Metal Cluster Ion Formation in Electrospray Ionization Mass Spectrometry. *Anal. Chem.* **1998**, *70*, 873-881.

12. Wang, G.; Cole R. B. Charged Residue versus Ion Evaporation for Formation of Alkali Metal Halide Cluster Ions in ESI (Electrospray Ionization). *Anal. Chim Acta* **2000**, *406*, 53-65.

13. Kebarle, P; Peschke, M. On the Mechanisms by which the Charged Droplets Produced by Electrospray Lead to Gas Phase Ions. *Anal. Chim. Acta* **2000**, *406*, 11-35.

14. Kebarle, P; Tang, L. From Ions in Solution to Ion in the Gas Phase - the Mechanism of Electrospray Mass Spectrometry. *Anal. Chem.* **1993**, *65*, 972A-986A.

15. Tang, L; Kebarle, P. Dependence on Ion Intensity in Electrospray Mass Spectrometry on the Concentration of the Analytes in the Electrosprayed Solution. *Anal. Chem.* **1993**, *65*, 3654-3668.

16. Zhou, S.; Hamburger, M. Formation of Sodium Cluster Ions in Electrospray Mass Spectrometry. *Rapid Cammun. Mass Spectrom.* **1996**, *10*, 797-800.

17. Hao, C.; March, R. E.; Croley, T. R.; Smith, J. C.; Rafferty, S. P. Electrospray Ionization Tandem Mass Spectrometric Study of Salt Cluster Ions. Part 1-Investigations of Alkali Metal Chloride and Sodium Salt Cluster Ions. *J. Mass Spectrom.* **2001**, *36*, 79-96.

18. Hao, C.; March, R. E. Electrospray Ionization Tandem Mass Spectrometric Study of Salt Cluster Ions. Part 2-Salts of Polyatomic Acid Groups and of Multivalent Metals. *J. Mass Spectrom.* **2001**, *36*, 509-521.

19. Pauling, L. *The Nature of the Chemical Bond.* Cornell University Press: Ithaca, New York, 1960; pp 514.

20. Waddington, T. C. Lattice Energies and Their Significance in Inorganic Chemistry. *Adv. Inorg. Chem. Radiochem.* (H. J. Emeléus and A. G. Sharpe, Eds., copyright by Academic Press, Inc) **1959**, *1*, 157-221.

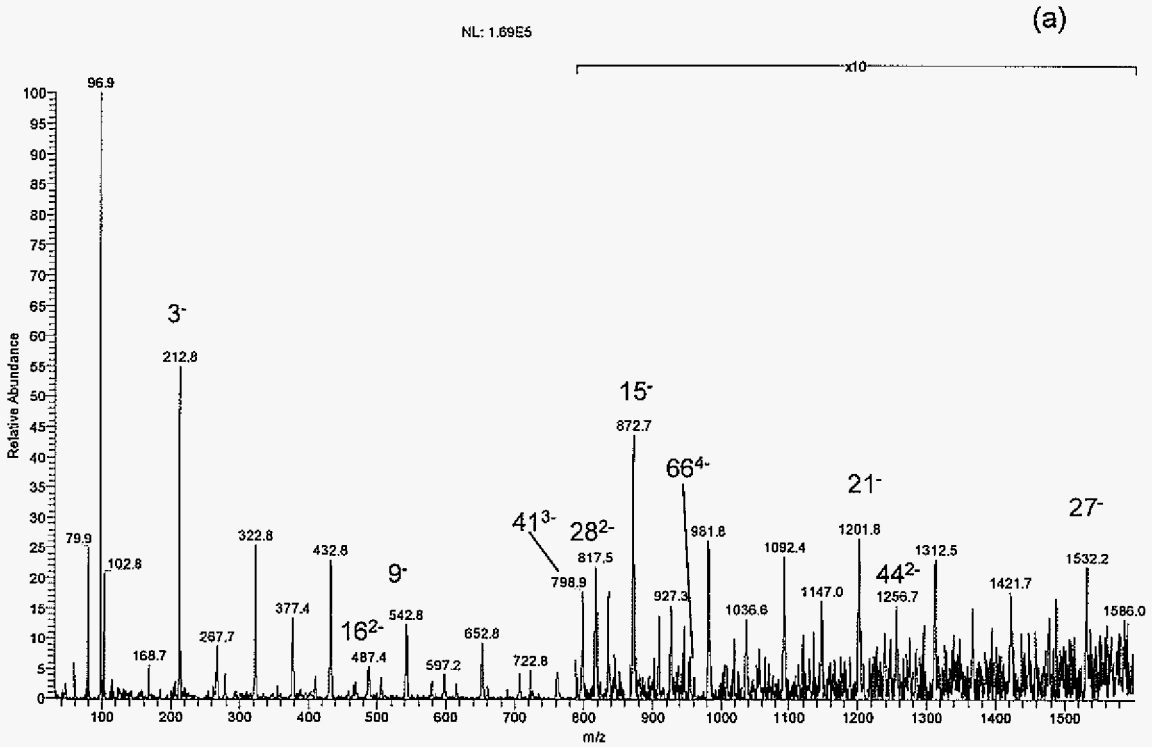

Figure 1. (a) Mass spectrum of 1 mM $LiSO_4$ in 50/50 H_2O/MeOH. The numbers above some peaks represent the number of Li^+ cations present, while the superscript denotes the charge state. (b) Mass spectrum of 1 mM $NaSO_4$ in 50/50 H_2O/MeOH. The numbers above some peaks represent the number of Na^+ cations present, while the superscript denotes the charge state. (c) Mass spectrum of 1 mM $CsSO_4$ in 50/50 H_2O/MeOH. The numbers above some peaks represent the number of Cs^+ cations present, while the superscript denotes the charge state. The intensity listed at the top of the figure corresponds to the most intense peak in the mass spectrum.

(b)

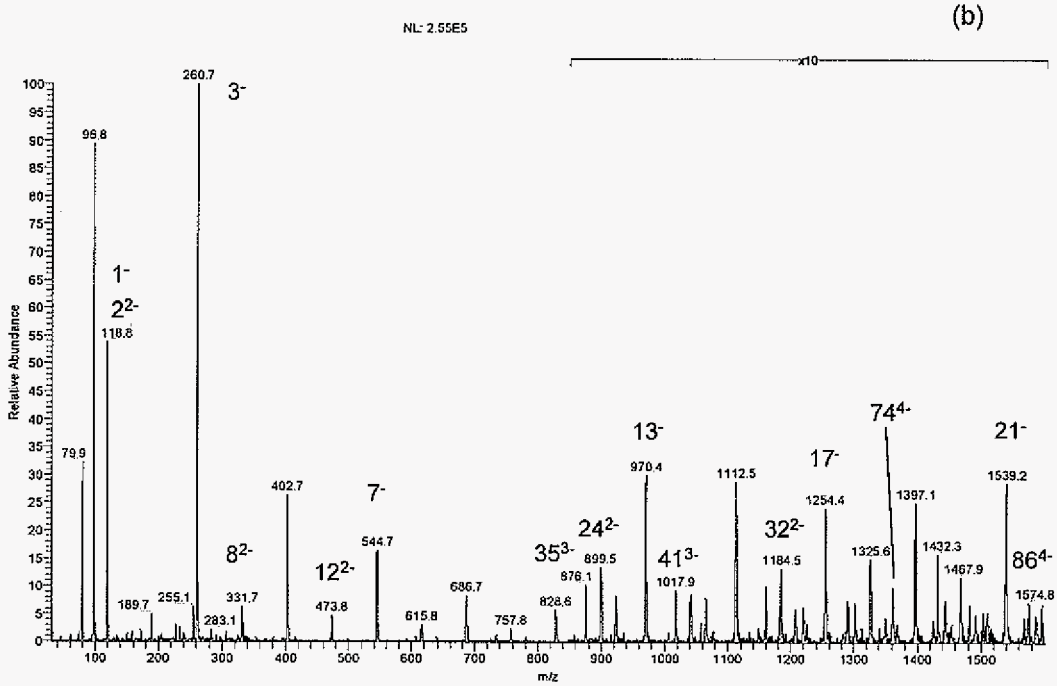
NL: 2.55E5
x10
Relative Abundance
m/z
260.7
3-
96.8
1-
2 2-
118.8
79.9
402.7
7-
544.7
8 2-
12 2-
473.8
331.7
189.7
255.1
283.1
615.8
686.7
757.8
828.6
35 3-
876.1
899.5
24 2-
970.4
13-
41 3-
1017.9
1112.5
17-
1254.4
32 2-
1184.5
1325.6
74 4-
1397.1
1432.3
1467.9
21-
1539.2
86 4-
1574.8

(c)

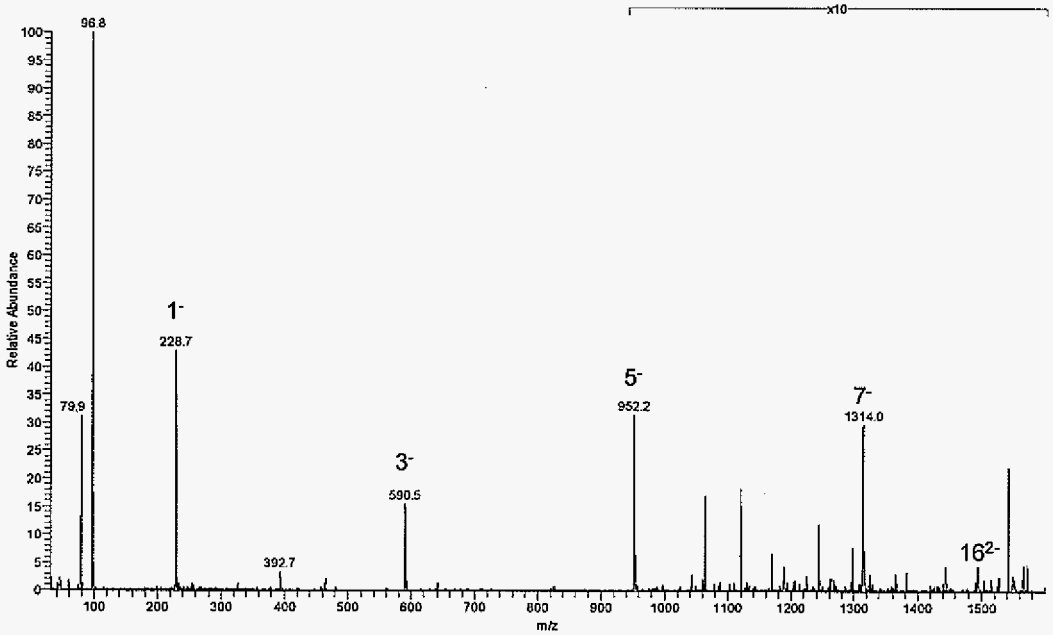
NL: 1.68E5
x10
Relative Abundance
m/z
96.8
1-
228.7
79.9
3-
590.5
392.7
5-
952.2
7-
1314.0
16 2-

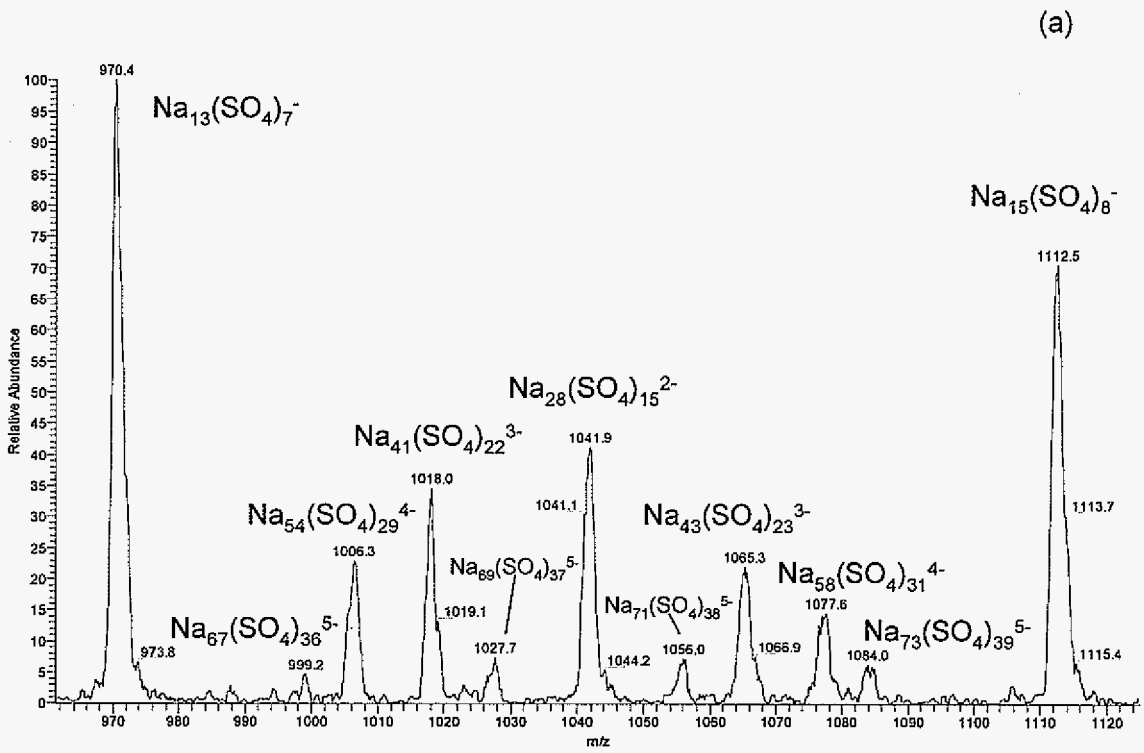

Figure 2. (a) Mass spectrum showing the m/z 965 – 1120 region of a 1 mM $NaSO_4$ solution in 50/50 H_2O/MeOH obtained on the TSQ-7000 instrument. Mass spectra showing the (b) m/z 965-1120 and (c) m/z 1250-1400 regions of a 1 mM $NaSO_4$ solution in 50/50 H_2O/MeOH obtained on the Agilent instrument. The numbers above some peaks represent the number of Na^+ cations present, while the superscript denotes the charge state. Peak assignments are based on calculated mass to charge.

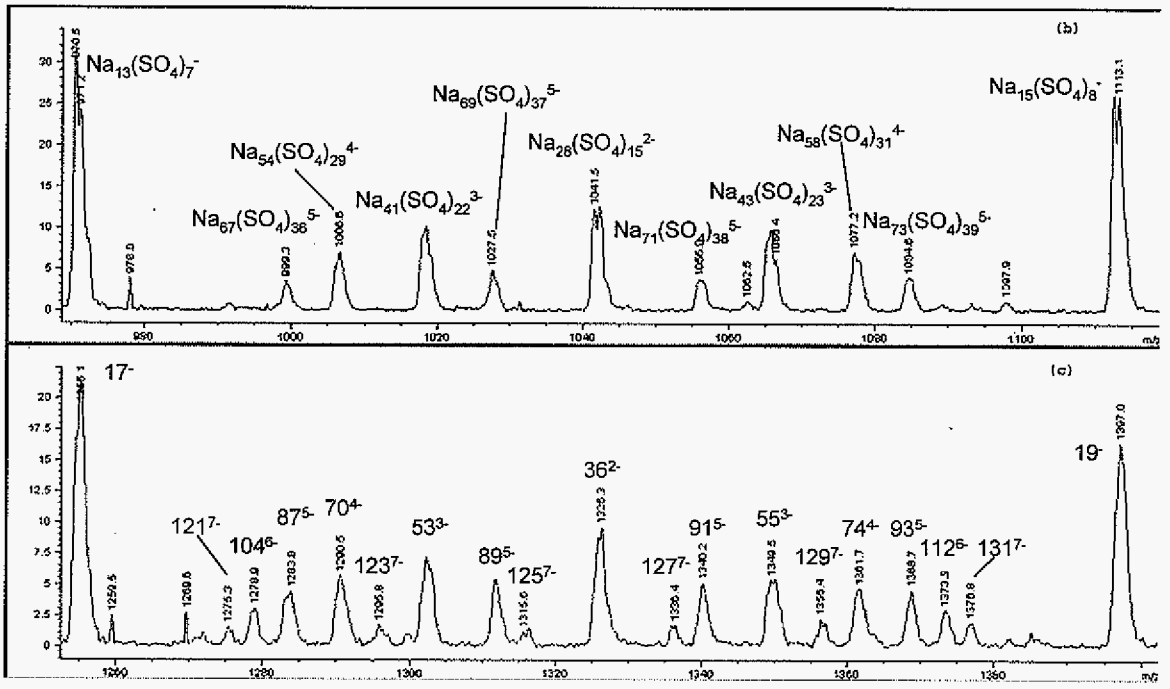
(b)
$Na_{13}(SO_4)_7^-$
$Na_{69}(SO_4)_{37}^{5-}$
$Na_{15}(SO_4)_8^-$
$Na_{54}(SO_4)_{29}^{4-}$
$Na_{26}(SO_4)_{15}^{2-}$
$Na_{58}(SO_4)_{31}^{4-}$
$Na_{43}(SO_4)_{23}^{3-}$
$Na_{67}(SO_4)_{36}^{5-}$
$Na_{41}(SO_4)_{22}^{3-}$
$Na_{71}(SO_4)_{38}^{5-}$
$Na_{73}(SO_4)_{39}^{5-}$
(c)
17^-
19^-
36^{2-}
121^{7-}
104^{6-}
87^{5-}
70^{4-}
53^{3-}
123^{7-}
89^{5-}
125^{7-}
127^{7-}
91^{5-}
55^{3-}
129^{7-}
74^{4-}
93^{5-}
112^{6-}
131^{7-}

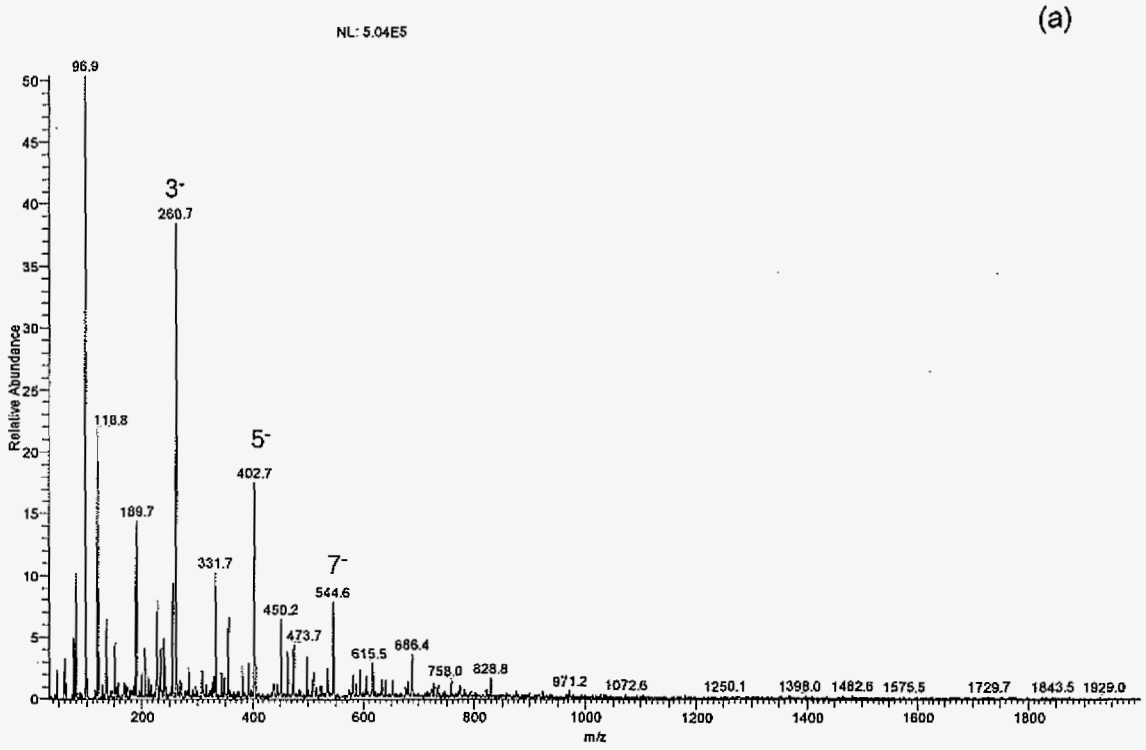

Figure 3. Effects of changing capillary and tube lens voltage on a 1 mM $NaSO_4$ solution in 50/50 H_2O/MeOH. The numbers above some peaks represent the number of Na^+ cations present, while the superscript denotes the charge state. The mass spectra capillary voltages are (a) 50, (b) 137 and (c) 150 V. The mass spectra tube lens voltages are (d) 5, (e) 60 and (f) 100 V. The intensity listed at the top of the figure corresponds to the most intense peak in the mass spectrum.

(b)

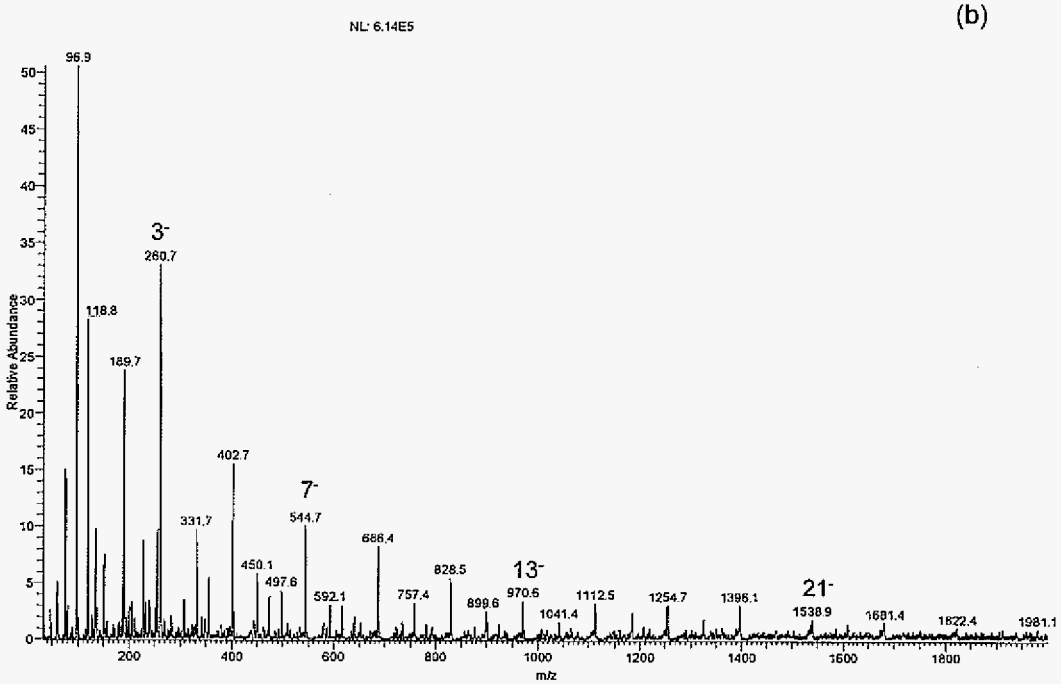
NL: 6.14E5
Relative Abundance
m/z
96.9
3-
260.7
118.8
189.7
402.7
7-
544.7
331.7
686.4
450.1
497.6
828.5
13-
970.6
592.1
757.4
899.6
1041.4
1112.5
1254.7
1396.1
21-
1538.9
1681.4
1822.4
1981.1

(c)

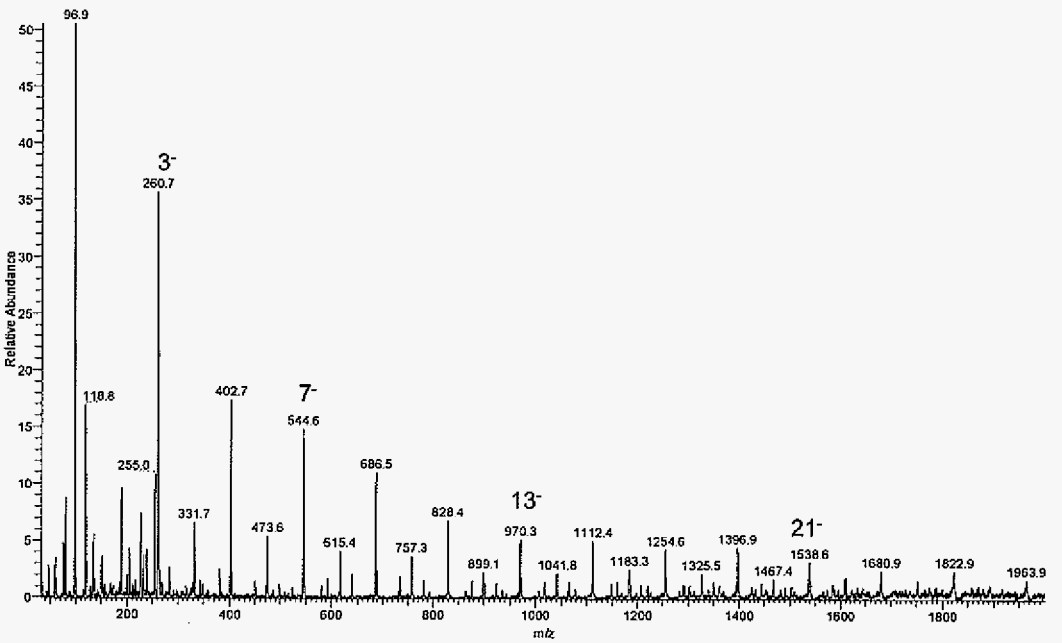
NL: 4.70E5
Relative Abundance
m/z
96.9
3-
260.7
118.8
255.0
402.7
7-
544.6
331.7
473.6
686.5
515.4
828.4
13-
757.3
970.3
899.1
1041.8
1112.4
1183.3
1254.6
1325.5
1396.9
21-
1467.4
1538.6
1680.9
1822.9
1963.9

(d)

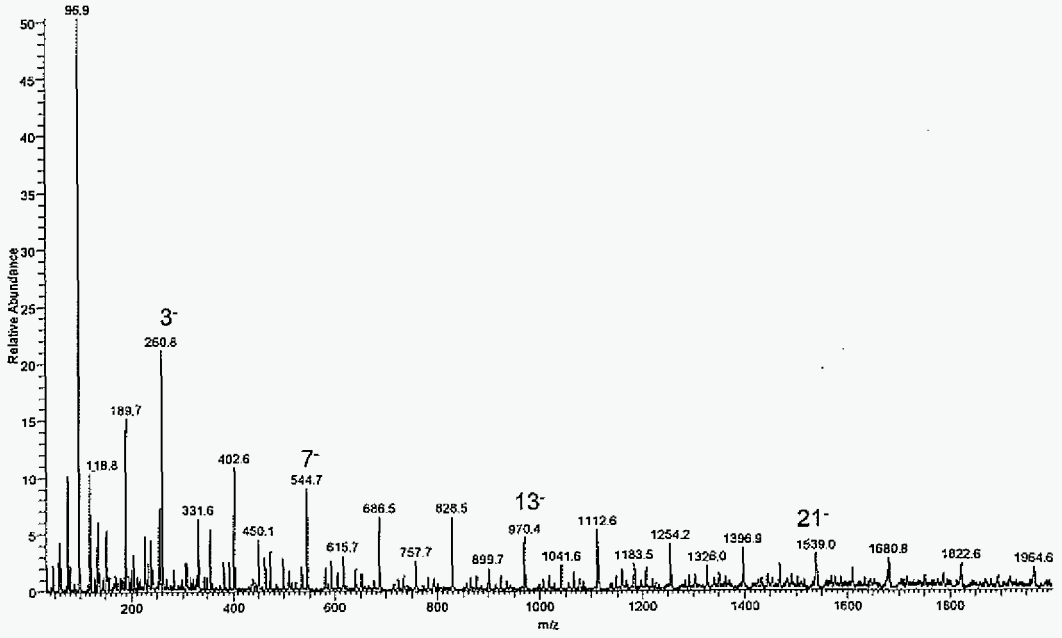
NL: 5.24E5
Relative Abundance
m/z
96.9
260.6
189.7
118.8
402.6
544.7
331.6
450.1
615.7
686.5
757.7
828.5
899.7
970.4
1041.6
1112.6
1183.5
1254.2
1326.0
1396.9
1539.0
1680.8
1822.6
1964.6
3-
7-
13-
21-

(e)

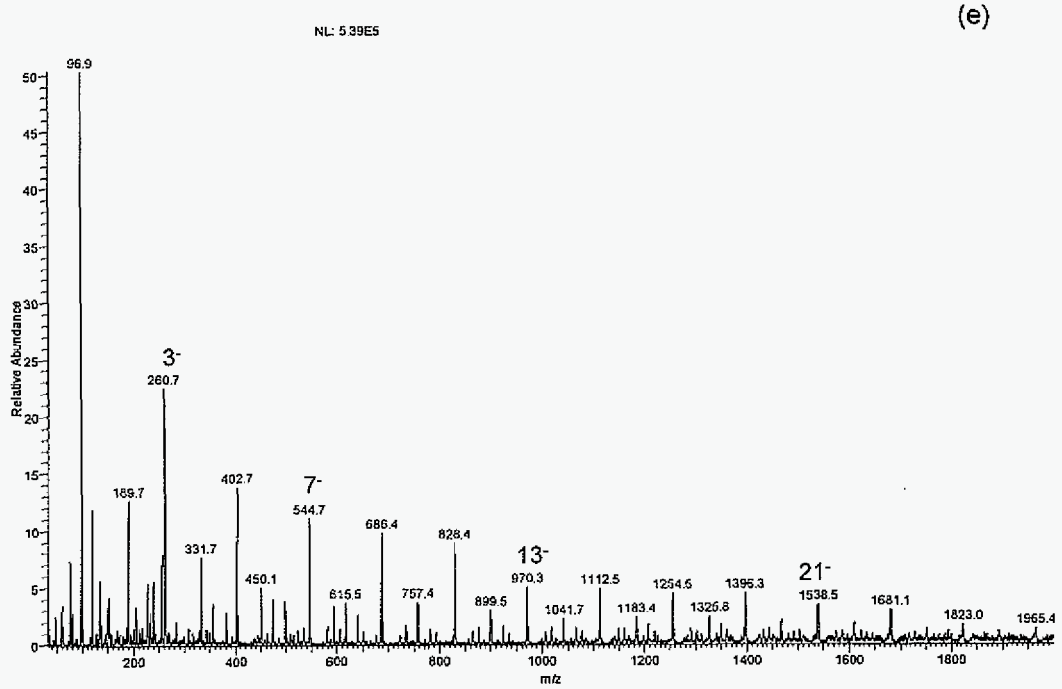
NL: 5.39E5
Relative Abundance
m/z
96.9
260.7
189.7
402.7
544.7
331.7
450.1
615.5
686.4
757.4
828.4
899.5
970.3
1041.7
1112.5
1183.4
1254.5
1326.8
1395.3
1538.5
1681.1
1823.0
1965.4
3-
7-
13-
21-

(f)

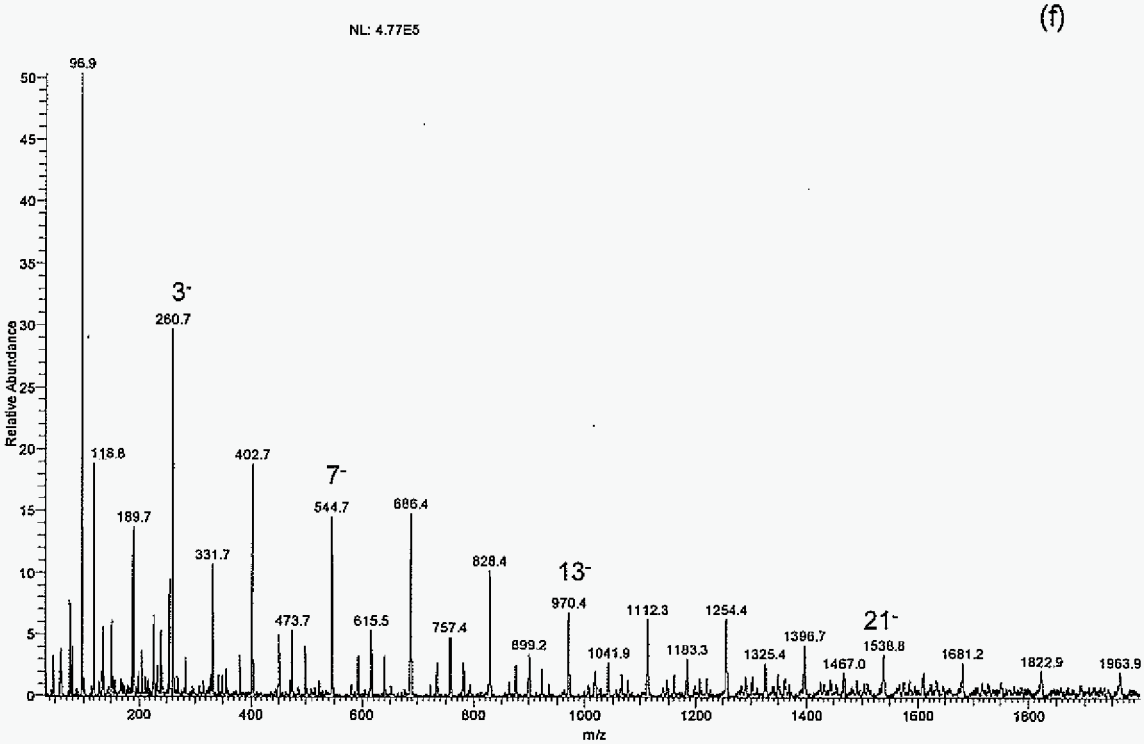
NL: 4.77E5
Relative Abundance
m/z
96.9
118.8
189.7
260.7
3-
331.7
402.7
473.7
544.7
7-
615.5
686.4
757.4
828.4
899.2
970.4
13-
1041.9
1112.3
1183.3
1254.4
1325.4
1396.7
1467.0
1538.8
21-
1681.2
1822.9
1963.9

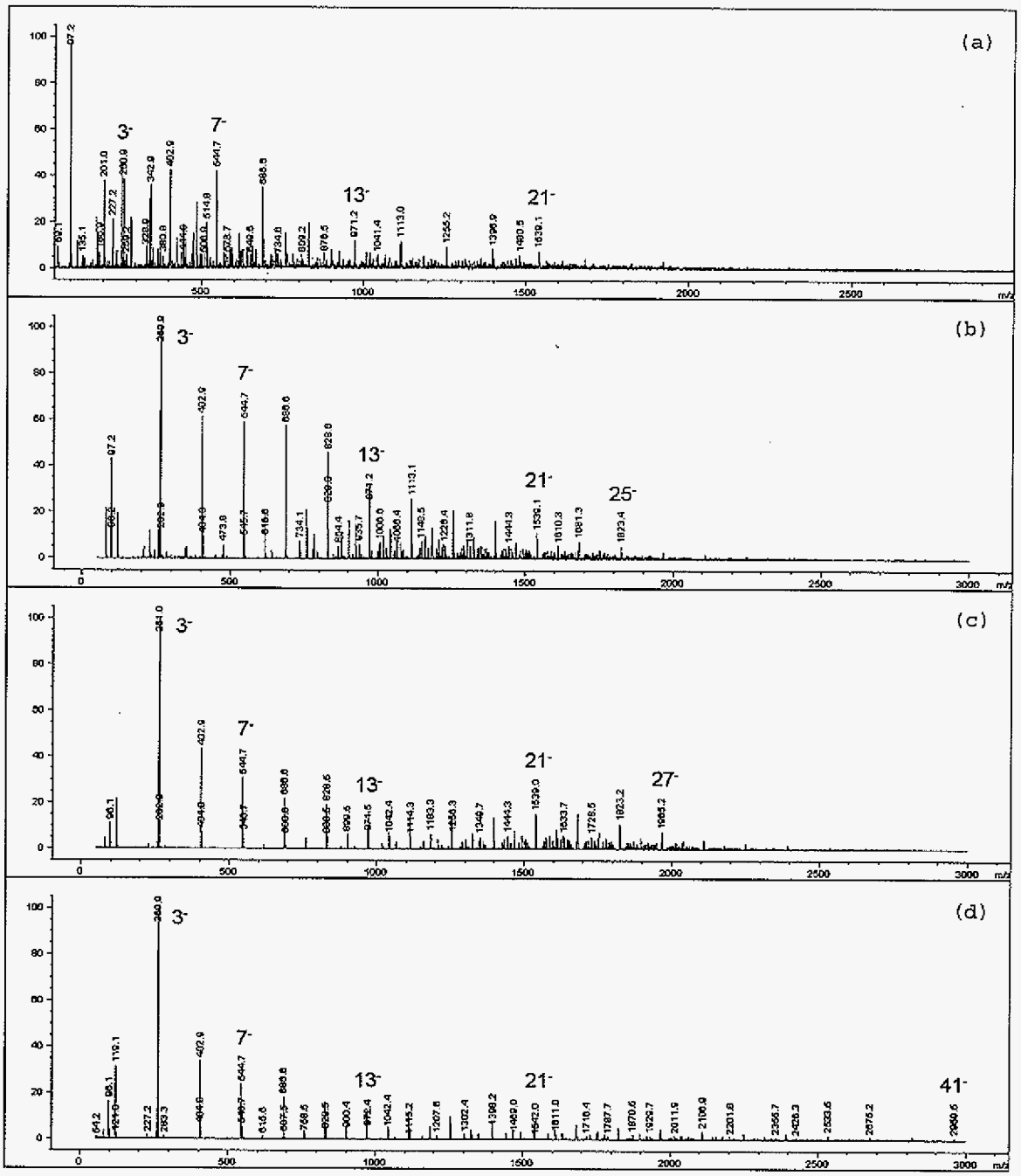

Figure 4. Mass spectra of a 1 mM $NaSO_4$ solution, 50/50 H_2O/MeOH, obtained with an Agilent single quadrupole instrument at fragmentor voltages of (a) 50, (b) 150, (c) 250 and (d) 400 V. .

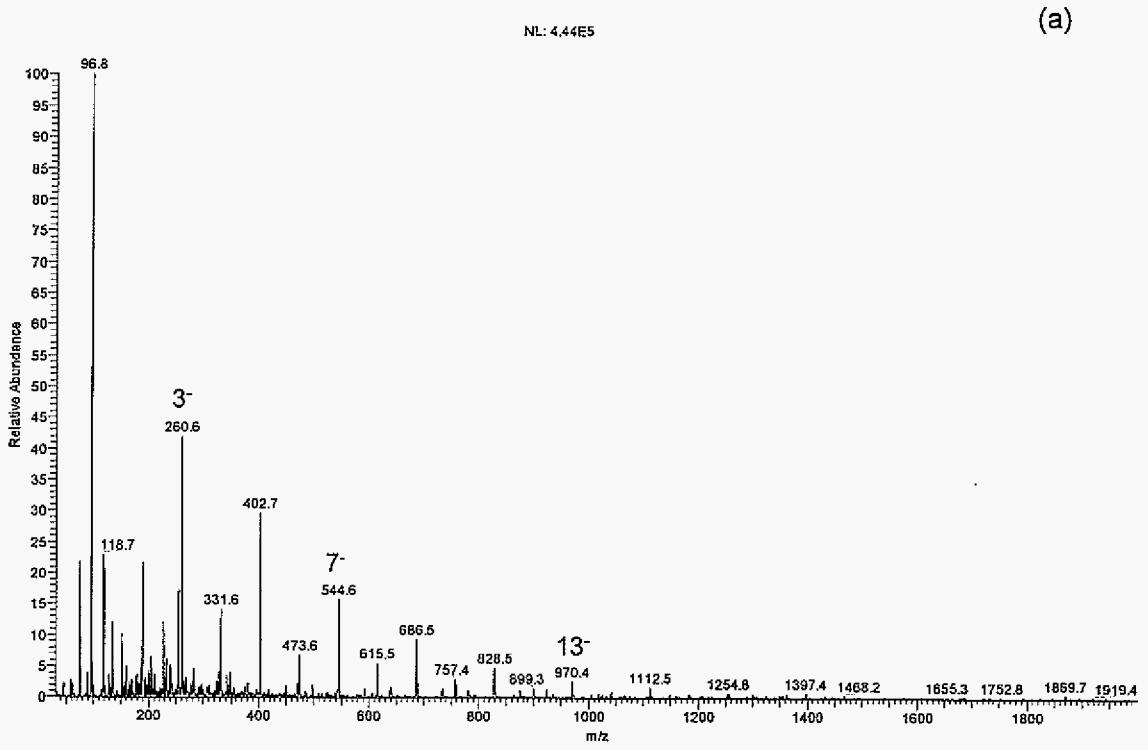

Figure 5. Mass spectra of a 1mM $NaSO_4$ solution in (a) 50/50 H_2O/MeOH, (b) 75/25 H_2O/MeOH, (c) 25/75 H_2O/MeOH, (d) 1/99 H_2O/MeOH and (e) 50/50 H_2O/IPA. The numbers above some peaks represent the number of Na^+ cations present, while the superscript denotes the charge state. The intensity listed at the top of the figure corresponds to the most intense peak in the mass spectrum.

(b)

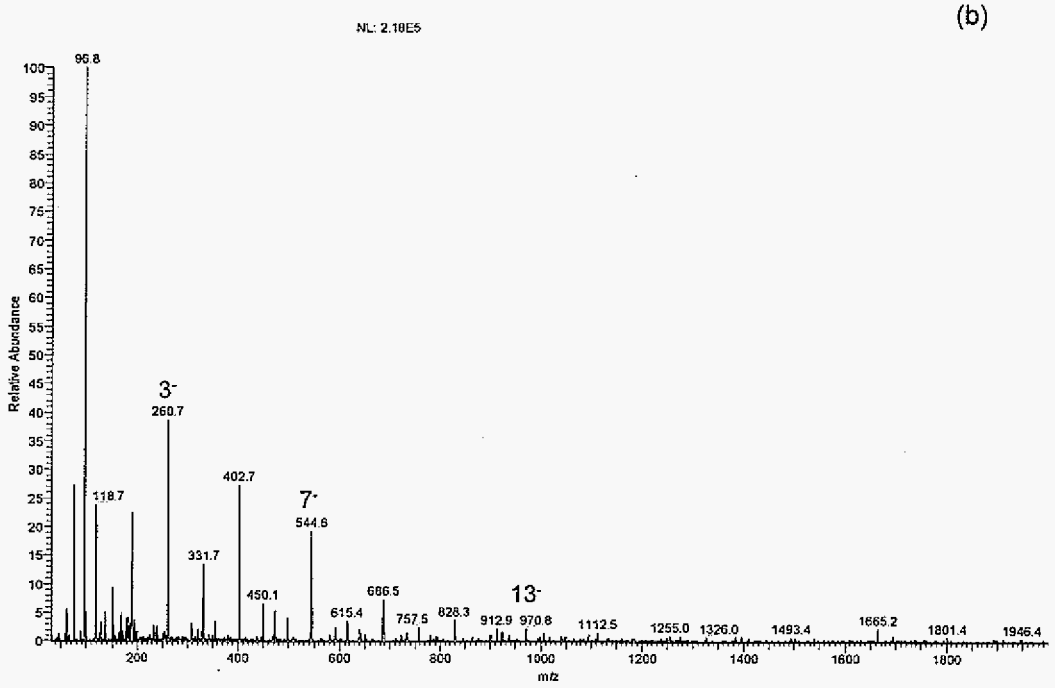
NL: 2.18E5
Relative Abundance
m/z
96.8
260.7
3-
118.7
331.7
402.7
450.1
544.6
7-
615.4
686.5
757.5
828.3
912.9
970.8
13-
1112.5
1255.0
1326.0
1493.4
1665.2
1801.4
1946.4

(c)

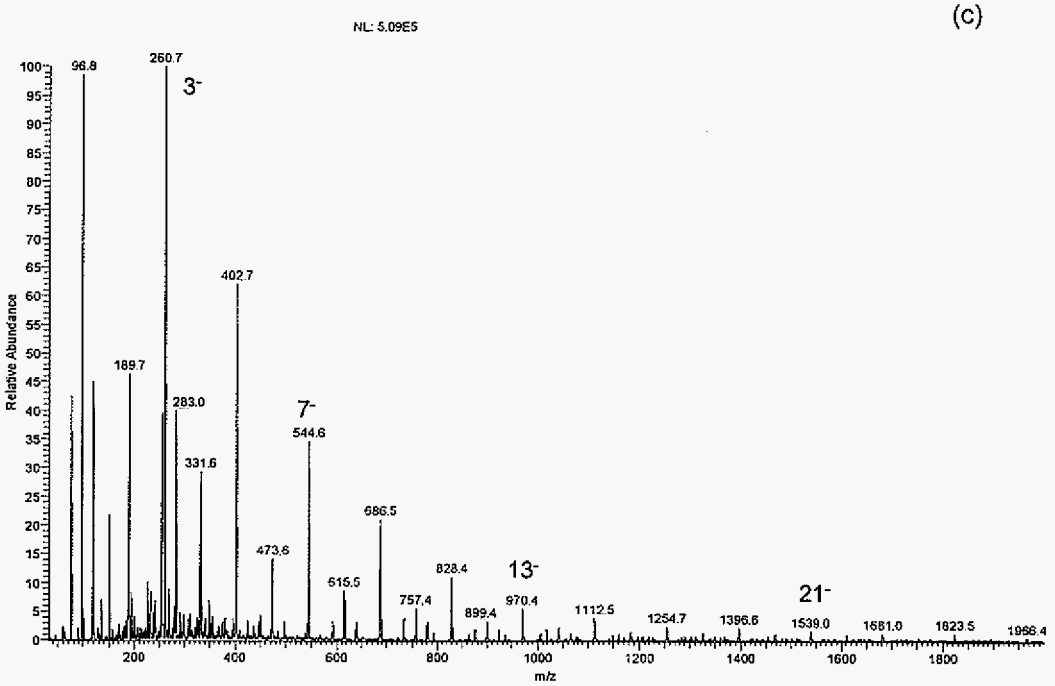
NL: 5.09E5
Relative Abundance
m/z
96.8
260.7
3-
189.7
283.0
331.6
402.7
473.6
544.6
7-
615.5
686.5
757.4
828.4
899.4
970.4
13-
1112.5
1254.7
1396.6
1539.0
21-
1681.0
1823.5
1966.4

(d)

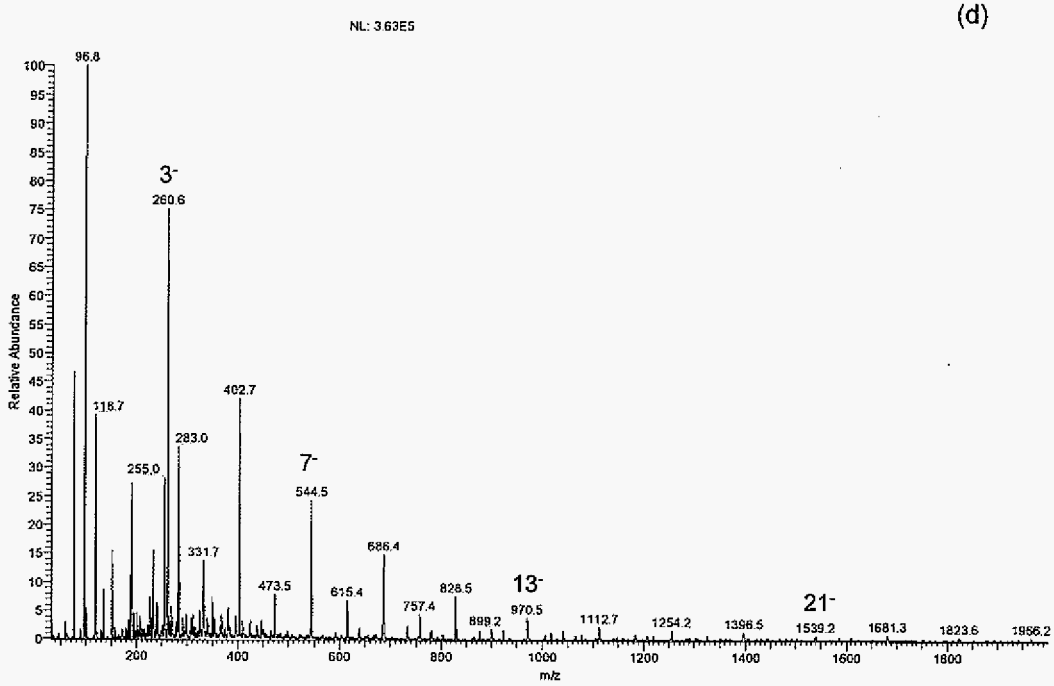
NL: 3.63E5
Relative Abundance
m/z
96.8
3-
260.6
118.7
283.0
255.0
402.7
7-
544.5
331.7
473.5
615.4
686.4
757.4
828.5
13-
970.5
899.2
1112.7
1254.2
1396.5
21-
1539.2
1681.3
1823.6
1956.2

(e)

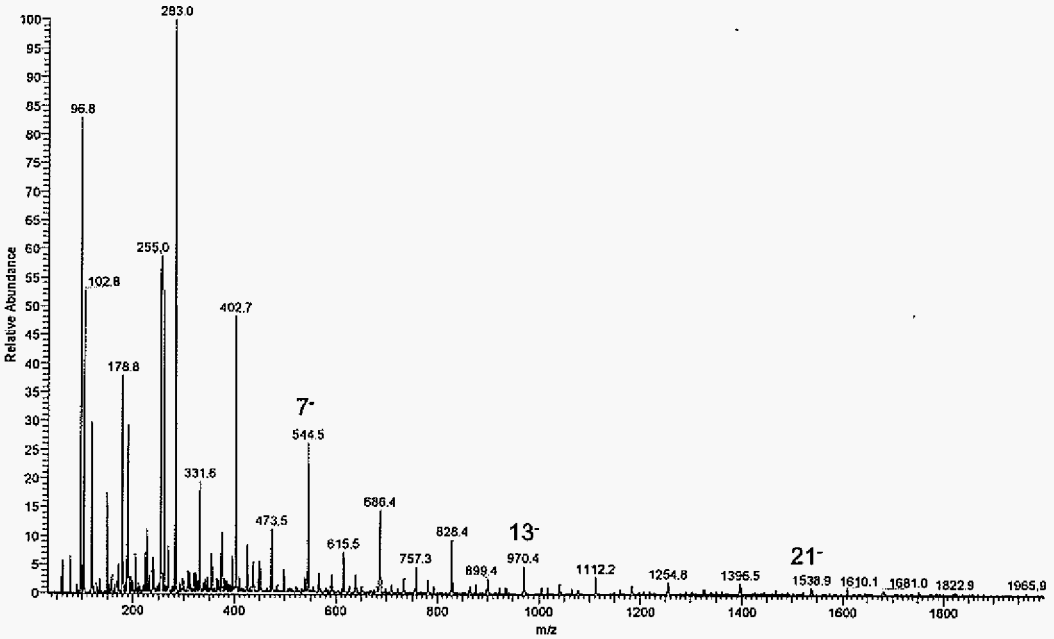
NL: 5.83E5
Relative Abundance
m/z
283.0
96.8
255.0
102.8
402.7
178.8
7-
544.5
331.6
473.5
686.4
615.5
828.4
13-
757.3
899.4
970.4
1112.2
1254.8
1396.5
21-
1538.9
1610.1
1681.0
1822.9
1965.9

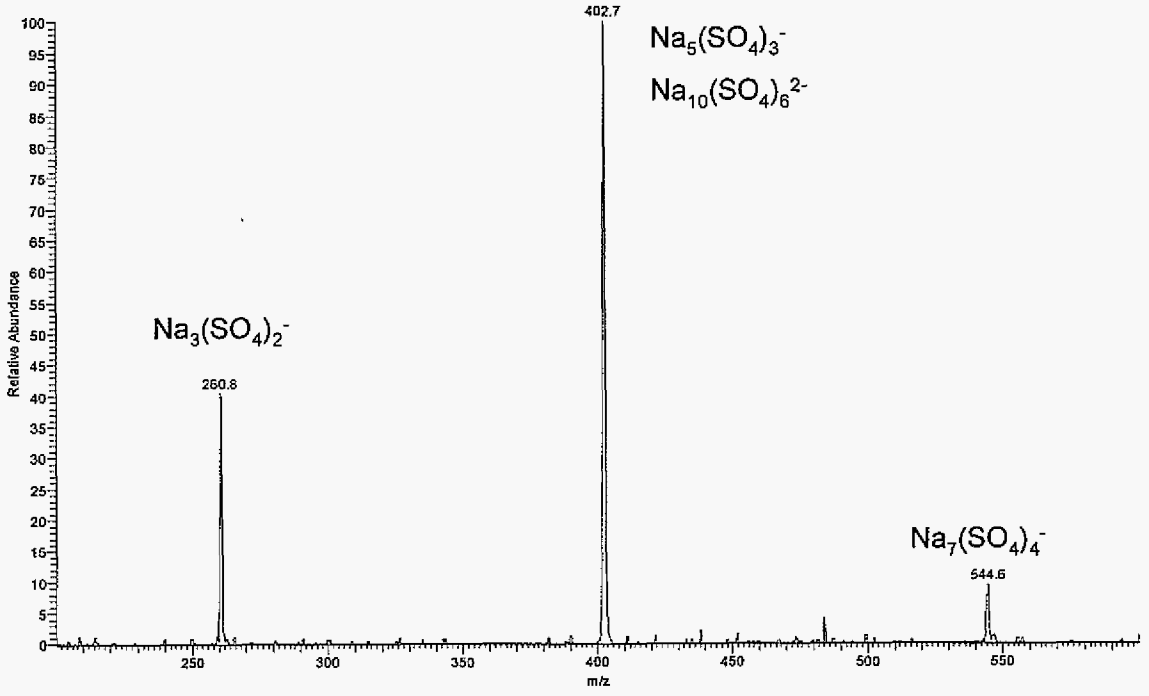

Figure 6. CID product spectrum for the $Na_5(SO_4)_3^-$ and $Na_{10}(SO_4)_6^{2-}$ ions at m/z 402.7. The collision energy and collision gas pressure were 25 eV and 0.20 Pa. The resolution of the first quadrupole was reduced to transmit the ^{32}S and ^{34}S isotopes. The inset shows the isotope distribution for $Na_7(SO_4)_4^-$, m/z 544.6. Except for $Na_3(SO_4)_2^-$ and $Na_7(SO_4)_4^-$, other unlabeled apparent peaks are just noise spikes.

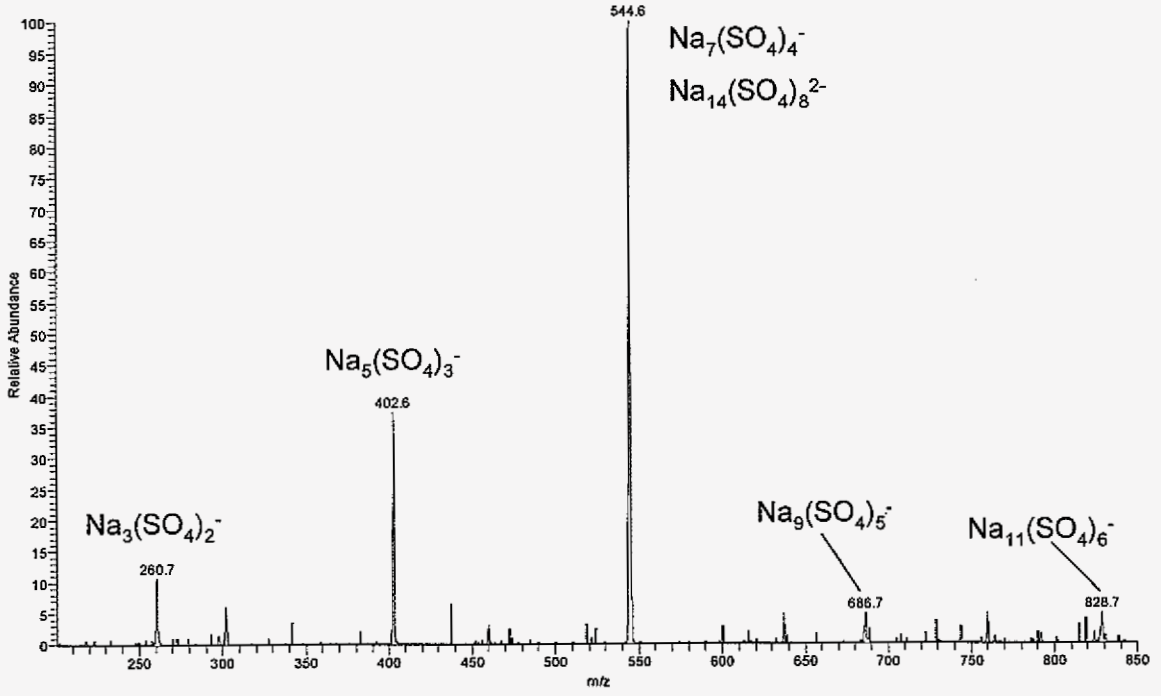

Figure 7. CID product spectrum for the $Na_7(SO_4)_4^-$ and $Na_{14}(SO_4)_8^{2-}$ ions at m/z 544.6. The collision energy and collision gas pressure were 29 eV and 0.21 Pa. Unlabeled peaks are just noise spikes.

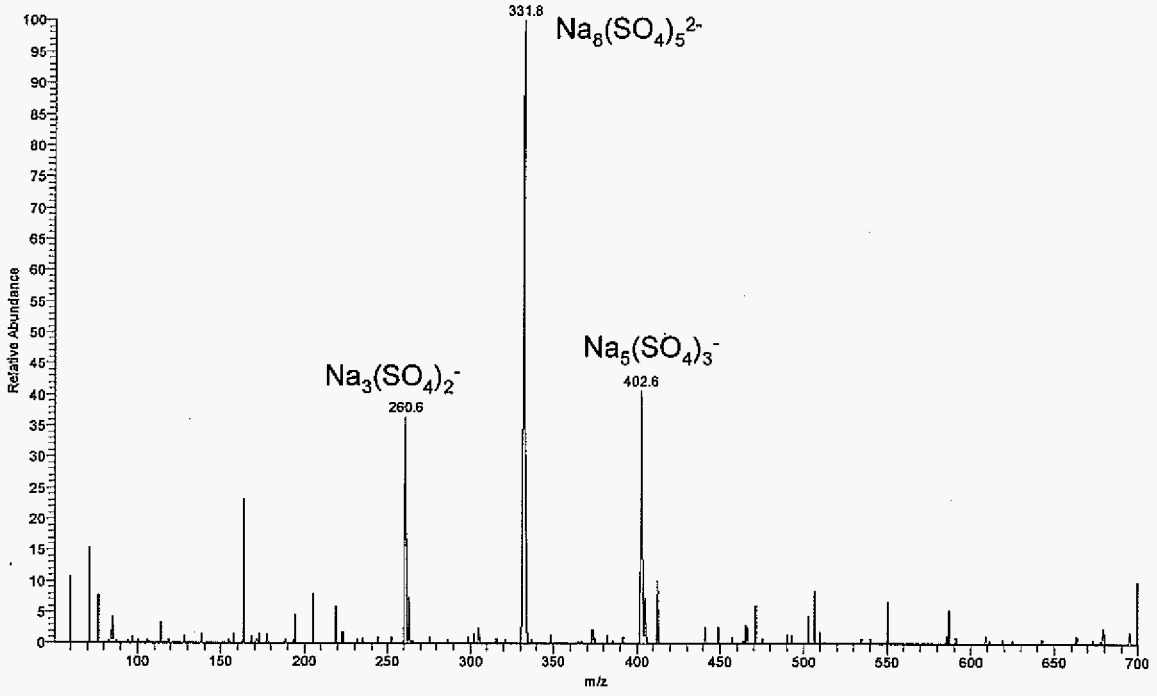

Figure 8. CID product spectrum for the $Na_8(SO_4)_5^{2-}$ ion at m/z 331.8. The collision energy and collision gas pressure were 20 eV and 0.13 Pa. Unlabeled peaks are just noise spikes.

CHAPTER 4. NEGATIVE ION MODE ELECTROSPRAY IONIZATION MASS SPECTROMETRY OF MIXED METAL CLUSTER IONS

A paper to be submitted to the *Journal of the American Society for Mass Spectrometry*

N. B. Lentz, T. C. Hutcheson, and R. S. Houk

Abstract

Solutions comprising two metal chloride compounds were analyzed in negative ion mode by electrospray ionization mass spectrometry. Various metal clusters, $M_xCl_z^-$ (M = Ce^{3+}, Co^{2+}, Zn^{2+} or Ho^{3+}) or $Ce_xM_yCl_z^-$ (M = Co^{2+}, Zn^{2+}, or Ho^{3+}) were present in the mass spectra. No multiply charged ions were observed. Lower heated capillary temperatures favored mixed metal cluster ions. The abundances of the mixed metal clusters increased when a 50/50 isopropyl alcohol/water solution was used compared to a 96/4 isopropyl/water solution. Collision induced dissociation of cerium/cobalt mixed metal clusters revealed that the Co^{2+} ion generally leaves as part of a neutral fragment, and the negatively charged fragment retains the Ce^{3+} ion.

Introduction

Cluster ions have many interesting applications with new and novel applications constantly being developed. Gas phase clusters are generally created by the laser ablation of solid materials. After the discovery of the C_{60} buckminsterfullerene cluster, synthesizing clusters via laser ablation has received great interest [1]. This method requires the sample to be a solid, and the plumes from two ablated solids have to be mixed. A soluble sample has to

have the solvent evaporated, or go through a crystallization process which can present difficulties. This process is also matrix dependent because laser coupling efficiency depends on the type of matrix [2].

Electrospray ionization mass spectrometry (ESI-MS) [3-6] has established itself as the premier analytical technique for polymers, biological systems, organic, and inorganic chemistry [7-10]. Since ESI is a soft ionization technique, it has the ability to transfer or even create gas phase ions that are not normally seen in solution. There is also minimal fragmentation which allows for the transfer of intact ions to the mass spectrometer.

There has been an increasing interest in cluster ion research using ESI-MS over the last 10-15 years. The soft ionization of ESI allows for unique cluster ions to be created in the source region. ESI-MS has been used to study alkali metal [11, 12], amino acid [13, 14], protein/drug [15, 16], organic [9, 17], and inorganic clusters [9, 18]. Not only have cluster ions been studied for their unique properties, but ions like $Cs_xI_y^+$ have also been used to calibrate the m/z scale in ESI-MS [19, 20]. Cluster ions have also provided valuable information regarding the ionization process of ESI [21-23].

March and coworkers have systematically examined how source conditions, solvents, and mass spectrometer interfaces affect the cluster ion distributions seen in mass spectra [24, 25]. They found that the cluster ion distributions varied greatly under different source conditions [24]. In their work, they focused on clusters with metal ions from only one element.

The goal of this paper is to explore the properties of mixed metal clusters and how various solvents, heated capillary temperatures, and interface conditions affect the cluster ions seen in the mass spectra. The mixed metal clusters were made by adding various metal

ions to solutions of Ce^{3+} ions. Metal ions with both 2+ and 3+ charge states were examined. Chloride anions were used to coordinate the metal ions. Only a stoichiometric amount of chloride was present. No extra chloride was added to the solutions.

Experimental

Samples and Sample Preparation

The chloride salts and solvents were purchased from Sigma (St. Louis, MO) and used without further purification. The samples were dissolved in isopropyl alcohol (IPA)/H_2O (Millipore 18.2 MΩ, Bedford, MA). The water was needed to dissolve the metal chloride salts. The percent composition of each solvent was altered during some experiments, but a 96/4 IPA/H_2O solution was used unless otherwise noted. The concentration of the chloride salts was 1 mM.

ESI-MS

A triple quadrupole (QoQ) mass spectrometer (TSQ-7000, Thermo Finnigan, San Jose, CA) with an on-axis ESI source and a heated capillary interface, was used for the experiments. Samples were continuously infused at 5 μL/min with a syringe pump (Model 22, Harvard Apparatus, Southnatic, MA). Nitrogen (60 PSI) and high purity argon were used as the nebulizing gas and collision gas, respectively. The electrospray needle voltage was set to -2.5 kV and the heated capillary was kept at 200 °C, -136 V, for most experiments. The voltages on the ring electrode (tube lens) and first octopole were -85 and +3.0 V, respectively. The skimmer is at ground on this instrument. The conditions were adjusted to obtain a stable signal with maximum intensity over the mass range investigated. The scan

range was 50 to 2000 m/z. Data were collected for 2 to 5 minutes at 2 seconds per scan. For CID studies, the collision pressure was 1.0-1.6 mtorr, and the collision voltage was 25 eV (lab frame). The resolution of the first quadrupole was reduced to increase ion transmission into the collision cell for CID experiments. Nevertheless, product ions do not show all Ce and Cl isotope peaks corresponding to natural abundance.

A single quadrupole MS (6130A, Agilent Technologies, Santa Clara, CA) with an orthogonal ESI source was also used for some experiments as noted. This instrument employs a heated nitrogen counter-current gas flow, a metal capped glass transfer capillary, and a skimmer with an adjustable fragmentor voltage. The electrospray needle was set to -3.5 kV and the drying gas temperature was set to 250 °C. Nitrogen was used for the nebulizing gas (35 psi) and for the drying gas. The scan range was 50 to 3000 m/z. The 1 mM samples were introduced via a high pressure liquid chromatography (HPLC) system (model 12000, Agilent Technologies, Santa Clara, CA) at a flow rate of 50 µl/min. No column was used for any of the experiments. The amount of sample injected was 100 µL, which allowed for 2 minutes of data to be averaged for each mass spectrum.

Results and Discussion

Cerium Chloride Clusters

The clustering capability of cerium ions with chloride was evaluated. Figure 1 shows the mass spectrum of a 5 mM $CeCl_3$ solution in 96/4 IPA/H_2O. Cerium chloride clusters are present throughout the whole mass range investigated. As m/z increases, the cluster ions decay gradually with no magic number clusters present. Only singly charged clusters are present in the mass spectrum. The identity of the cluster ions was confirmed by comparing

the calculated and experimental isotope distribution. The inset to Figure 1 shows the isotope distribution for the $Ce_3Cl_{10}^-$ ion. The black bars show the calculated isotope distribution. The experimental and calculated isotope distributions show excellent agreement which allows for accurate ion identification. $Ce_7Cl_{22}^-$ was the largest cerium chloride cluster ion present in the mass spectrum.

At each cerium chloride cluster, there are other cluster ions present at m/z above and below the cluster ion. These ions represent the substitution of a chloride with NO_3^- or other background gas molecules/ions present in the interface region. As the solvent evaporates during the ESI process, the background molecules can compete with chloride to bind to the cerium ions present. The larger cerium chloride cluster ions have more substitutions from the background molecules. This is probably because there are more chloride ions present, and therefore a greater probability for ligand substitution.

For example, there are two oxo chloro cluster ions below $Ce_3Cl_{10}^-$, m/z 773.0. The ions at m/z 718.9 and m/z 754.2 are $Ce_3OCl_8^-$ and $Ce_3OCl_9^-$, respectively. Oxygen is present is the 2- charge state in $Ce_3Cl_8^-$, and present in the 1- charge state in $Ce_3OCl_9^-$.

Mixed Metal Clusters: Ce^{3+} and Co^{2+}

Two metal chloride salts were added to a solution to see if cluster ions with each metal ion could be observed. Three different metal chloride salts (Co^{2+}, Ho^{3+}, and Zn^{2+}) were added along with cerium chloride to make various solutions, each with 2 metal ions. Figure 2 shows the mass spectrum of a 1 mM $CeCl_3$ and 1 mM $CoCl_2$ solution in 96/4 IPA/H_2O. Five cluster ion distributions are present in the mass spectrum. The first two distributions correspond to cerium chloride and cobalt chloride cluster ions, starting with

$CeCl_4^-$ and $CoCl_3^-$. If only a cobalt or cerium solution was sprayed, these would be the expected clusters. These single metal cluster distributions are the most intense ions in the spectrum.

The next two cluster ion patterns correspond to mixed metal clusters. In the third distribution, one cerium ion replaces a cobalt ion, beginning with $CeCoCl_6^-$. As the cluster ions get larger, the number of cobalt and chloride ions increase, but only one cerium ion is present in the clusters. Only a few clusters of this type are present in the mass spectrum. The largest cluster ion present in Figure 2 is $CeCo_3Cl_{10}^-$, m/z 670.1.

The fourth distribution is similar to the third, but this time only one cobalt ion and multiple cerium ions are present in each cluster. The first ion in this distribution is $CeCoCl_6^-$, which is the starting ion as in the previous distribution. The largest cluster ion present is m/z 1397, which is $Ce_5CoCl_{18}^-$. This cluster pattern is more prevalent than the pattern with multiple cobalt ions and only one cerium ion. This indicates that Ce^{3+} has a stronger interaction with chloride than Co^{2+}.

The fifth cluster distribution in Figure 2 has two or more cerium and two or more cobalt ions present in each cluster ion. This cluster distribution starts at m/z 786.1, $Ce_2Co_2Cl_{11}^-$, and stops at m/z 1408, $Ce_4Co_3Cl_{19}^-$. The cluster ions in this distribution are low in intensity, but are intense enough to be accurately identified. The isotope patterns are also consistent with these assignments.

Mixed Metal Clusters: Ce^{3+} and Zn^{2+}

Cerium and zinc did not work well for mixed metal clusters. Only $CeZnCl_6^-$, m/z 417.5, and $Ce_2ZnCl_9^-$, m/z 664.4 were present in the mass spectrum when a 1 mM $CeCl_3$, 0.5

mM $ZnCl_2$ solution was sprayed (data not shown). These two ions were very low in intensity. $ZnCl_3^-$ accounted for most of the Zn^{2+} ions present in the mass spectrum (data not shown). Further studies on cerium and zinc mixed metal clusters were not conducted.

Mixed Metal Clusters: Ce^{3+} and Ho^{3+}

The clustering properties of a 1mM $CeCl_3$ and $HoCl_3$ solution were examined. Like cerium, holmium is also a 3+ lanthanide ion and so the two metals should easily make mixed metal clusters. Figure 3 shows the mass spectrum with both cerium and holmium ions present in solution. This spectrum was taken with the Agilent single quadrupole instrument. The mixed metal clusters are of equal or higher intensity than the $Ce_xCl_y^-$ and $Ho_xCl_y^-$ clusters of similar m/z. This shows that cations of similar size, Table 1, exhibit a higher degree of mixed metal cluster ion formation. It is likely that the similarly sized metal ions allow for less strain on the overall structure. The similarly sized cations will also have similar charge densities. This allows the chloride anions to evenly distribute within the ion.

The cerium/holmium clusters have the same distributions as seen with the cerium/cobalt clusters. The largest mixed metal ion present in Figure 3 is present at m/z 1367, $Ho_4CeCl_{16}^-$. This is the largest cluster in the pattern where there are multiple holmium ions, and one cerium ion present in the cluster. Cluster ions are also present in which there are more than one cerium and more than one holmium ion present. For example, the ions of $HoCe_3Cl_{13}^-$ (m/z 1045) and $Ho_2Ce_2Cl_{13}^-$ (m/z 1070) are present in Figure 3.

Effects of Heated Capillary Temperature

The heated capillary temperature was systematically changed for a 1 mM cerium/cobalt chloride solution to determine its influence on mixed metal cluster ion intensity and distribution. In Figures 4a-e, the heated capillary temperature was decreased in 50 or 25 °C increments from 250 to 125 °C to see if the heated capillary temperature has any effect on the mixed metal clusters. A heated capillary temperature of 250 °C (Figure 4a) produced the least intense mass spectrum. Perhaps the ions fragment if the capillary is too hot. The intensity is more than doubled when the heated capillary temperature is reduced from 250 to 200 °C (Figure 4b). The mixed metal cluster peak at m/z 410.7 showed an increase from 12 abundance units to 20 abundance units when the heated capillary temperature was reduced to 200 °C (see Figures 3a and 3b).

This trend is continued in Figure 4c at a heated capillary temperature of 175 °C. On the vertical scale, the mixed metal cluster ion intensity has increased approximately 10 more abundance units, and the intensity has remained the same. The peaks between m/z 400 and 800 increased in intensity more than the other peaks in the mass spectrum.

At 150 °C, Figure 4d, there is another 10 abundance unit increase in the m/z 410.7 peak. There was no significant change in the mass spectrum when the heated capillary temperature was reduced from 150 to 125 °C (Figure 4e). In Figures 4d and 4e, the higher m/z clusters, both single and mixed metal, are no longer seen in the mass spectra. It is likely that the interface conditions have changed and favor the formation of the lower m/z clusters instead of the larger m/z clusters. The cerium chloride clusters also decrease in intensity in Figures 4d and 4e. The lower heated capillary temperatures enhance the formation of the mixed metal clusters. The cerium chloride cluster signal decreases because more of the

cerium ions are present in the mixed metal clusters. Even at the low heated capillary temperatures, no doubly charged clusters were present in the mass spectra.

As the heated capillary temperature was decreased, the amount of free Cl^- present in the mass spectra also decreased. At a heated capillary temperature of 250 °C, Figure 4a, the abundance of the free chloride is 17 abundance units. At a heated capillary temperature of 125 °C, Figure 4e, the abundance of the free chloride drops to 10 abundance units. In Figures 4a-4e, the free chloride signal shows a consistent drop. If the free chloride is an indication of the cluster ion formation, the lower heated capillary temperatures generate more cluster ions, thus using up more Cl^-. Since the single metal cluster signals also decreased, more mixed metal clusters are present at lower heated capillary temperatures.

Solvent Effects

Different ratios of IPA and water were examined to determine the role that the solvent plays in mixed metal cluster ion formation. Methanol and other solvents were not used because they did not generate an appreciable amount of these ions. Figures 5a-c show the mass spectra of a 1 mM cerium chloride and cobalt chloride solution in 96/4, 50/50 and 25/75 IPA/H_2O, respectively. The 96/4 IPA/H_2O solution produces the most intense mass spectrum with twice the intensity of the other two spectra. Figures 5b and 5c had similar signal intensities with 5c (25/75 IPA/H_2O) being slightly more intense.

In Figures 5b and 5c, the mixed metal clusters are higher in abundance relative to the largest peak in the mass spectrum. The additional water allows for more mixed metal clusters to be formed. This could contribute to the lower intensity of the most intense peak

which is a cobalt chloride cluster ion. The mixed metal clusters are similar in abundance in Figures 5b and 5c even though 25 percent more water is present in Figure 5c.

It is interesting to note the signal of the free chloride peaks. In Figures 4a-e, the mixed metal clusters increased in intensity as the free chloride decreased. In Figures 5a-c, both the free chloride and the mixed metal cluster peaks increased in intensity when a 50/50 IPA/H_2O solution was used. This shows that solvent conditions affect the droplet dynamics in the source region. It is also possible that the free chloride peak increased due to increased ionization efficiency with more water present in solution.

CID of Mixed Metal Clusters

CID studies were carried out to examine the mixed metal cluster fragmentation patterns. Figure 6 shows the CID mass spectrum of the mixed metal cluster ion at m/z 410.6, $CeCoCl_6^-$. The proposed CID fragmentation equation for Figure 6 is as follows:

$CeCoCl_6^- \rightarrow CeCl_4^- + \mathit{CoCl_2}$

The species in italics are the inferred neutral products. The only product ion present is $CeCl_4^-$ at m/z 281.6. Apparently, the rest of the parent ion left as the neutral fragment $CoCl_2$. The more highly charged Ce^{3+} keeps the extra chloride ion instead of Co^{2+}. It is also interesting to note that no Cl^- ions are seen in the CID spectrum. All of the chloride ions remain coordinated with either the Ce^{3+} or Co^{2+} ion.

Figure 7 shows the CID mass spectrum of $CeCo_2Cl_8^-$ at m/z 541.8. When this ion undergoes CID, three product ions are observed in the mass spectrum: $CeCoCl_6^-$, $CeCl_4^-$, and $CoCl_3^-$. The neutral fragments that correspond to these ions are $CoCl_2$, $2CoCl_2$, and

$CeCl_3/CoCl_2$, respectively. The proposed CID fragmentation equations for Figure 7 are as follows:

$CeCo_2Cl_8^- \rightarrow CeCoCl_6^- + CoCl_2$
$CeCo_2Cl_8^- \rightarrow CeCl_4^- + 2CoCl_2$
$CeCo_2Cl_8^- \rightarrow CoCl_3^- + CeCl_3 + CoCl_2$
(or $CeCoCl_5$)

Although the neutral products can only be inferred, the absence of a Cl^- product ion supports these neutral fragments. This is the smallest cluster that yields a product ion with only Co^{2+} present in the spectrum. It is likely that ions with only Co^{2+} will also be present with larger cluster ions due to their larger size and number of Co^{2+} ions present.

Conclusion

Mixed metal clusters were observed through ESI-MS. When "softer" source conditions were used, there was an increase in the intensity of the mixed metal cluster ions. This means that the mixed metal clusters are weakly associated and are subject to source fragmentation at normal operating conditions. Even when "softer" source conditions are used, the single metal chloride cluster distributions (e.g. $CeCl_4^-$...) were the most intense ions in the mass spectra.

The expected oxidation states (Cl^-, Ce^{3+}, Ho^{3+}, and Co^{2+}) were the only species seen in the mass spectra. If metal ions were reduced during negative ion mode ESI, the ions may reduce all the way to neutral ions and thus are not observed in the mass spectra. Metals with more than one stable oxidation state could be used to determine the extent of metal oxidation during the ESI process for mixed metal clusters.

It would be interesting to conduct computer modeling to ascertain the structure of the different mixed metal cluster ions. There are a few possible structures, and the CID data cannot distinguish one cluster from another because similar product ions would appear for all of the possible structures.

Acknowledgements

Ames Laboratory is operated by Iowa State University for the U.S. Department of Energy, contract no. W-7405-Eng-82. This work was supported by the Chemical and Biological Sciences Program, Office of Basic Energy Sciences, Division of Chemical Sciences. The authors thank L. Huang and Bayer Company for donating the TSQ-7000 triple quadrupole instrument and Agilent Technologies for the loan of their instrument.

References

1. Kroto, H. W.; Heath, J. R.; O'Brien, S. C.; Curl, R. F.; Smalley, R. E. C_{60}: Buckminsterfullerene. *Nature* **1985**, *318*, 162-163.
2. Günther, D.; Horn, I.; Hattendorf, B. Recent Trends and Developments in Laser Ablation-ICP-Mass Spectrometry. *Fresenius J. Anal. Chem.* **2000**, *368*, 4-14.
3. Dole, M.; Mack, L. L.; Hines, R. L.; Mobley, R. C.; Ferguson, L. D.; Alice, M. B. Molecular Beams of Macroions. *J. Chem. Phys.* **1968**, *49*, 2240-2249.
4. Yamashita, M.; Fenn, J. B. Electrospray Ion Source. Another Variation on the Free-Jet Theme. *J. Phys. Chem.* **1984**, *88*, 4451-4459.
5. Yamashita, M.; Fenn, J. B. Negative Ion Production with the Electrospray Ion Source. *J. Phys. Chem.* **1984**, *88*, 4671-4675.

6. Whitehouse, C. M.; Dreyer, R. N.; Yamashita, M; Fenn, J. B. Electrospray Interface for Liquid Chromatographs and Mass Spectrometers. *Anal. Chem.* **1985**, *57*, 675-679.

7. Smith, R. D.; Cheng, X.; Bruce, J. E.; Hofstadler, S. A.; Anderson, G. A. Trapping, Detection and Reaction of Very Large Single Molecular Ions by Mass Spectrometry. *Nature* **1994**, *369*, 137-139.

8. Cole, R. B. *Electrospray Ionization Mass Spectrometry* John Wiley & Sons: New York, NY, 1997; pp 385-419.

9. Henderson, W.; McIndoe, J. S. *Mass Spectrometry of Inorganic and Organometallic Compounds* John Wiley & Sons: England, 2005.

10. Dyson, P. J.; Hearley, A. K.; Johnson, B. F. G.; McIndoe, J. S.; Langridge-Smith, P. R. R.; Whyte, C. Combining Energy-Dependent Electrospray Ionisation with Tandem Mass Spectrometry for the Analysis of Inorganic Compounds. *Rapid Commun. Mass Spectrom.* **2001**, *15*, 895-897.

11. Zhang, D.; Cooks, R. G. Doubly Charged Cluster Ions $[(NaCl)_m(Na)_2]^{2+}$: Magic Numbers, Dissociation, and Structure. *Int. J. Mass Spectrom.* **2000**, *195/196*, 667-684.

12. Charles, L.; Pépin, D.; Gonnet, F.; Tabet, J. Effects of Liquid Phase Composition on Salt Cluster Formation in Positive Ion Mode Electrospray Mass Spectrometry: Implications for Clustering Mechanism in Electrospray. *J. Am. Soc. Mass Spectrom.* **2001**, *12*, 1077-1084.

13. Schalley, C. A.; Weis, P. Unusually Stable Magic Number Clusters of Serine with a Surprising Preference for Homochirality. *Int. J. Mass Spectrom.* **2002**, *221*, 9-19.

14. Nemes, P.; Schlosser, G.; Vékey, K. Amino Acid Cluster Formation Studied by Electrospray Ionization Mass Spectrometry. *J. Mass Spectrom.* **2005**, *40*, 43-49.

15. Loo, J. A. Studying noncovalent protein complexes by electrospray ionization mass spectrometry. *Mass Spectrom. Rev.* **1997**, *16*, 1-23.

16. Tian, R.; Xu, S.; Lei, X.; Jin, W.; Ye, M.; Zou, H. Characterization of Small-Molecule-Biomacromolecule Interactions: From Simple to Complex. *Trends Anal. Chem.* **2005**, *24*, 810-825.

17. Lentz, N. B.; Houk, R. S. Negative Ion Mode Electrospray Ionization Mass Spectrometry Study of Ammonium-Counter Ion Clusters. *J. Am. Soc. Mass Spectrom.* **2007**, *18*, 285-293.

18. Mollah, S.; Pris, A. D.; Johnson, S. K.; Gwizdala, A. B., III; Houk, R. S. Identification of Metal Cations, Metal Complexes, and Anions by Electrospray Mass Spectrometry in the Negative Ion Mode. *Anal. Chem.* **2000**, *72*, 985-991.

19. Anacleto, J. F.; Pleasance, S.; Boyd, R.K. Calibration of Ion Spray Mass Spectra using Cluster Ions. *Org. Mass Spectrom.* **1992**, *27*, 660-666.

20. Moini, M.; Jones, B.L.; Rogers, R. M.; Jiang, L. Sodium Trifluoroacetate as a Tune/Calibration Compound for Positive- and Negative-Ion Electrospray Ionization Mass Spectrometry in the Mass Range of 100-4000 Da. *J. Am. Soc. Mass Spectrom.* **1998**, *9*, 977-980.

21. Kebarle, P; Tang, L. From Ions in Solution to Ion in the Gas Phase - the Mechanism of Electrospray Mass Spectrometry. *Anal. Chem.* **1993**, *65*, 972A-986A.

22. Tang, L; Kebarle, P. Dependence on Ion Intensity in Electrospray Mass Spectrometry on the Concentration of the Analytes in the Electrosprayed Solution. *Anal. Chem.* **1993**, *65*, 3654-3668.

23. Zhou, S.; Hamburger, M. Formation of Sodium Cluster Ions in Electrospray Mass Spectrometry. *Rapid Commun. Mass Spectrom.* **1996**, *10*, 797-800.

24. Hao, C.; March, R. E.; Croley, T. R.; Smith, J. C.; Rafferty, S. P. Electrospray Ionization Tandem Mass Spectrometric Study of Salt Cluster Ions. Part 1-Investigations of Alkali Metal Chloride and Sodium Salt Cluster Ions. *J. Mass Spectrom.* **2001**, *36*, 79-96.

25. Hao, C.; March, R. E. Electrospray Ionization Tandem Mass Spectrometric Study of Salt Cluster Ions. Part 2-Salts of Polyatomic Acid Groups and of Multivalent Metals. *J. Mass Spectrom.* **2001**, *36*, 509-521.

26. Shannon, R. D.; Prewitt, C. T. Revised Values of Effective Ionic Radii. *Acta Crystallogr.* **1970**, *B26*, 1046-1048.

Table 1. Ionic radii of Ce^{3+}, Ho^{3+}, and Co^{2+} in Å [26].

	Coordination number			
Ion	4	6	8	12
Ce^{3+}		1.01	1.14	1.29
Co^{2+}	0.57	0.65 or 0.74		
Ho^{3+}		0.90	1.02	

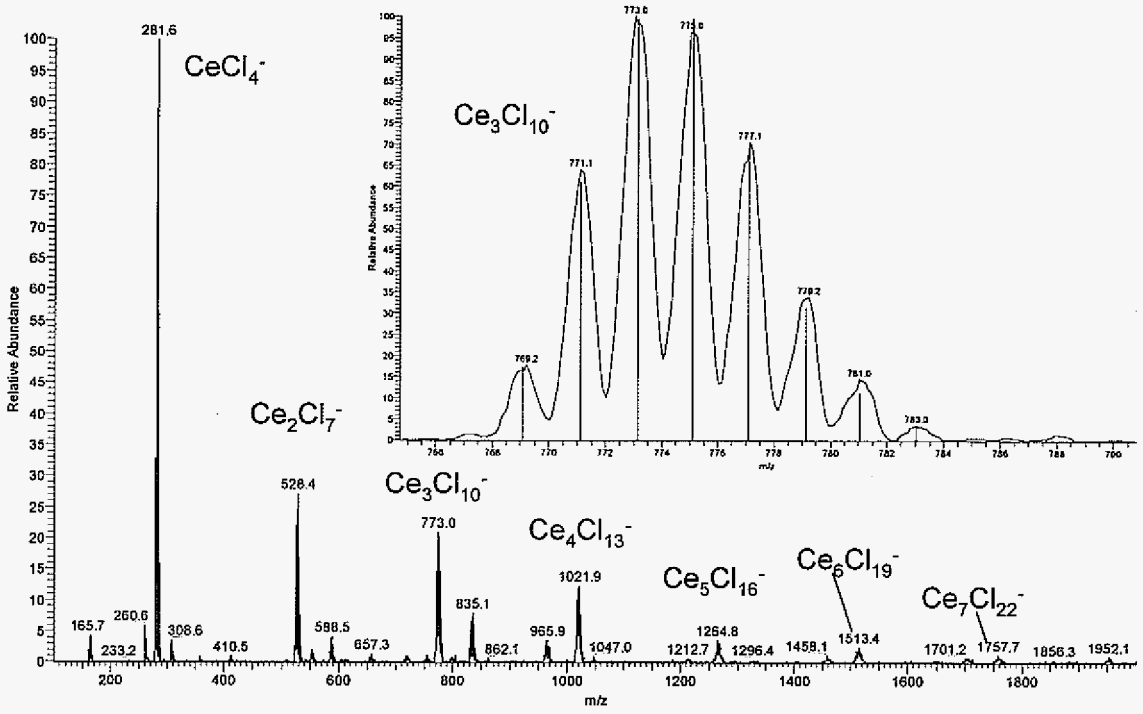

Figure 1. Mass spectrum of a 1 mM cerium chloride solution in 96/4 IPA/H_2O. Inset shows the experimental peaks and calculated isotope distribution (black bars) for $Ce_3Cl_{10}^-$.

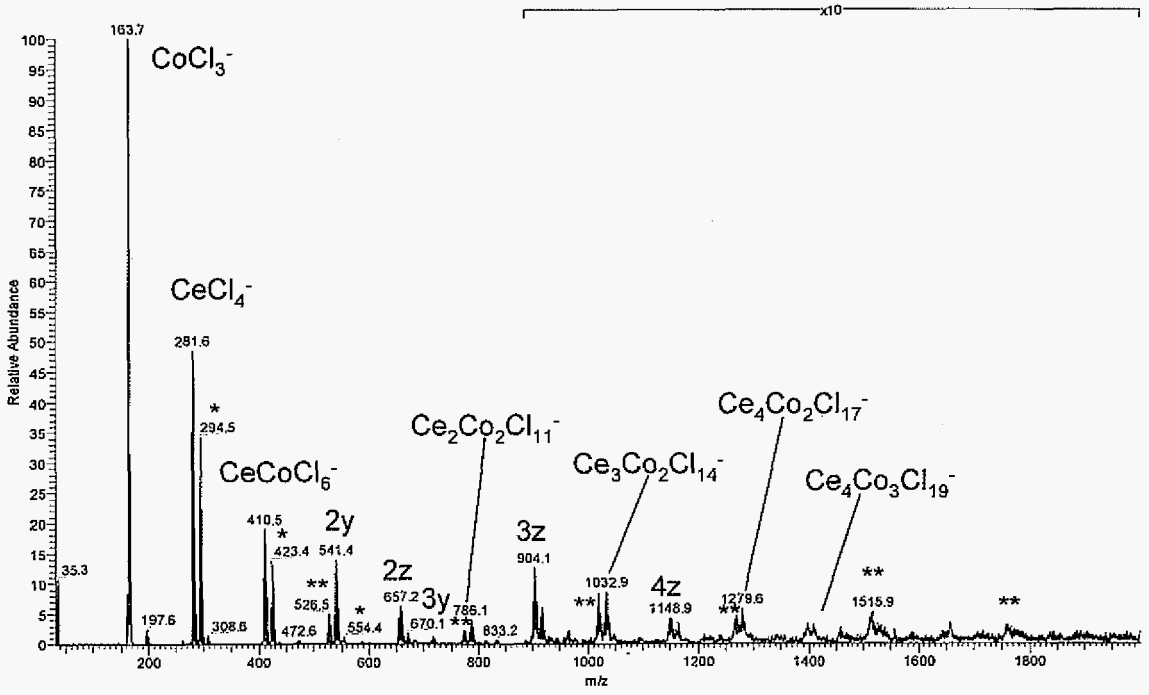

Figure 2. Mass spectrum of 1 mM cerium and cobalt chloride solution in 96/4 IPA/H_2O. The peaks labeled with an "*" and "**" contain only Ce and Co metal ions, respectively. The 2y and 3y numbers denote $CeCo_yCl^-$ cluster ions, and the 2z pattern denotes Ce_zCoCl^- cluster ions. Note vertical scale zoom at m/z > 850.

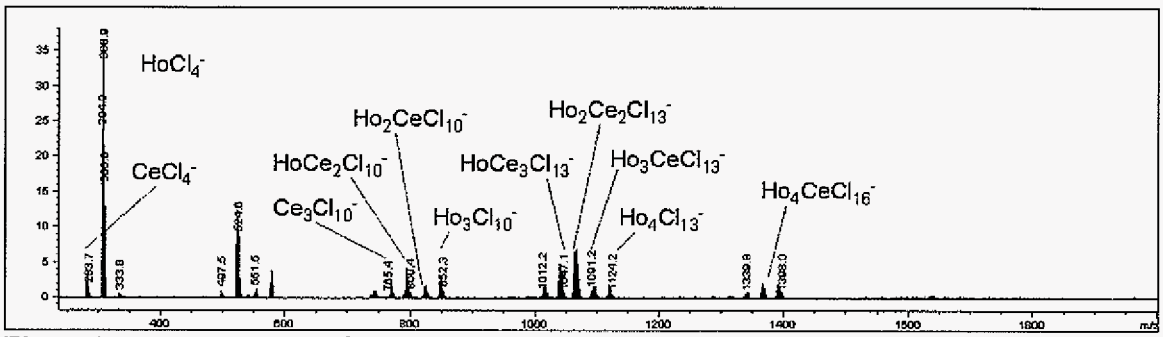

Figure 3. Mass spectrum of a 1 mM cerium and holmium chloride solution in 96/4 IPA/H_2O collected on the Agilent single quadrupole instrument.

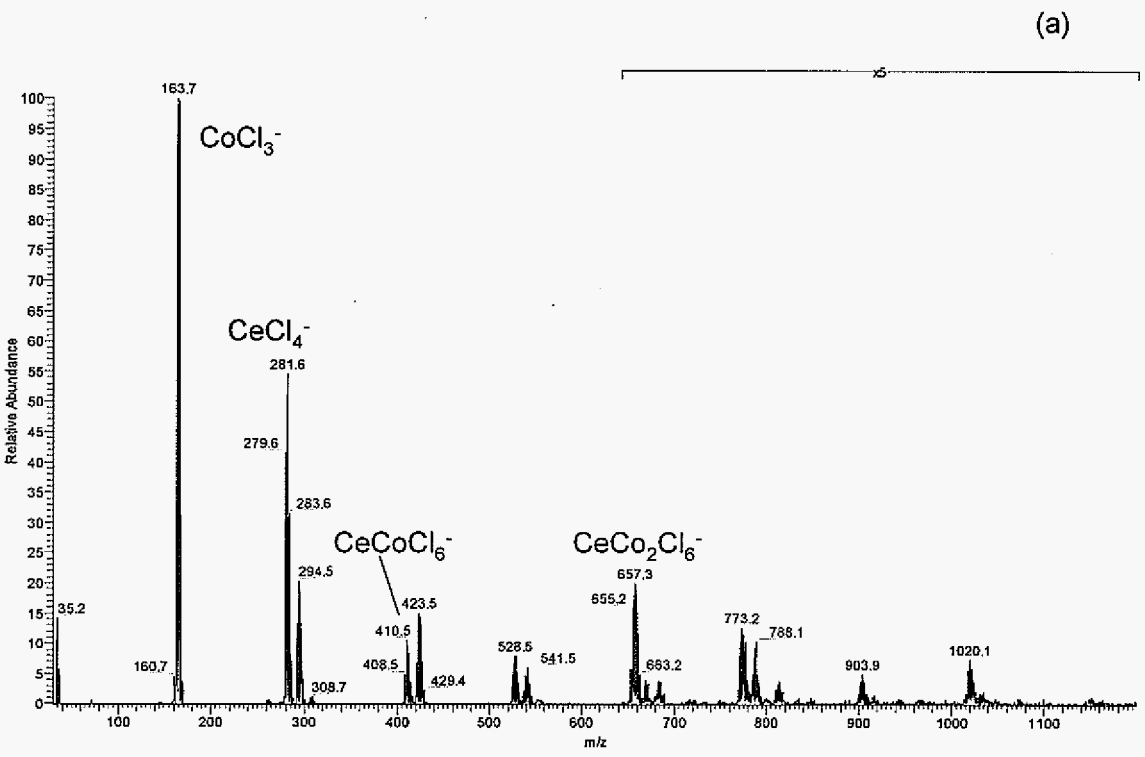

Figure 4. Heated capillary temperature effects on a 1 mM cerium and cobalt chloride solution in 96/4 IPA/H_2O. The heated capillary temperatures for (a), (b), (c), (d), and (e) are 250, 200, 175, 150, and 125 °C, respectively. Note vertical scale zoom at m/z > 640.

(b)

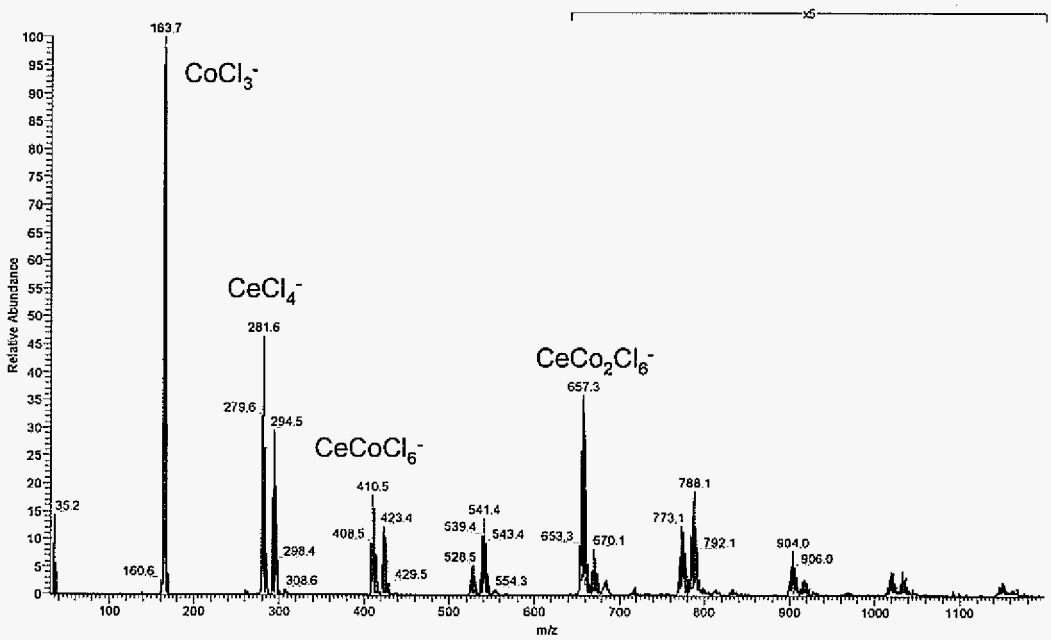
x5
163.7
CoCl3-
CeCl4-
281.6
279.6
294.5
CeCoCl6-
410.5
423.4
408.5
298.4
308.6
429.5
541.4
539.4
543.4
528.5
554.3
CeCo2Cl6-
657.3
653.3
670.1
788.1
773.1
792.1
904.0
906.0
35.2
160.6
Relative Abundance
m/z

(c)

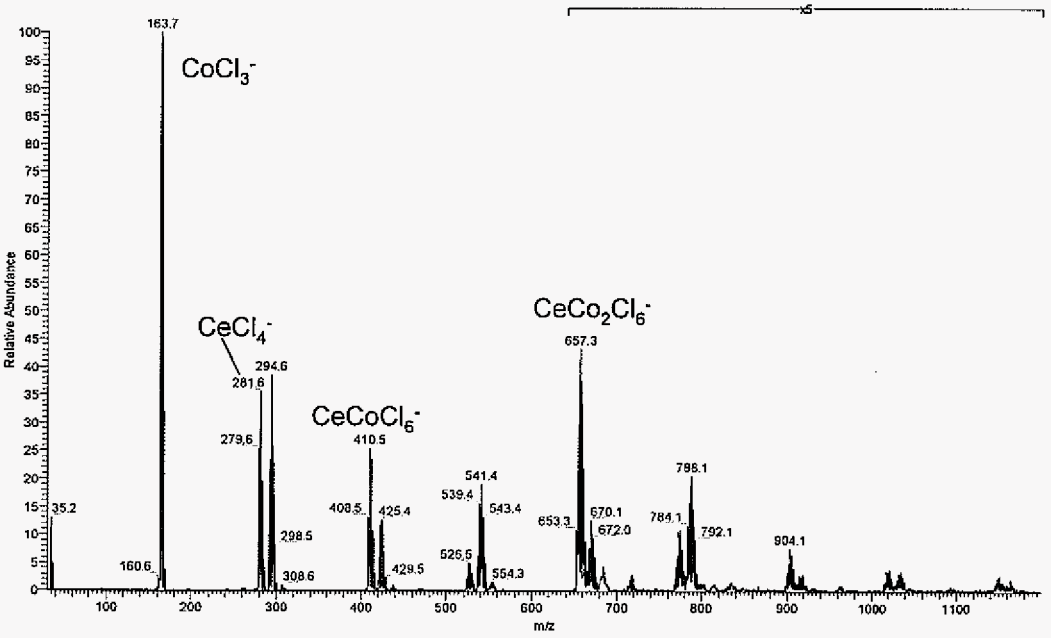
x5
163.7
CoCl3-
CeCl4-
281.6
294.6
279.6
CeCoCl6-
410.5
425.4
408.5
298.5
308.6
429.5
541.4
539.4
543.4
526.5
554.3
CeCo2Cl6-
657.3
653.3
670.1
672.0
798.1
784.1
792.1
904.1
35.2
160.6
Relative Abundance
m/z

(d)

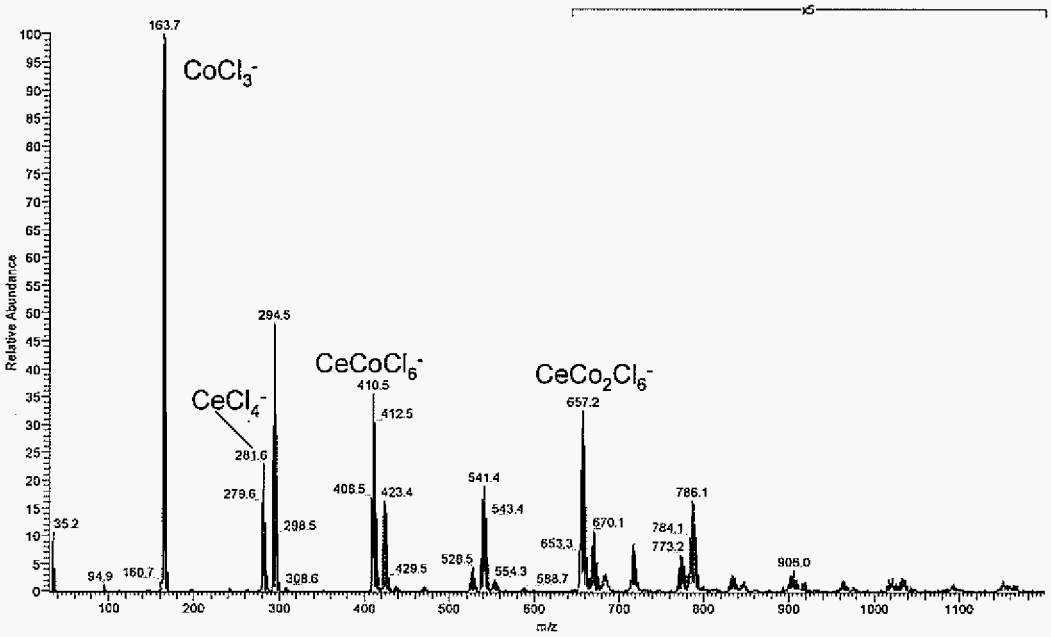
x5
163.7
CoCl3-
294.5
CeCoCl6-
410.5
412.5
CeCl4-
281.6
279.6
408.5
423.4
298.5
308.6
429.5
541.4
543.4
526.5
554.3
588.7
CeCo2Cl6-
657.2
670.1
653.3
784.1
773.2
786.1
908.0
35.2
94.9
160.7
Relative Abundance
m/z

(e)

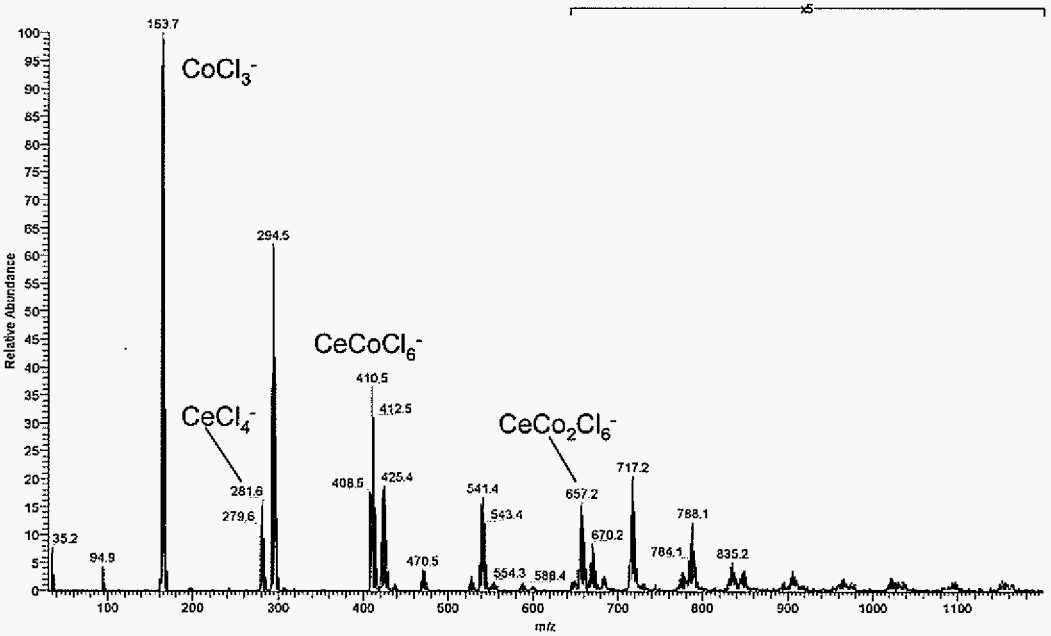
x5
153.7
CoCl3-
294.5
CeCoCl6-
410.5
412.5
CeCl4-
281.6
279.6
408.5
425.4
470.5
541.4
543.4
554.3
588.4
CeCo2Cl6-
657.2
670.2
717.2
784.1
788.1
835.2
35.2
94.9
Relative Abundance
m/z

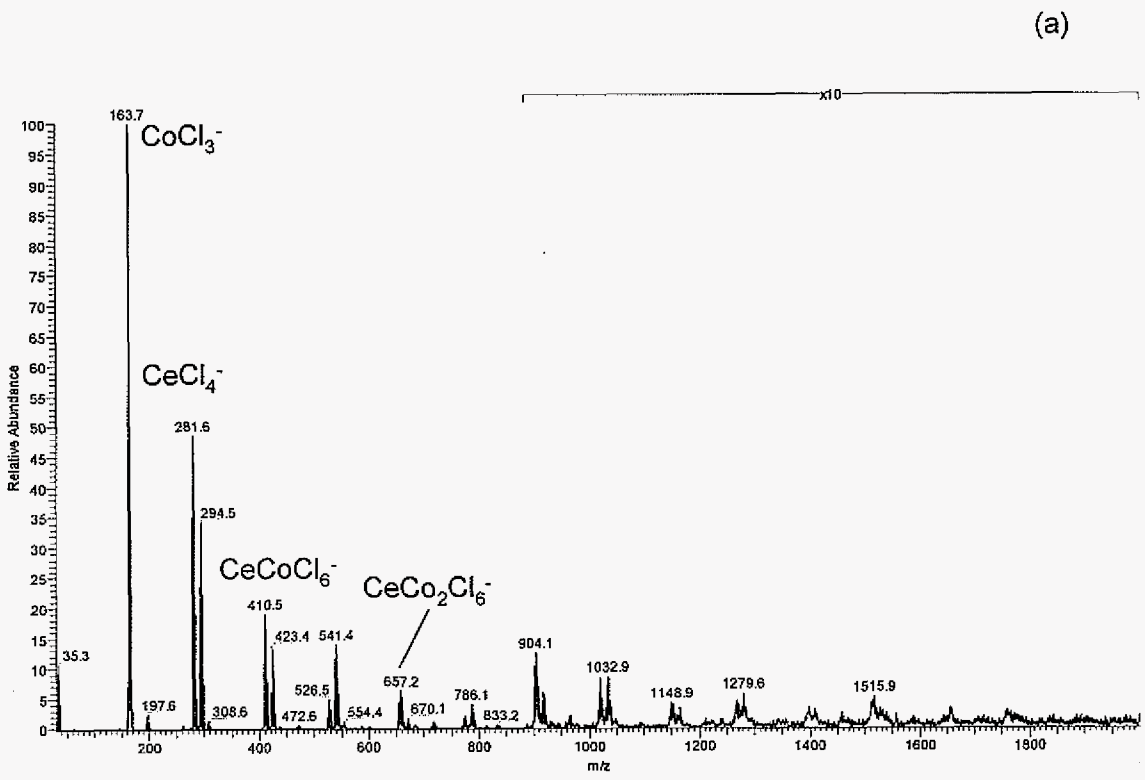

Figure 5. Solvent effects on a 1 mM cerium and cobalt chloride solution. The solvent compositions are (a) 96/4 IPA/H_2O, (b) 50/50 IPA/H_2O, (c) 25/75 IPA/H_2O. Note vertical scale zoom at m/z > 900.

(b)

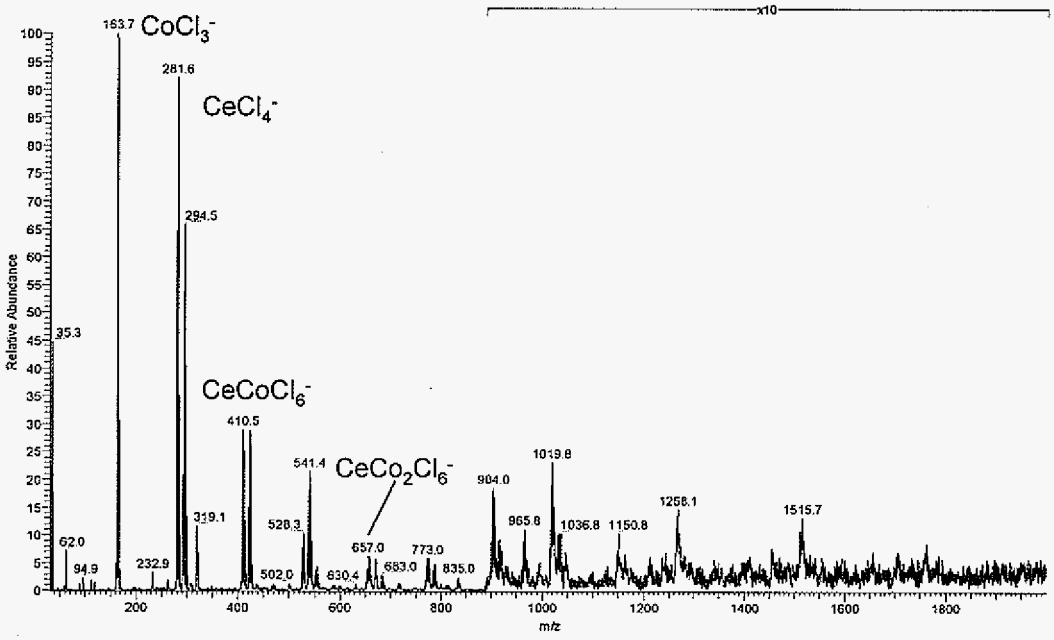
x10
163.7 $CoCl_3^-$
281.6
$CeCl_4^-$
294.5
35.3
$CeCoCl_6^-$
410.5
541.4
$CeCo_2Cl_6^-$
1019.8
904.0
339.1
528.3
657.0
773.0
965.8
1036.8
1150.8
1258.1
1515.7
62.0
94.9
232.9
502.0
630.4
683.0
835.0
Relative Abundance
m/z

(c)

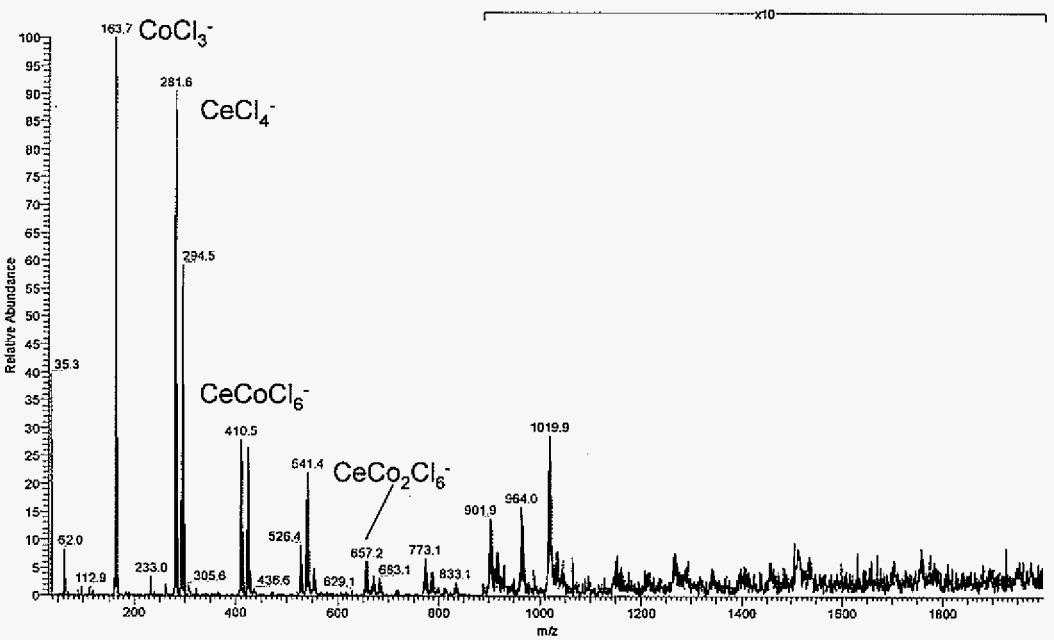
x10
163.7 $CoCl_3^-$
281.6
$CeCl_4^-$
294.5
35.3
$CeCoCl_6^-$
410.5
641.4
$CeCo_2Cl_6^-$
1019.9
964.0
901.9
526.4
657.2
773.1
62.0
112.9
233.0
305.6
436.6
629.1
683.1
833.1
Relative Abundance
m/z

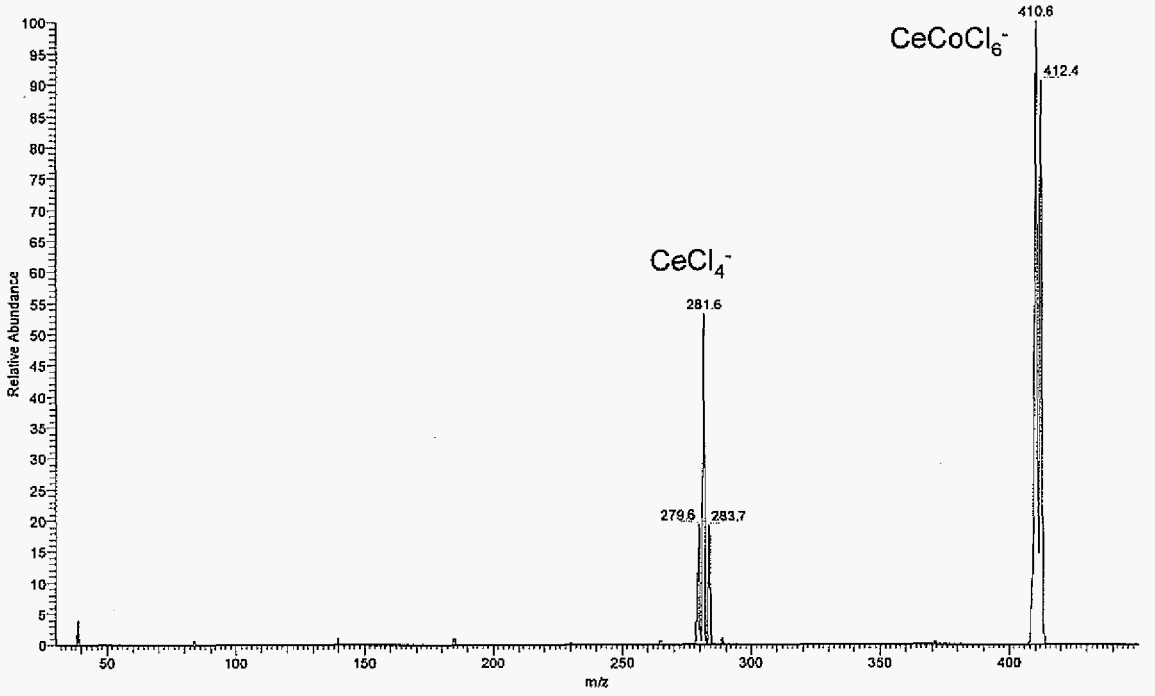

Figure 6. CID product spectrum for the $CeCoCl_6^-$ ion at m/z 410.6. The collision energy and collision gas pressure were 25 eV and 0.067 Pa, respectively.

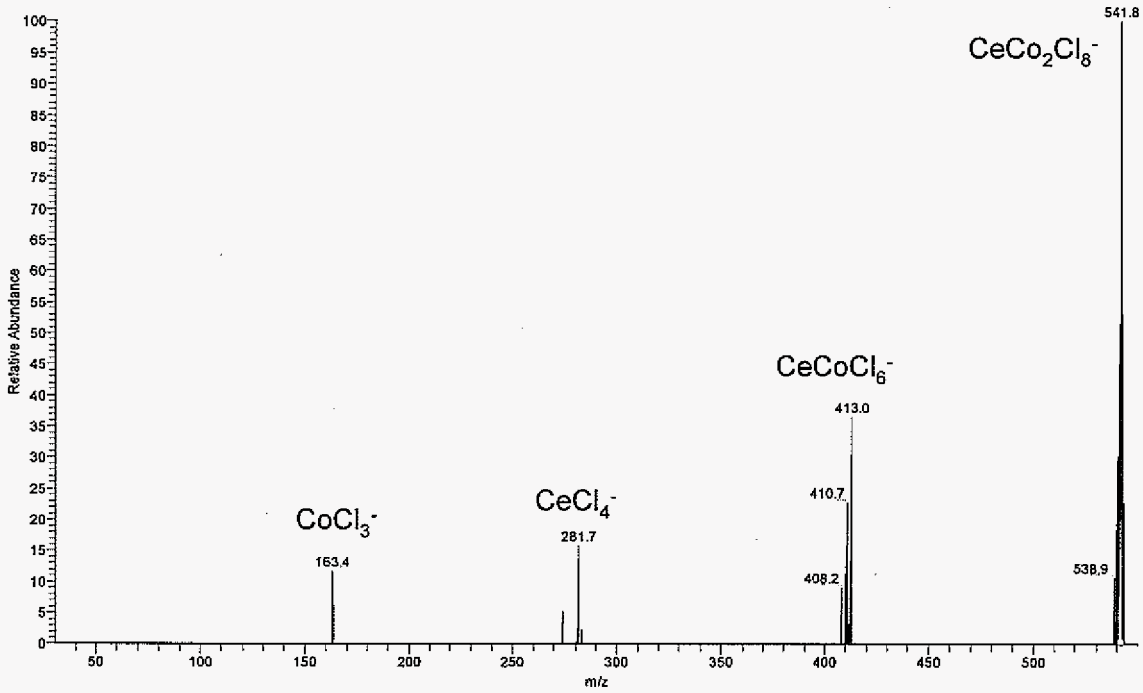

Figure 7. CID product spectrum for the $CeCo_2Cl_8^-$ ion at m/z 541.8. The collision energy and collision gas pressure were 25 eV and 0.067 Pa, respectively.

CHAPTER 5. INTERACTION OF TOXIC METAL IONS WITH THE [Gln^{11}]-AMYLOID β-PROTEIN FRAGMENT (1-16) STUDIED BY ELECTROSPRAY IONIZATION MASS SPECTROMETRY

A paper submitted to the *Journal of Biological Inorganic Chemistry*

N. B. Lentz and R. S. Houk

Abstract

Electrospray ionization mass spectrometry (ESI-MS) was used to evaluate toxic metal binding to the [Gln^{11}]-amyloid β-protein fragment (1-16). Cd and Pb bound to the amyloid fragment; Hg did so weakly. Collision induced dissociation (CID) studies found that Pb and Cd attached to the same binding site as the essential element Zn. Competition studies found that Pb and Cd have a higher affinity for the binding site than Zn. The signal ratio (Cd + peptide)/(Zn + peptide) was 1.39, and the ratio (Pb + peptide)/(Zn + peptide) was 1.85. Cadmium and lead displaced about 80 percent of the bound Zn ions, but an excess of Zn did not remove the bound toxic metals.

Introduction

Some metal ions play a critical role in biological systems and are needed for many biological functions [1]. Not all metal ions are essential for biological systems. Once present in a biomolecule, toxic metals are often hard to remove and can accumulate over time. Other toxic metals can cause improper folding in proteins, cause enzymes to lose their

function, compete for specific binding sites with the desired metal ion, and cause many unknown reactions within the biological system [2].

Many well established instrumental methods such as absorption spectroscopy, circular dichroism (CD) [3], nuclear magnetic resonance (NMR) spectroscopy [3,4], electron paramagnetic resonance (EPR) spectroscopy [3], extended x-ray absorption fine structure (EXAFS) [5-7], and x-ray crystallography [8, 9] have been used to study the interaction between metal ions and biological entities. While these methods yield detailed structural information, they often are slow and require large amounts of purified protein sample.

Since its beginning [10], electrospray ionization mass spectrometry (ESI-MS) has revolutionized the analysis of proteins and peptides [11, 12]. Over the past fifteen years, ESI-MS has become a valuable method for studying the binding of metal ions to peptides and proteins [13-42]. The advantages of mass spectrometry were best described by McLafferty as specificity, speed, and sensitivity [43]. For studying metal ion binding to peptides and proteins with ESI-MS, Loo added stoichiometry as another advantage of mass spectrometry [16]. Stoichiometry can provide accurate information regarding the number of metal ions associated with proteins or peptides. The low total amounts of protein/peptide and small sample volumes of ESI-MS make it advantageous for studying biological materials which are expensive to extract or synthesize in large amounts.

Most of the metal ion binding studies have focused on the alkali [21, 22], alkali earth [23-25], and the biologically essential first row transition metals [14, 15, 44, 26-42]. Very little mass spectrometry research has involved the investigation of toxic metal binding to peptides [18, 45-49]. Of these papers, only a select few have utilized ESI-MS [18, 48].

In this paper, the binding of toxic metals to the [Gln^{11}]-amyloid β-protein fragment (1-16) is investigated using ESI-MS. This amyloid fragment represents a wide class of peptides that have histidine residues at the site for metal coordination. Information obtained with this peptide can be used to predict or model the behavior of other peptides that may bind the toxic metals studied in this paper. As discussed by Tabet et al. [13], beta sheet formation of the amyloid β-protein has been implicated in triggering the onset of Alzheimer's disease. In this protein, the amyloid β-protein fragment (1-16) has been identified as the smallest peptide able to coordinate metal ions and has been used as a model for the full protein in metal ion coordination studies [50]. Instead of using the whole amyloid β-protein, the [Gln^{11}]-amyloid β-protein fragment (1-16) was chosen because it is commercially available and generates a simple mass spectrum.

The main aim of this paper is to evaluate whether ESI-MS can determine the binding location and relative affinity of toxic metal ions compared to zinc ions in peptides. CID studies were performed to determine the metal ion binding location(s). Competition studies were performed in solution to determine the relative binding affinity of the different metal ions toward the peptide of interest.

Materials and Methods

Samples and Sample Preparation

The [Gln^{11}]-amyloid β-protein fragment (1-16), DAEFRHDSGYQVHHQK, and metal salts ($ZnCl_2$, $PbCl_2$, $CdCl_2$, and $HgCl_2$) were purchased from Sigma (St. Louis, MO), and used without further purification. The methanol was also purchased from Sigma.

Samples for ESI-MS were prepared as either 5:1 or 10:1 molar ratios (metal to peptide) in 50/50 H_2O/MeOH. The peptide concentration was kept constant at 25 μM during all experiments. The solution pH was 6.

ESI-MS

A TSQ-7000 (Thermo Finnigan, San Jose, CA) was used for this study. This triple quadrupole (QoQ) instrument has a heated capillary interface and an angled octopole collision cell. Samples were infused at a flow rate of 4 μL/min with a syringe pump (Model 22, Harvard Apparatus, Southnatic, MA) through a 250 μL gas-tight syringe (Hamilton, Reno, NV). The electrospray needle voltage was set to 5 kV, and the heated capillary temperature was kept at 250 °C. Nitrogen (60 psi) was used as the sheath gas, and high purity-argon was used as the collision gas. The mass range was calibrated using a standard MRFA peptide/myoglobin solution in 49.5/49.5/1 H_2O/MeOH/acetic acid. The collision gas pressure was 0.293 Pa, and the collision energy was 30 eV, lab frame. For CID studies, the resolution of the first quadrupole was reduced in order to transmit the entire multiply charged peak. CID spectra were smoothed for better product ion detection.

Results and Discussion

Metal-Amyloid Complexes

Tabet et al. [13] investigated the binding properties Zn, Ni, Mn, and Co to amyloid β-protein fragment (1-16). Zinc exhibited the highest binding strength when competition studies were performed [13]. In the current study, spectra were obtained after addition of 125 μM $ZnCl_2$ to the 25 μM amyloid fragment solution. The mass spectrum in Figure 1

shows the 2+ to 5+ charge states of the peptide, and the Zn/peptide complexes. Most of the peptide remains in the free form, but a significant amount, about 20 percent, incorporates one Zn^{2+} ion. Other low abundance peaks represent peptide + two Zn^{2+} ions, and peptide + Zn^{2+} + $2H_2O$. These peaks are present for each charge state in the mass spectrum. It is tempting to calculate a binding constant based on the relative signals in this spectrum, but the signal ratios (metal peptide/peptide) observed by ESI-MS can depend on instrument conditions, pH, and the type of instrument used [16]. These operating conditions are kept constant in subsequent experiments.

In order to determine the Zn^{2+} binding location, CID was performed on the $[M + Zn + 2H]^{4+}$ ion. The CID spectrum (Figure 2) gave the following fragment ions y_2^+, y_3^+, y_{10}^{2+}, $[y_{15} + H + Zn]^{4+}$, $[a_6 - H + Zn]^{2+}$, $[b_6 - H + Zn]^{2+}$, $[a_{14} + Zn]^{3+}$, $[b_{14} + Zn]^{3+}$, and $[a_{15} + Zn]^{3+}$. The nomenclature for the peptide fragmentation pattern is based on normal convention, with the addition of a superscript to indicate the charge state [51]. The fragment ions are consistent with coordination of Zn^{2+} to the histidine residues as previously described [13].

Initial studies were carried out to see if Cd, Hg, and Pb would bind to the amyloid peptide fragment. Each toxic metal was added at 125 μM to a different vial containing peptide at 25 μM. Thus, the mole ratio toxic metal/peptide was 5:1; same as for the Zn^{2+}/peptide studies above. Thus, the mole ratio toxic metal/peptide complexes were found for all three toxic metals investigated (data not shown). The intensities of the toxic metal/peptide complex ions were comparable to the intensities found for the Zn/peptide complex.

In order to determine the binding location of toxic metals, CID studies were performed on the toxic metal/peptide complexes. Cd/peptide and Pb/peptide complexes,

fragment similarly during CID. Figure 3 shows the CID spectrum for the $[M + Cd + 2H]^{4+}$ ion. In this mass spectrum, the product ions are y_2^+, y_3^+, y_{10}^{2+}, $[a_6 - H + Cd]^{2+}$, $[b_6 - H + Cd]^{2+}$, $[y_{15} + H + Cd]^{4+}$, $[a_{14} + Cd - H_2O]^{3+}$, $[b_{14} + Cd]^{3+}$, $[y_9 - H + Cd]^{2+}$, and $[a_{15} + Cd - H_2O]^{3+}$. Figure 4 shows the CID spectrum for the $[M + Pb + 2H]^{4+}$ ion.

Scheme 1 shows the fragmentation pattern for the $[M + Cd + 2H]^{4+}$ and $[M + Pb + 2H]^{4+}$ ions. The fragmentation pattern for the $[M + Zn + 2H]^{4+}$ ion is included for comparison purposes. The arrows pointing left indicate abc ions, and the arrows pointing to the right indicate xyz ions. The fragmentation pattern for the Cd and Pb peptides is similar to that of the Zn peptide. All three metal/peptide ions have D^1-A^2, H^6-D^7, H^{13}-H^{14}, H^{14}-Q^{15}, and Q^{15}-K^{16} bond dissociations.

Most of the bond dissociation is centered on the histidine residues for all three complexes. The similar fragmentation patterns confirm that Cd and Pb are attached to the same binding site as Zn. In other words, the histidine residues serve as the binding site for Cd and Pb as well as Zn. This indicates the possibility that the toxic metals compete with zinc for the same binding site. A strong affinity for lead and/or cadmium may have detrimental effects on the biological function of the protein. In order to address this issue, competition studies were carried out on the peptide fragment.

Competition Studies between Zn and Toxic Metals

Equimolar amounts of Zn and each toxic metal were added simultaneously to the amyloid fragment solution in ratios of 5:5:1. All solutions were equilibrated at room temperature overnight. The signals of the 2+ to 4+ metal/peptide charge states were summed

to compare the intensities of the Zn and toxic metal bound to the peptide. Peaks with two metal ions associated to the peptide were also included.

Figure 5 shows the mass spectrum of a 5:5:1 Zn:Cd:peptide solution. The inset shows a close-up view of the $[M + 2H + Zn]^{4+}$ and $[M + 2H + Cd]^{4+}$ ions. The 4+ ions represent the most intense charge state in the mass spectrum. The signal for the Cd peptide complex is higher than that for the Zn peptide complex by about 40%. Thus, more Cd^{2+} ions occupy the active site than Zn^{2+} ions, if the ESI-MS sensitivity is similar for both metal peptide ions.

As seen in Figure 6, the Pb peptide peak is twice as intense as the Zn peptide peak. The inset shows the 4+ peaks of $[M + 2H + Zn]^{4+}$ and $[M + 2H + Pb]^{4+}$. Nearly twice as many Pb^{2+} ions are bound compared to Zn^{2+}.

Figure 7 shows the mass spectrum of a 5:5:1 Zn:Hg:peptide solution. The peak at m/z 541 is a contaminant Pb peptide peak from previous samples. The inset to Figure 7 shows that the signal ratio Hg peptide/Zn peptide is only ~ 0.1. Mercury does not displace much Zn from the metal ion binding site of the amyloid fragment. It is possible that certain toxic metals preferentially interact with specific metal binding sites, or other factors determine toxic metal ion binding strength.

Toxic Metal/Peptide Complex in the Presence of Excess Zn^{2+}

The question of whether the toxic metals actually displace zinc already in the binding site is addressed next. The free peptide peaks remain the most abundant peaks in the spectra (Figures 1, 5, and 6), even when 5:1 excess Cd or Pb is added. Perhaps the toxic metals only interact with the excess apopeptide and do not disturb the Zn peptide complex. If this

hypothesis is true, adding the toxic metal to a solution that already contains the Zn peptide complex would only make additional toxic metal – peptide ions and not affect the Zn peptide/peptide ratio.

In order to address this issue, the study outlined in Scheme 2 was carried out. A 1 mL solution of 5:1 Zn:peptide was prepared, and allowed to equilibrate overnight. This sample is referred to as the Zn peptide solution. Part of this solution, 200 μL, is transferred to another vial and remains the 5:1 Zn:peptide solution. One toxic metal (Cd or Pb) is added to the original vial to make a 5:10:1 Zn:toxic metal:peptide solution. This two-fold excess of toxic metal to zinc solution is called the Cd or Pb spike and is allowed to equilibrate overnight. The Cd and Pb spike solutions are then evenly divided into two vials. To one of the vials, an excess of Zn is added to make a 20:10:1 Zn:toxic metal:peptide solution. This solution is called the toxic metal:Zn spike. Note that the Cd, Pb and Zn spikes are added to solutions whose compositions have already equilibrated, so these are replacement studies rather than competitions.

Figures 8a-c show the results of this experiment for cadmium. In the following discussion, only the 4+ charge state is discussed because it was the most intense charge state present in the mass spectra. Figure 8a represents the 5:1 Zn:peptide solution. This solution has no Cd, Pb or Hg, and a Zn peptide peak is present at about 23 percent of the apopeptide peak. At the pH used in this study, much of the peptide does not bind the metal ion. Some of the histidine residues at the metal binding site remain protonated and unable to bind the metal ions. For the following experiments, the 23 percent value can serve as a rough guideline for the maximum amount of metal ions that can be bound to the peptide. When the Cd spike is added (Figure 8b), the Zn peptide peak decreases by about 20 abundance units, and the Cd

peptide peak becomes the most abundant metal peptide peak. Since there is a notable change in the Zn peptide peak, the Cd must displace some of the Zn that was bound to the peptide and not simply bind to some of the free peptide present. The total amount of zinc and cadmium bound to the peptide is 19 percent, which is comparable to the 23 percent when only zinc was bound to the peptide.

When additional zinc is added to create the 20:10:1 Zn:Cd:peptide solution (Figure 8c), the Zn peptide peak increases to about 14 abundance units, but remains about half the initial value when cadmium was absent. The intensity of the Cd peptide peak is reduced by four percent, but the majority of the cadmium remains bound to the peptide. This indicates that a small amount of the free peptide may have bound some Zn, and that a small amount of the Cd may have been displaced by Zn. The total amount of metal bound to the peptide is once again 23 percent, which is the same as when only the zinc ions were present in solution. These spectra show that a) Cd^{2+} has a higher affinity for the binding site because it displaces much of the bound Zn^{2+}, and b) Cd^{2+} largely stays bound in the presence of extra Zn.

When this experiment is performed with lead, similar results are obtained. Table 1 summarizes the results for the lead experiments. Figures 9a-c show the mass spectra of the 4+ charge states of the 5:1 Zn:peptide, 5:10:1 Zn:Pb:peptide, and 20:10:1 Zn:Pb:peptide complexes, respectively. When the Pb spike is introduced (Figure 9b), the Zn peptide peak decreases by over 20 abundance units. The Pb peptide peak now towers over the Zn peptide peak and has about the same intensity as the Cd peptide peak in Figure 8b. The total amount of metal bound to the peptide is 16 percent, which is slightly lower than the original value of approximately 23 percent. When the extra Zn is added (Figure 9c), the abundance for the lead peptide peak remains unchanged, and the Zn peptide peak increases to 12 percent. Since

the amount of lead bound to the peptide remains unchanged, the excess zinc must bind to some of the free peptide in solution. In Figure 9c, the total amount of metal ions bound to the peptide is 25 percent, which is close to the original value of 23 percent.

Table 1 shows the relative abundances of the Zn peptide and toxic metal peptide peaks normalized to the $[M + 4H]^{4+}$ apopeptide peak. All of the metal peptide complex peak signals for all the observed charge state throughout the whole mass range investigated are summed in Table 1. All of the possible metal peptide peaks are examined to account for all of the metal bound to the peptide.

In contrast to Cd^{2+} and Pb^{2+}, Hg^{2+} did not displace a significant amount of the Zn bound to the peptide. Figures 10a-c show the 4+ charge states of the peptide and the corresponding holopeptide peaks with Hg^{2+} and Zn^{2+}. Figure 10a shows the 5:1 Zn:peptide solution without any Hg^{2+} ions present. The peak at m/z 541 corresponds to a Pb peptide peak arising from Pb carryover from previous experiments with Pb^{2+}. When the Hg spike was added (Figure 10b), the Zn peptide peak remains the predominant metal peptide peak with a slight Hg peptide peak present at m/z 539. The intensity of the Hg peptide peak is much smaller than the intensities of the Pb peptide and Cd peptide peaks. When extra zinc is added (figure 10c) the Hg peptide peak is reduced to near baseline levels. This shows that Hg has a much weaker binding affinity for the peptide than Zn.

Conclusion

Electrospray ionization mass spectrometry is used to probe the binding of Pb, Cd, and Hg to the [Gln^{11}]-amyloid β-protein fragment (1-16). The toxic metals primarily bind in a 1:1 stoichiometry; a few peptides contain two metal ions. CID studies confirm that Pb and

Cd bind in the same location as Zn due to similar fragmentation patterns at the histidine residues. Competition studies show that Pb^{2+} and Cd^{2+} ions have a higher affinity for the amyloid binding site than the zinc ions. The amount of Pb and Cd bound to the amyloid fragment remains consistent, even in the presence of a two fold excess of Zn. The peptide binds Hg^{2+} much less extensively than Zn^{2+}. Unlike Pb and Cd, zinc was able to displace the Hg ions that were bound to the amyloid peptide. Tabet [13] found that Zn^{2+} bound to the amyloid peptide more strongly than several other first row transition metals. We find that Cd^{2+} and Pb^{2+} bind more strongly than Zn^{2+}. Lead binds the peptide more extensively than cadmium, because none of the lead bound to the peptide was displaced by excess zinc whereas cadmium showed a slight decrease in the amount bound to the peptide (see figures 8c and 9c).

A variety of additional studies could be carried out to address the implications of the toxic metal binding to the amyloid fragment. Circular dichroism (CD) studies would provide valuable information regarding the conformation of the Pb peptide and Cd peptide complexes. These results could be compared to the Zn/peptide CD information to show if the amyloid fragment maintains the same folded confirmation with Cd and Pb in the binding site. Ion mobility studies could also be used to evaluate the gas phase conformations and these could be compared to solution conformations. The binding of toxic metals to other peptides and proteins should be examined by ESI-MS to see if there is a pattern. These studies are currently underway in our lab.

Acknowledgments

Ames Laboratory is operated by Iowa State University for the U.S. Department of Energy, contract no. W-7405-Eng-82. This work was supported by the Chemical and Biological Sciences Program, Office of Basic Energy Sciences, Division of Chemical Sciences. The authors thank L. Huang and Bayer Company for donating the triple quadrupole instrument.

References

1. Voet, D.; Voet, J. G.; Pratt, C. W. *Fundamentals of Biochemistry* John Wiley & Sons: New York, NY, 1999.
2. Lippard, S. J.; Berg, J. M. *Principles of Bioinorganic Chemistry* University Science Books: Mill Valley, CA, 1994.
3. Riordan, J. F.; Vallee, B. L., Eds. *Metallobiochemistry, Part D, Physical and Spectroscopic Methods for Probing Metal Ion Environments in Metalloproteins.* **1993**, *227*.
4. Bertini,-L; Turano, P.; Villa, A. J. Nuclear Magnetic Resonance of Paramagnetic Metalloproteins. *Chem. Rev.* **1993**, *93*, 2833-2932.
5. Dent, A. J.; Beyersmann, C.; Block, C.; Hasnain, S. S. Two Different Zinc Sites in Bovine 5-Aminolevulinate Dehydraase Distinguished by Extended X-ray Absorption Fine Structure. *Biochemistry.* **1990**, *29*, 7822-7828.
6. Eggers-Borkenstein, P.; Priggemeyer, S.; Krebs, B.; Henkel, G.; Simmonis, U.; Pettifer, R. F.; Nolting, H.-F.; Hermes, C. Extended X-ray Absorption Fine Structure

(EXAFS) Investigations of Model Compounds for Zinc Enzymes. *Eur. J. Biochem.* **1989**, *186*, 667-675.

7. Hubbard, S. R.; Bishop, W. R.; Kirschmeier, P.; George, S. J.; Cramer, S. P.; Henrickson, W. A. Identification and Characterization of Zinc Binding Sites in Protein Kinase C. *Science*. **1991**, *254*, 1776-1779.
8. Krebs, J. F.; Fierke, C. A.; Alexander, Richard S.; Christianson, David W. Conformational Mobility of His-64 in the Thr-200 .fwdarw. Ser Mutant of Human Carbonic Anhydrase II. *Biochemistry*. **1991**, *30*, 9153-9160.
9. Vallee, B. L.; Auld, D. S. Active-Site Zinc Ligands and Activated H_2O of Zinc Enzymes. *Proc. Natl. Acad. Sci. USA*. **1990**, *87*, 220-224.
10. Yamashita, M.; Fenn J. B. Electrospray ion source. Another variation on the Free-Jet Theme. *J. Phys. Chem.* **1984**, *88*, 4451-4459.
11. Fenn, J. B.; Mann, M.; Meng, C. K.; Wong, S. F.; Whitehouse, C. M. Electrospray Ionization for Mass Spectrometry of Large Biomolecules. *Science* **1989**, *246*, 64-71.
12. Cole, R. B. *Electrospray Ionization Mass Spectrometry* John Wiley & Sons: New York, NY, 1997; pp 385-419.
13. Zirah, S.; Rebuffat, S.; Kozin, S. A.; Debey, P.; Fournier, F.; Lesage, D.; Tabet, J.-C. Zinc Binding Properties of the Amyloid Fragment Aβ(1–16) Studied by Electrospray-Ionization Mass Spectrometry. *Int. J. Mass Spectrom.* **2003**, *228*, 999-1016.
14. Loo, J. A.; Hu, P.; Smith, R. D. Interaction of Angiotensin Peptides and Zinc Metal Ions Probed by Electrospray Ionization Mass Spectrometry. *J. Am. Soc. Mass Spectrom.* **1994**, *5*, 959-965.

15. Loo, J. A.; Hu, P. Gas-Phase Coordination Properties of Zn^{2+}, Cu^{2+}, Ni^{2+}, and Co^{2+} with Histidine-Containing Peptides. *J. Am. Chem. Soc.* **1995**, *117*, 11314-11319.

16. Loo, J. A. Studying Noncovalent Protein Complexes by Electrospray Ionization Mass Spectrometry. *Mass Spectrom. Rev.* **1997**, *16*, 1-23.

17. Loo, J. A. Electrospray Ionization Mass Spectrometry: A Technology for Studying Noncovalent Macromolecular Complexes. *Int. J. Mass Spectrom.* **2000**, *200*, 175.

18. Boysen, R. I.; Hearn, M. T. W. The Metal Binding Properties of the CCCH Motif of the 50S Ribosomal Protein L36 from *Thermus thermophilus*. *J. Peptide Res.* **2001**, *57*, 19-28.

19. Sinz, A.; Jin, A. J; Zschörnig, O. Evaluation of the Metal Binding Properties of a Histidine-Rich Fusogenic Peptide by Electrospray Ionization Fourier Transform Ion Cyclotron Resonance Mass Spectrometry. *J. Mass Spectrom.* **2003**, *38*, 1150-1159.

20. Ho, Y.-P.; Li, H.-P.; Lu, L.-C. Probing the Interactions of Oxidized Insulin Chain A and Metal Ions using Electrospray Ionization Mass Spectrometry. *Int. J. Mass Spectrom.* **2003**, *227*, 97-109.

21. Kanai, M; Iida, A.; Nagaoka, Y.; Wada, S.; Fujita, T. Fungal metabolites. XXI.[1] Characteristics of Low Energy Collision Induced Dissociation of $[M + 2H]^{2+}$, $[M + H + Na]^{2+}$ and $[M + 2Na]^{2+}$ of Peptaibols using Electrospray Ionization Mass spectrometry *J. Mass Spectrom.* **1996**, *31*, 177-183.

22. Ngoka, L. C. M.; Gross, M. L. Location of Alkali Metal Binding Sites in Endothelin A Selective Receptor Antagonists, cyclo(D-Trp-D-Asp-Pro-D-Val-Leu) and cyclo(D-Trp-D-Asp-Pro-D-Ile-Leu), from Multistep Collisionally Activated decompositions. *J. Mass Spectrom.* **2000**, *35*, 265-276.

23. Veenstra, T. D.; Johnson, K. L.; Tomlinson, A. J.; Kumar, R.; Naylor, S. Correlation of Fluorescence and Circular Dichroism Spectroscopy with Electrospray Ionization Mass Spectrometry in the Determination of Tertiary Conformational Changes in Calcium-Binding Proteins. *Rapid Commun. Mass Spectrom.* **1998**, *12*, 613-619.

24. Halgand, F.; Dumas, R.; Biou, V.; Andrieu, J. P.; Thomazeau, K.; Gagnon, J.; Douce, R.; Forest, E. Characterization of the Conformational Changes of Acetohydroxy Acid Isomeroreductase Induced by the Binding of Mg^{2+} Ions, NADPH, and a Competitive Inhibitor. *Biochemistry* **1999**, *38*, 6025-6034.

25. Nemirovskiy, O. V.; Gross, M. L. Determination of Calcium Binding Sites in Gas-Phase Small Peptides by Tandem Mass Spectrometry. *J. Am. Soc. Mass Spectrom.* **1998**, *9*, 1020-1028.

26. Surovoy, A.; Waidelich, D.; Jung, G. Nucleocapsid protein of HIV-1 and its Zn^{2+} Complex Formation Analysis with Electrospray Mass Spectrometry. *FEBS Lett.* **1992**, *311*, 259-262.

27. Reiter, A.; Adams, J.; Zhao, H. Intrinsic (Gas-Phase) Binding of Co2+ and Ni2+ by Peptides: A Direct Reflection of Aqueous-Phase Chemistry. *J. Am. Chem. Soc.* **1994**, *116*, 7827-7838.

28. Sullards, M. C.; Adams, J. On the use of Scans at a Constant ratio of B/E for studying Decompositions of Peptide Metal(II)-Ion Complexes Formed by Electrospray Ionization. *J. Am. Soc. Mass Spectrom.* **1995**, *6*, 608-610.

29. Witkowska, H. E.; Shackelton, C. H. L.; Dahlman-Wright, K; Kim, J. Y.; Gustafsson, J. A. Mass Spectrometric Analysis of a Native Zinc-Finger Structure: The

Glucocorticoid Receptor DNA Binding Domain. *J. Am. Chem. Soc.* **1995**, *117*, 3319-3324.

30. Gadhavi, P. L. An Electrospray Ionisation Mass Spectrometry (ESI-MS) Study to Probe the Metal Ion Binding Site in the DNA Binding Domain of the Yeast Transcriptional Activator GAL4. *FEBS Lett.* **1997**, *417*, 145-149.
31. Fabris, D.; Hathout, Y.; Fenselau, C. Investigation of Zinc Chelation in Zinc-Finger Arrays by Electrospray Mass Spectrometry. *Inorg. Chem.* **1999**, *38*, 1322-1325.
32. Volz, J.; Bosch, F. U.; Wunderlin, M.; Schuhmacher, M.; Melchers, K.; Bensch, K.; Steinhilber, W.; Schäfer, K. P.; Tóth, G.; Penke, B.; Przybylski, M. Molecular Characterization of Metal-Binding Polypeptide Domains by Electrospray Ionization Mass Spectrometry and Metal Chelate Affinity Chromatography. *J. Chromatogr. A* **1998**, *800*, 29-37.
33. Nemirovskiy, O. V.; Gross, M. L. Gas Phase Studies of the Interactions of Fe^{2+} with Cysteine-Containing Peptides. *J. Am. Soc. Mass Spectrom.* **1998**, *9*, 1285-1292.
34. Guy, P. A.; Anderegg, R. J.; Lim, A.; Saderholm, M. J.; Yan, Y.; Erickson, B. W. Metal-Ion Binding and Limited Proteolysis of Betabellin 15D, a Designed Beta-Sandwich Protein. *J. Am. Soc. Mass Spectrom.* **1999**, *10*, 969-974.
35. Whittal, R. M.; Ball, H. L.; Cohen, F. E.; Burlingame, A. L.; Prusiner, S. B.; Baldwin, M. A. Copper Binding to Octarepeat Peptides of the Prion Protein Monitored by Mass Spectrometry. *Protein Sci.* **2000**, *9*, 332-343.
36. Lippincott, J.; Fattor, T. J.; Lemon, D. D.; Apostol, I. Application of Native-State Electrospray Mass Spectrometry to Identify Zinc-Binding Sites on Engineered Hemoglobin. *Anal. Biochem.* **2000**, *284*, 247-255.

37. Morris, L. A.; Jaspars, M.; Kettenes-van den Bosch, J. J.; Versluis, K.; Heck, A. J. R.; Kelly, S. M.; Price, N. C. Metal Binding of *Lissoclinum patella* Metabolites. Part 1: Patellamides A, C and Ulithiacyclamide A. *Tetrahedron* **2001**, *57*, 3185-3197.

38. Payne, A. H.; Glish, G. L. Gas-Phase Ion/Ion Interactions Between Peptides or Proteins and Iron Ions in a Quadrupole Ion Trap. *Int. J. Mass Spectrom.* **2001**, *204*, 47-54.

39. Craig, T. A.; Benson, L. M.; Naylor, S.; Kumar, R. Modulation Effects of Zinc on the Formation of Vitamin D Receptor and Retinoid X Receptor α-DNA Transcription Complexes: Analysis by Microelectrospray Mass Spectrometry. *Rapid Commun. Mass Spectrom.* **2001**, *15*, 1011-1016.

40. Loo, J. A. Probing Protein–Metal Ion Interactions by Electrospray Ionization Mass Spectrometry: enolase and nucleocapsid protein. *Int. J. Mass Spectrom.* **2001**, *204*, 113-123.

41. Vachet, R. W.; Hartman, J. R.; Gertner, J. W.; Callahan, J. H. Investigation of Metal Complex Coordination Structure using Collision-Induced Dissociation and Ion–Molecule Reactions in a Quadrupole Ion Trap Mass Spectrometer. *Int. J. Mass Spectrom.* **2001**, *204*, 101-112.

42. Afonso, C.; Hathout, Y.; Fenselau, C. Qualitative Characterization of Biomolecular Zinc Complexes by Collisionally Induced Dissociation. *J. Mass Spectrom.* **2002**, *37*, 755-759.

43. McLafferty, F. W. Tandem Mass Spectrometry. *Science* **1981**, *214*, 280-287.

44. Brewer, D.; Lajoie, G. Evaluation of the Metal Binding Properties of the Histidine-Rich Antimicrobial Peptides Histatin 3 and 5 by Electrospray Ionization Mass Spectrometry. *Rapid Commun. Mass Spectrom.* **2000**, *14*, 1736-1745.

45. Razmiafshari, M.; Kao, J.; d'Avignon, A.; Zawia, N. H. NMR Identification of Heavy Metal-Binding Sites in a Synthetic Zinc Finger Peptide: Toxicological Implications for the Interactions of Xenobiotic Metals with Zinc Finger Proteins. *Toxicology and Applied Pharmacology*, **2001**, *172*, 1-10.

46. Razmiafshari, M.; Zawia, N. H. Utilization of a Synthetic Peptide as a Tool to Study the Interaction of Heavy Metals with the Zinc Finger Domain of Proteins Critical for Gene Expression in the Developing Brain. *Toxicology and Applied Pharmacology*, **2000**, *166*, 1-12.

47. Asmuss, M.; Mullenders, L. H. F.; Eker, A.; Hartwig, A. Differential Effects of Toxic Metal Compounds on the Activities of Fpg and XPA, Two Zinc Finger Proteins Involved in DNA Repair. *Carcinogenesis*. **2000**, *21*, 2097-2104.

48. Burford, N.; Eelman, M. D.; Groom, K. Identification of Complexes Containing Glutathione with As(III), Sb(III), Cd(II), Hg(II), Tl(I), Pb(II) or Bi(III) by Electrospray Ionization Mass Spectrometry. *J. Inorg. Biochem.* **2005**, *99*, 1992-1997.

49. Hartwig, A. Recent advances in metal carcinogenicity. *Pure Appl Chem.* **2000**, *72*, 1007-1014.

50. Kozin, S. A.; Zirah, S.; Rebuffat, S.; Hui Bon Hoa, G.; Debey, P. Zinc Binding to Alzheimers Aβ(1-16) Peptide Results in Stable Soluble Complex. *Biochem. Biophys. Res. Commun.* **2001**, 959-964.

51. Biemann, K. *Biomed. Environ. Mass Spectrom.* **1988**, *16*, 99-111.

Table 1. Relative intensities of the metal peptide complex ions from amyloid peptide solutions spiked with various metal ions. The intensities are averaged over all charge states in the mass spectra. The solutions were prepared sequentially in the order shown. See text and Scheme 2.

Sample	Mole ratios			Ion Signal Ratios		
peptide/Zn peptide	Cd	Zn	peptide	Zn peptide/peptide	Cd peptide/peptide	Cd
Zn + peptide	0	5	1	0.23	-	-
Zn + peptide + Cd spike	10	5	1	0.06	0.13	2.25
Zn + peptide + Cd spike + Zn spike	10	20	1	0.14	0.09	0.67

Sample	Mole ratios			Ion Signal Ratios		
peptide/Zn peptide	Pb	Zn	peptide	Zn peptide/peptide	Pb peptide/peptide	Pb
Zn + peptide	0	5	1	0.23	-	-
Zn + peptide + Pb spike	10	5	1	0.04	0.12	2.84
Zn + peptide + Pb spike + Zn spike	10	20	1	0.12	0.13	1.06

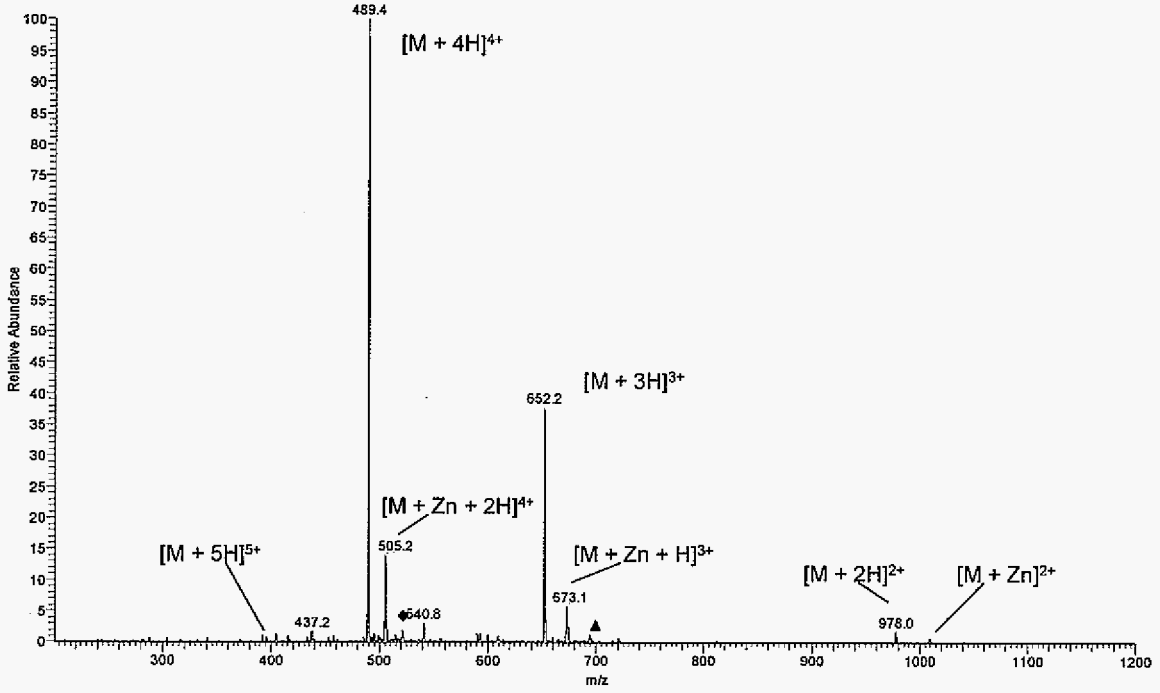

Figure 1. Mass spectrum of 25 μM [$Gln^{[1]}$]-amyloid β-protein fragment (1-16) in the presence of 125 μM $ZnCl_2$. The solvent was 50/50 H_2O/MeOH at a solution pH of 6. Symbols represent the $[M + 2Zn]^{4+}$ (diamond), and the $[M + 2Zn - H]^{3+}$ (triangle) ions.

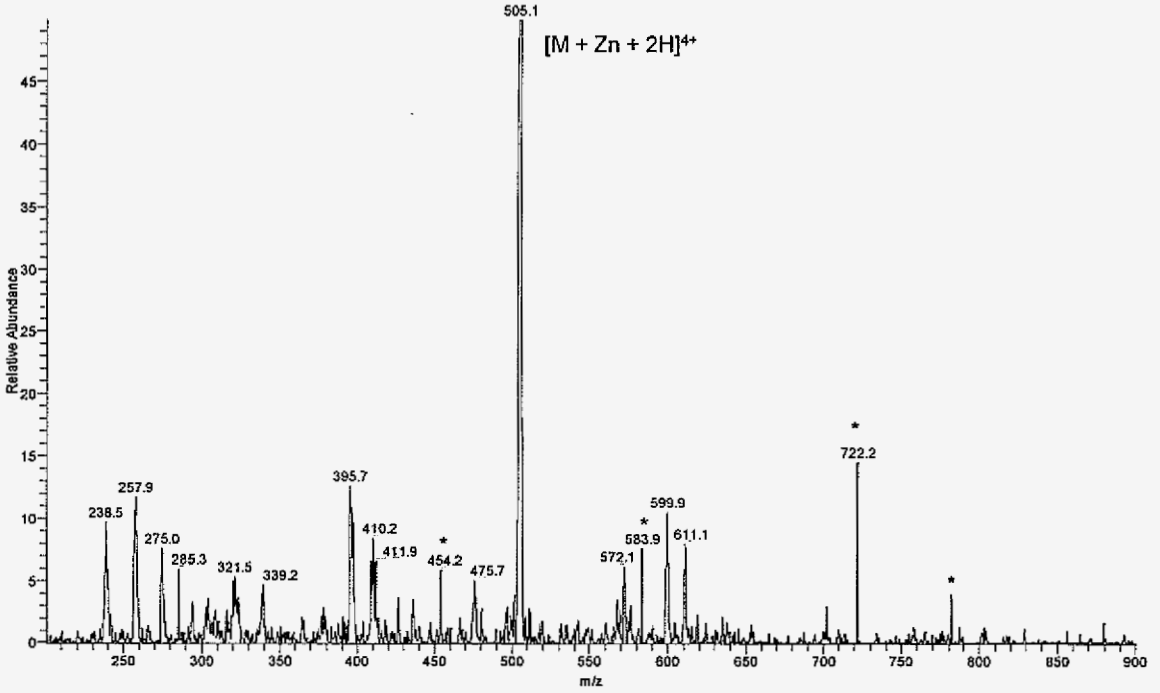

Figure 2. ESI-CID mass spectrum of the $[M + Zn + 2H]^{4+}$ ion of the $[Gln^{11}]$-amyloid β-protein fragment (1-16). The collision energy was 30 eV, lab frame, and the collision gas pressure was 0.293 Pa (argon collision gas). Features marked with an "*" are noise spikes.

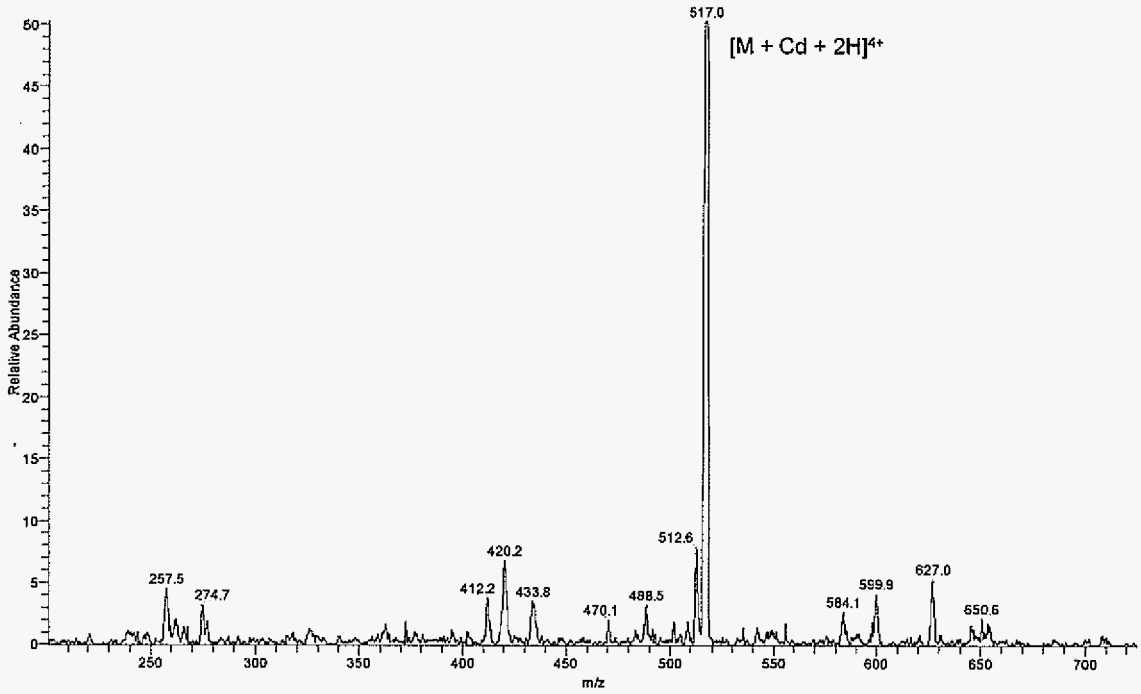

Figure 3. CID mass spectrum of the $[M + Cd + 2H]^{4+}$ ion of the $[Gln^{11}]$-amyloid β-protein fragment (1-16). The collision energy was 30 eV, and the collision gas pressure was 0.293 Pa.

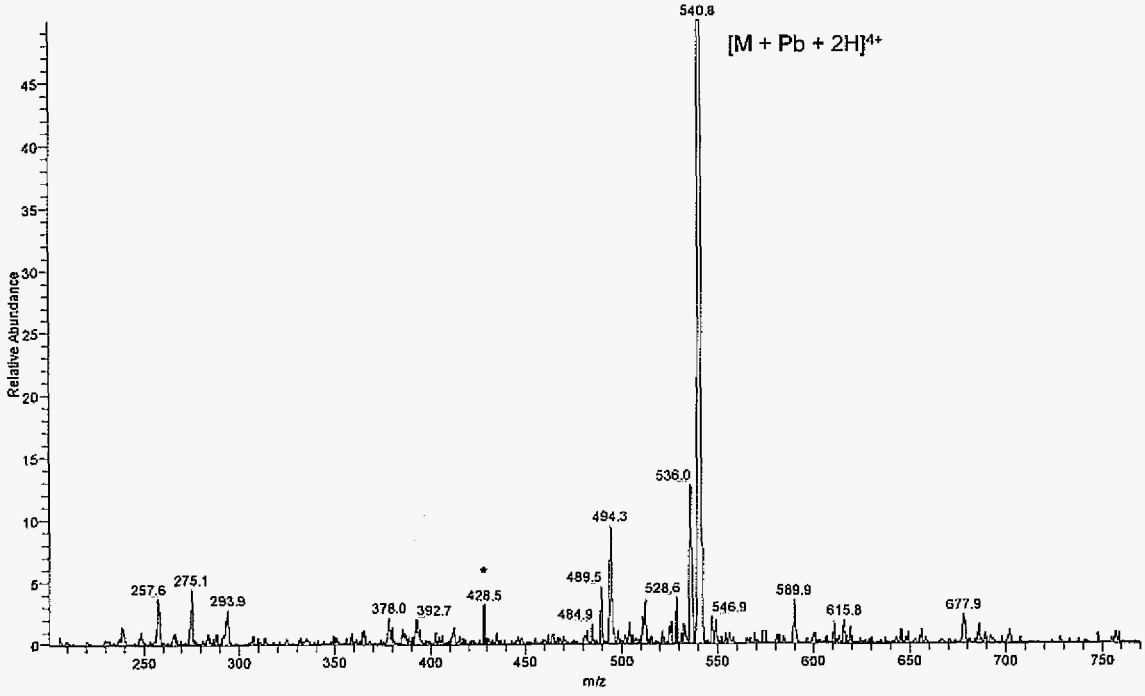

Figure 4. CID mass spectrum of the $[M + Pb + 2H]^{4+}$ ion of the [Gln^{11}]-amyloid β-protein fragment (1-16). The collision energy was 30 eV, and the collision gas pressure was 0.293 Pa. Features marked with an "*" are noise spikes.

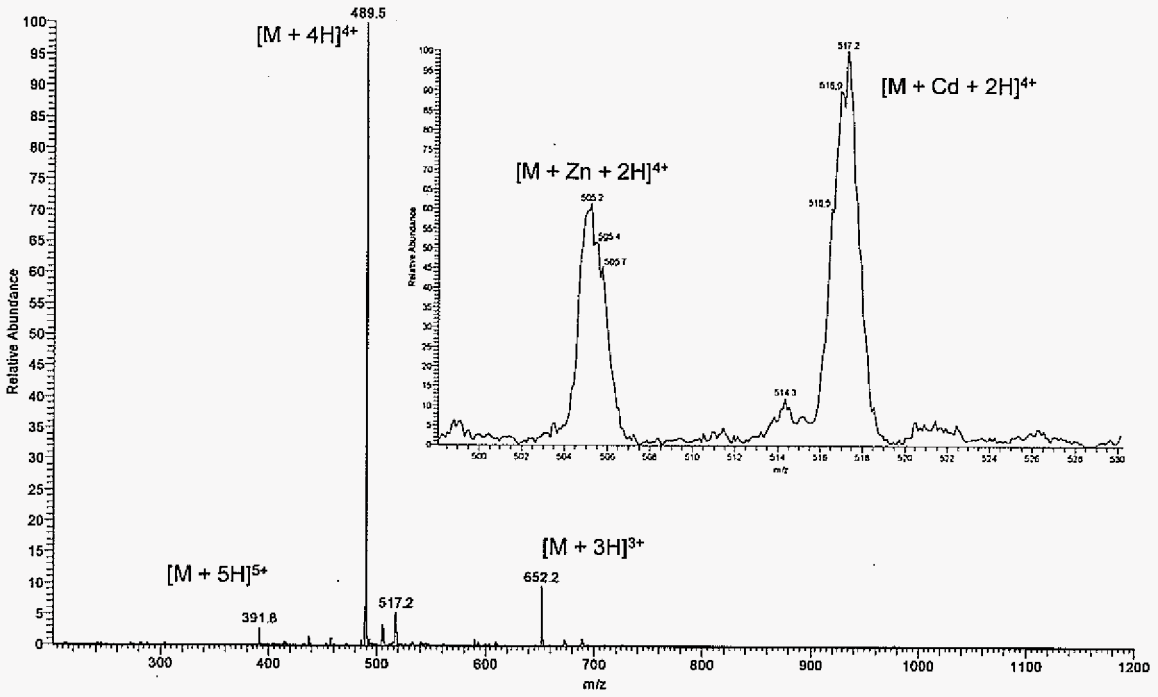

Figure 5. Mass spectrum of the [Gln^{11}]-amyloid β-protein fragment (1-16) in the presence of 5 Zn^{2+} and 5 Cd^{2+} equivalents. The inset shows the $[M + Zn + 2H]^{4+}$ and the $[M + Cd + 2H]^{4+}$ ions.

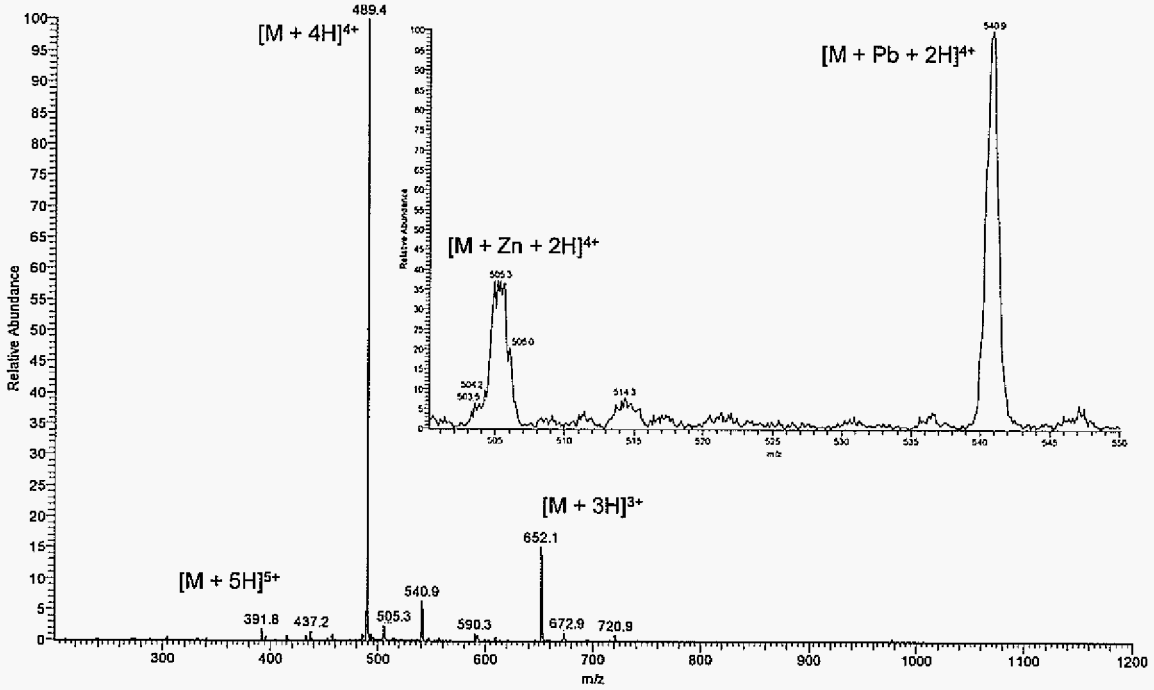

Figure 6. Mass spectrum of the [Gln^{11}]-amyloid β-protein fragment (1-16) in the presence of 5 Zn^{2+} and 5 Pb^{2+} equivalents. The inset shows the $[M + Zn + 2H]^{4+}$ and the $[M + Pb + 2H]^{4+}$ ions.

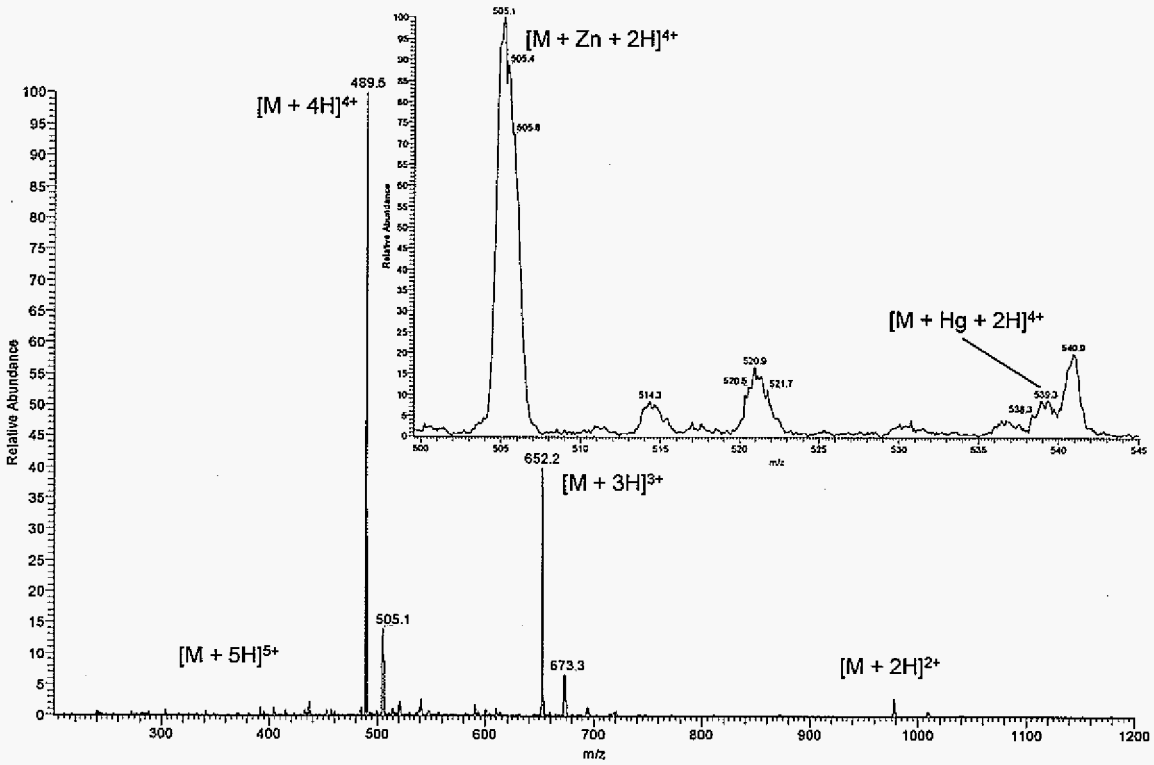

Figure 7. Mass spectrum of the [Gln^{11}]-amyloid β-protein fragment (1-16) in the presence of 5 Zn^{2+} and 5 Hg^{2+} equivalents. The inset shows the $[M + Zn + 2H]^{4+}$ and the $[M + Hg + 2H]^{4+}$ ions.

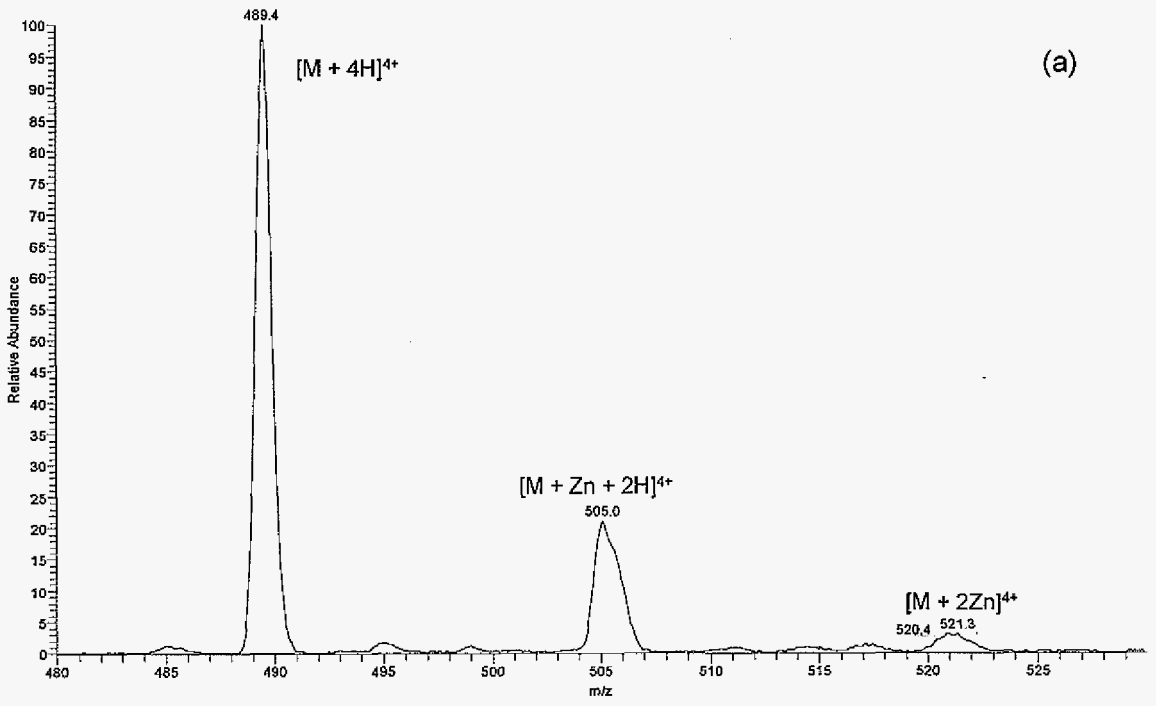

Figure 8. Replacement experiment with Cd. (a) Mass spectrum of the $[M + 4H]^{4+}$ and $[M + Zn + 2H]^{4+}$ ions of a 25 μM [Gln^{11}]-amyloid β-protein fragment (1-16) in the presence of 5 Zn^{2+} equivalents. (b) Mass spectrum of the $[M + 4H]^{4+}$, $[M + Zn + 2H]^{4+}$, and $[M + Cd + 2H]^{4+}$ ions. The solution ratios are 5:10:1 Zn:Cd:amyloid peptide. (c) Mass spectrum of the $[M + 4H]^{4+}$, $[M + Zn + 2H]^{4+}$, and $[M + Cd + 2H]^{4+}$ ions. The diamond and triangle represent the $[M + Zn + 2H_2O + 2H]^{4+}$ and $[M + 2Zn]^{4+}$ ions, respectively. The solution ratios are 20:10:1 Zn:Cd:amyloid peptide.

(b)

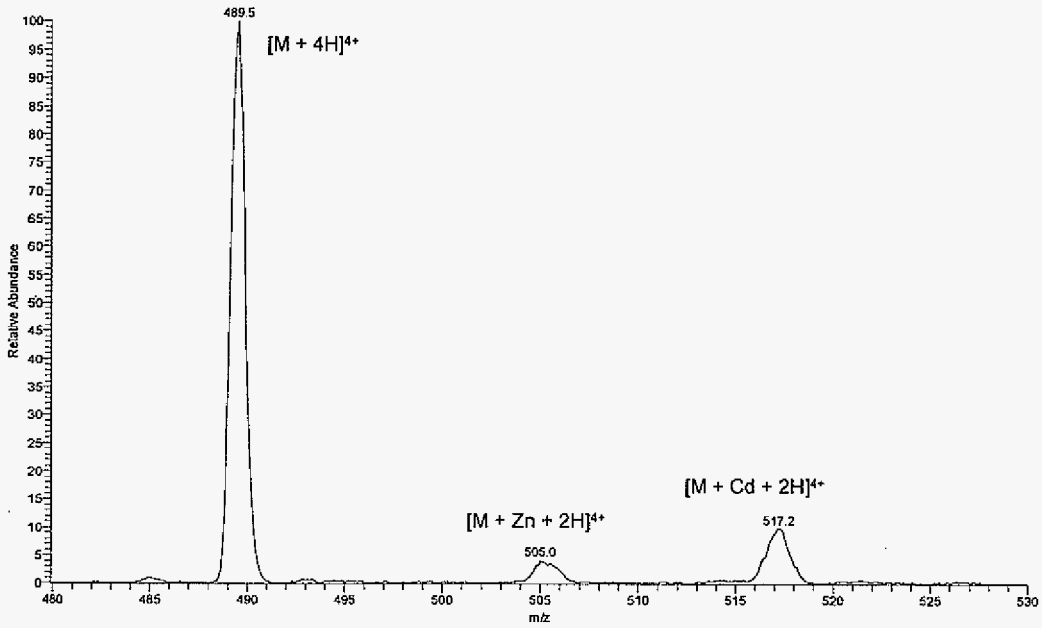
489.5
[M + 4H]4+
[M + Zn + 2H]4+
505.0
[M + Cd + 2H]4+
517.2
Relative Abundance
m/z

(c)

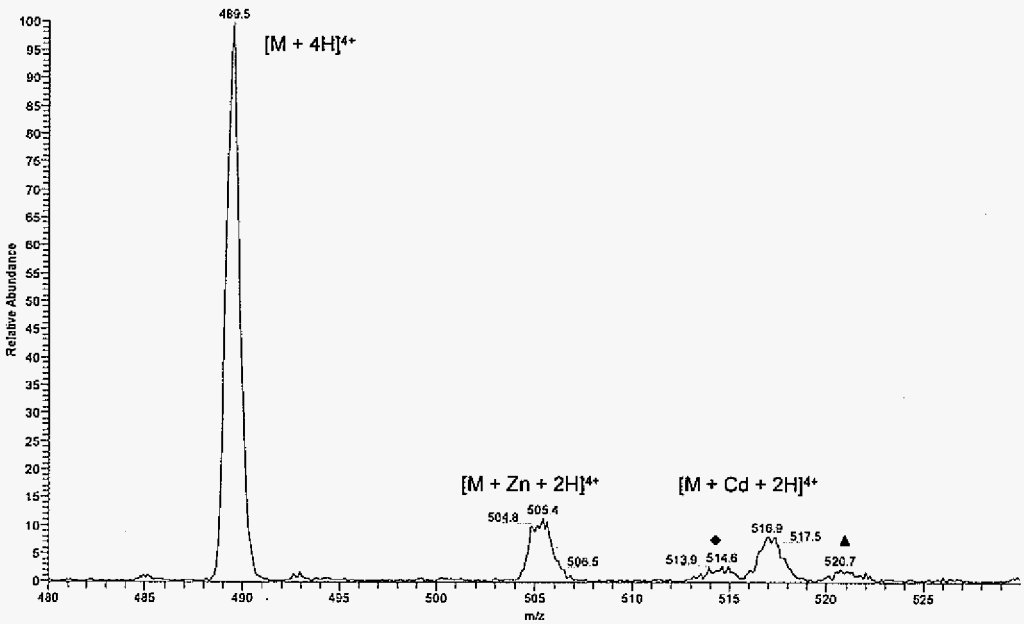
489.5
[M + 4H]4+
[M + Zn + 2H]4+
504.8
505.4
506.5
[M + Cd + 2H]4+
513.9
514.6
516.9
517.5
520.7
Relative Abundance
m/z

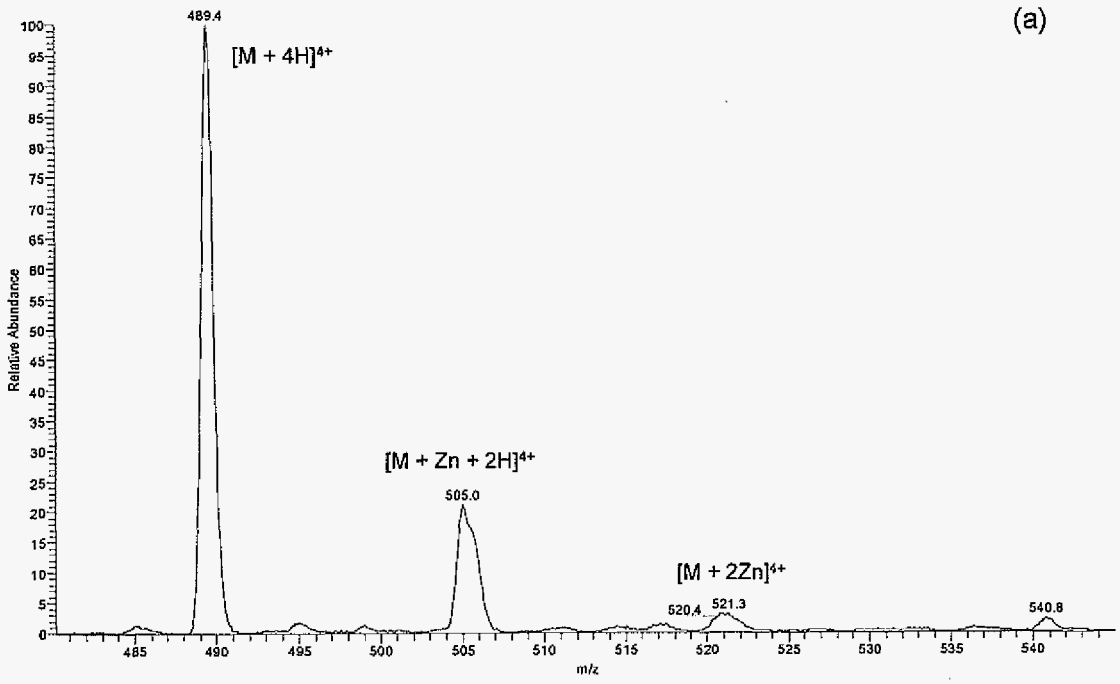

Figure 9. Replacement experiment with Pb. (a) Mass spectrum of the $[M + 4H]^{4+}$ and $[M + Zn + 2H]^{4+}$ ions of a 25 μM [Gln^{11}]-amyloid β-protein fragment (1-16) in the presence of 5 Zn^{2+} equivalents. (b) Mass spectrum of the $[M + 4H]^{4+}$, $[M + Zn + 2H]^{4+}$, and $[M + Pb + 2H]^{4+}$ ions. The solution ratios are 5:10:1 Zn:Pb:amyloid peptide. (c) Mass spectrum of the $[M + 4H]^{4+}$, $[M + Zn + 2H]^{4+}$, and $[M + Pb + 2H]^{4+}$ ions. The solution ratios are 20:10:1 Zn:Pb:amyloid peptide.

(b)

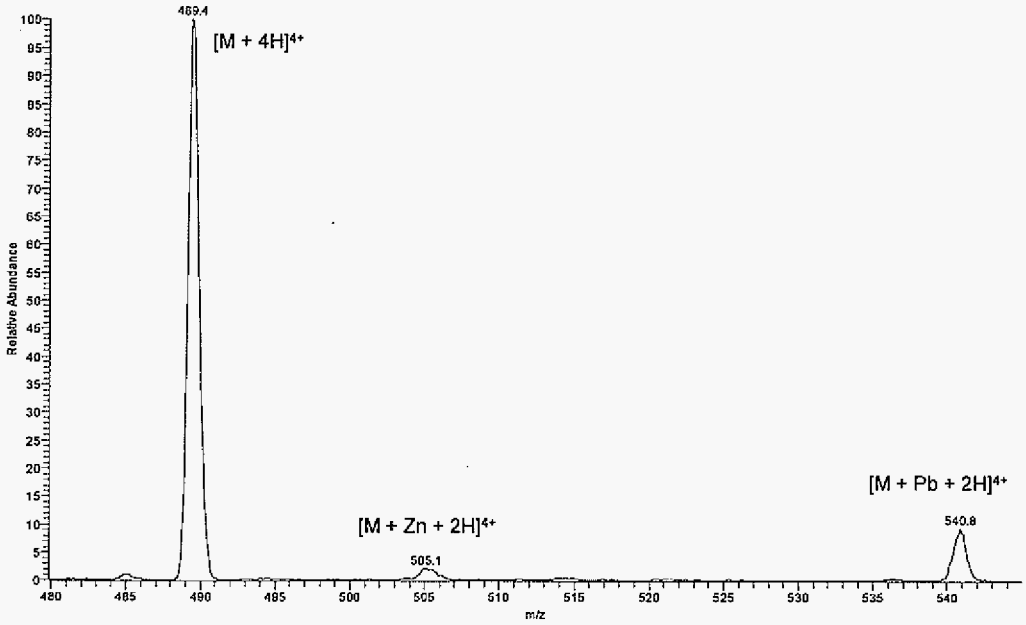
489.4
[M + 4H]4+
[M + Zn + 2H]4+
505.1
[M + Pb + 2H]4+
540.8
Relative Abundance
m/z

(c)

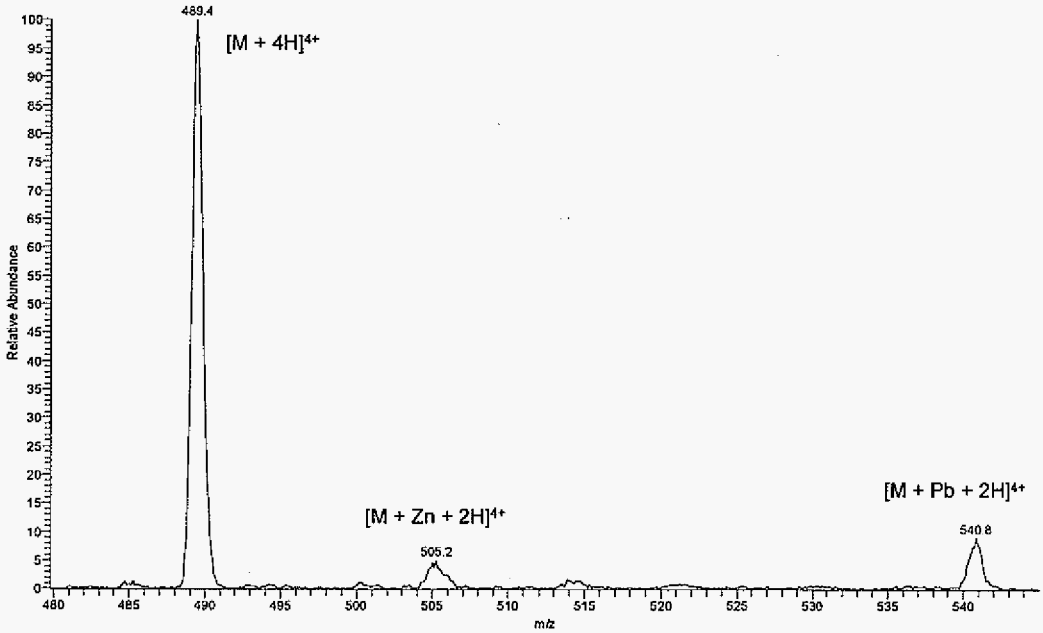
489.4
[M + 4H]4+
[M + Zn + 2H]4+
505.2
[M + Pb + 2H]4+
540.8
Relative Abundance
m/z

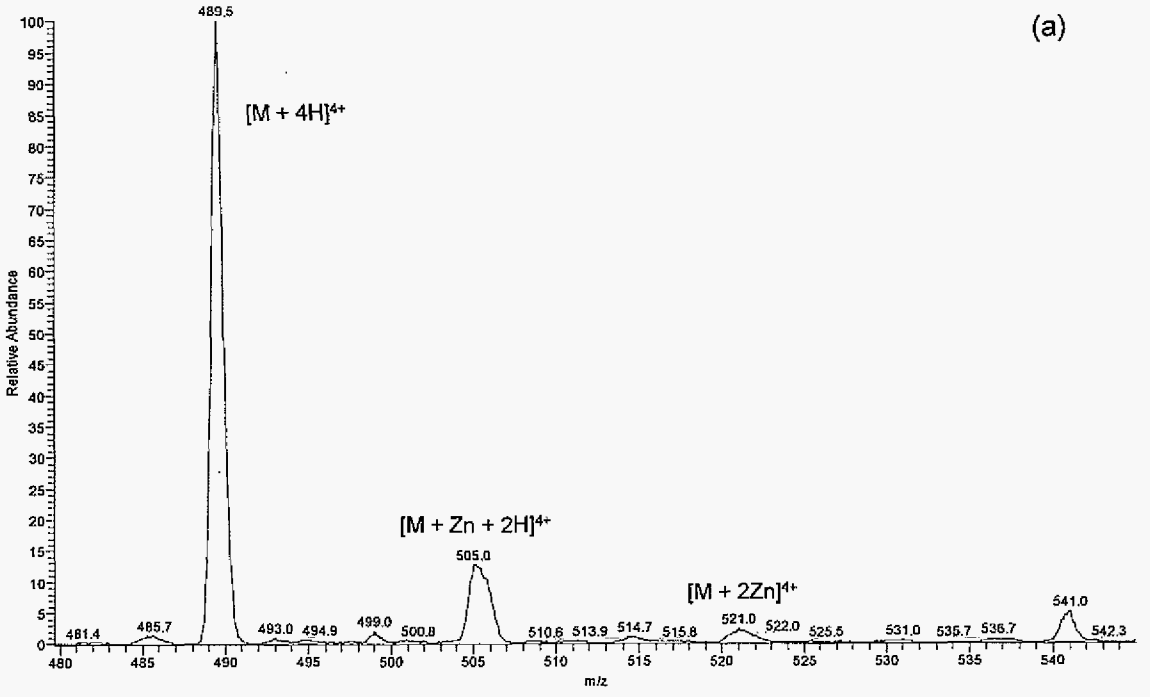

Figure 10. Replacement experiment with Hg. (a) Mass spectrum of the $[M + 4H]^{4+}$ and $[M + Zn + 2H]^{4+}$ ions of a 25 μM [Gln^{11}]-amyloid β-protein fragment (1-16) in the presence of 5 Zn^{2+} equivalents. (b) Mass spectrum of the $[M + 4H]^{4+}$, $[M + Zn + 2H]^{4+}$, and $[M + Hg + 2H]^{4+}$ ions. The solution ratios are 5:10:1 Zn:Hg:amyloid peptide. (c) Mass spectrum of the $[M + 4H]^{4+}$, $[M + Zn + 2H]^{4+}$, and $[M + Hg + 2H]^{4+}$ ions. The solution ratios are 20:10:1 Zn:Hg:amyloid peptide.

(b)

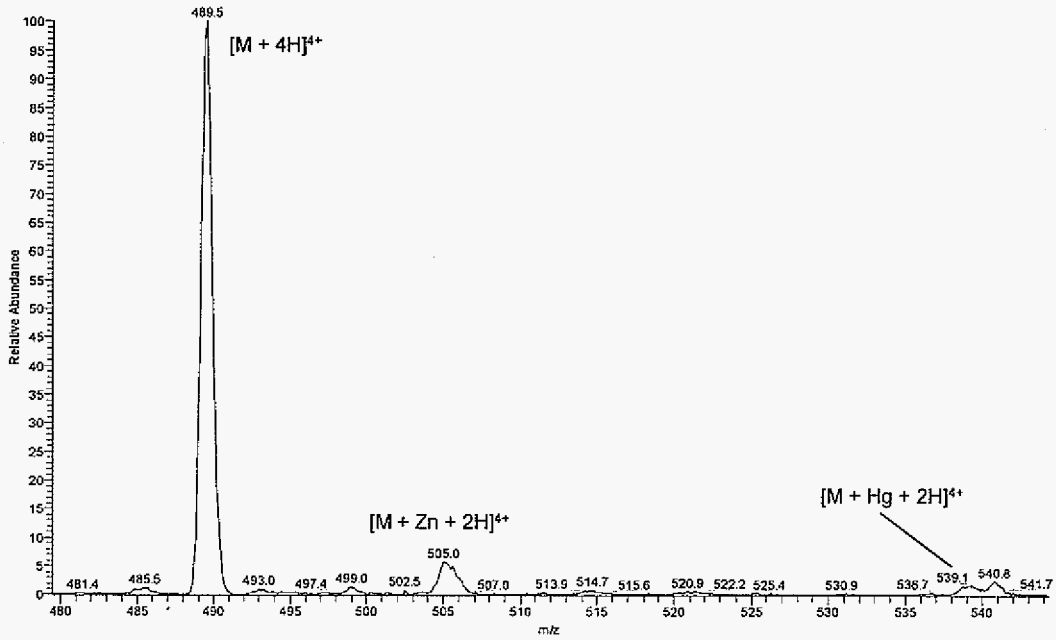
489.5
[M + 4H]4+
[M + Zn + 2H]4+
505.0
[M + Hg + 2H]4+
Relative Abundance
m/z

(c)

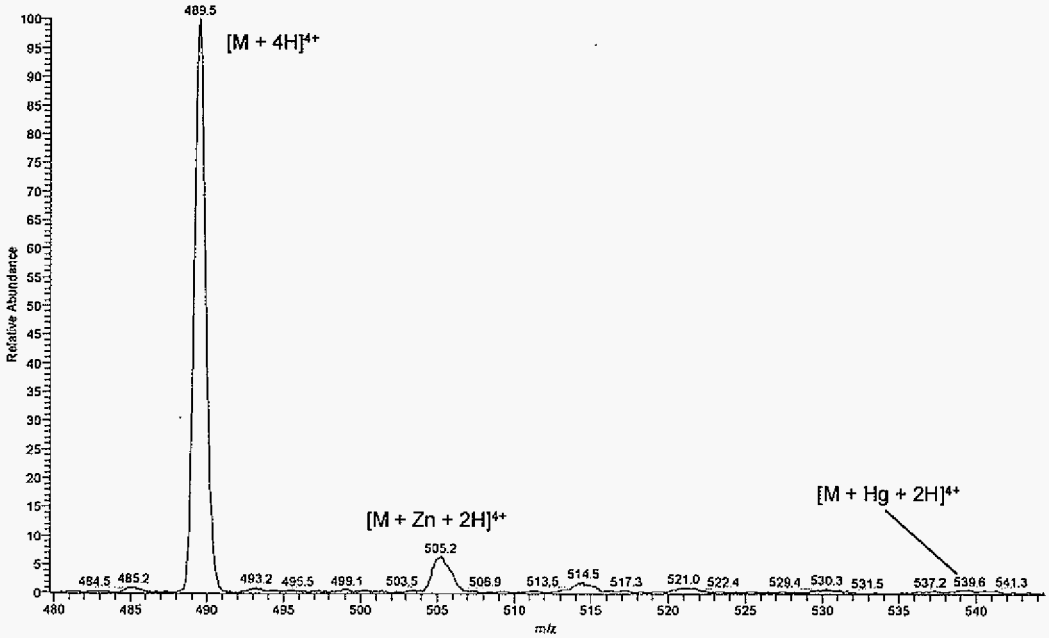
489.5
[M + 4H]4+
[M + Zn + 2H]4+
505.2
[M + Hg + 2H]4+
Relative Abundance
m/z

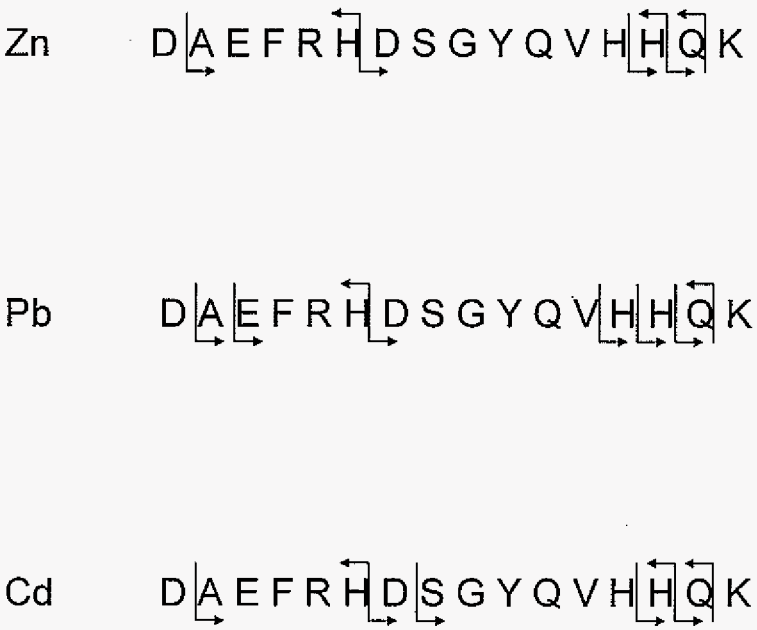

Scheme 1. CID fragmentation patterns for the Zn, Pb, and Cd metal:amyloid complexes. Arrows pointing to the left indicate abc ions, while arrows pointing to the right indicate xyz ions.

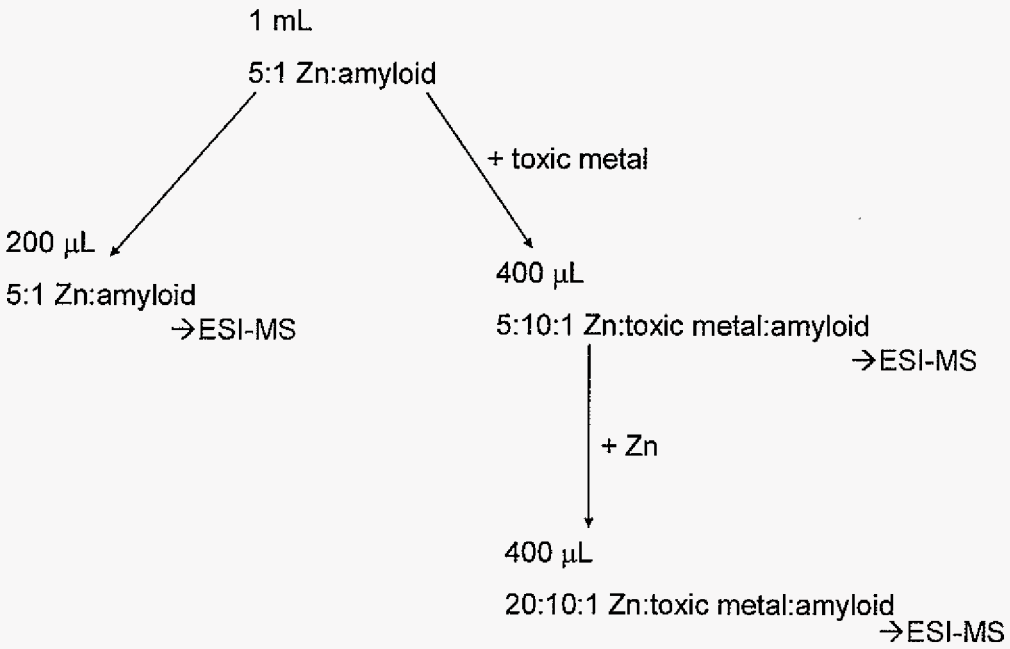

Scheme 2. Experimental flow chart for the replacement experiment.

CHAPTER 6. GENERAL CONCLUSIONS

This dissertation focused on using electrospray ionization mass spectrometry to study cluster ions and toxic metal ions in biology. In Chapter 2, it was shown that primary, secondary and quaternary amines exhibit different clustering characteristics under identical instrument conditions. Carbon chain length also played a role in cluster ion formation. In Chapters 3 and 4, the effects of solvent types/ratios and various instrumental parameters on cluster ion formation were examined. It was found that instrument interface design also plays a critical role in the cluster ion distribution seen in the mass spectrum. In Chapter 5, ESI-MS was used to investigate toxic metal binding to the [Gln^{11}]-amyloid β-protein fragment (1-16). Pb and Cd bound stronger than Zn, even in the presence of excess Zn. Hg bound weaker than Zn.

There are endless options for future work on cluster ions. Any molecule that is poorly ionized in positive ion mode can potentially show an increase in ionization efficiency if an appropriate anion is used to produce a net negative charge. It is possible that drug protein or drug/DNA complexes can also be stabilized by adding counter-ions. This would preserve the solution characteristics of the complex in the gas phase. Once in the gas phase, CID could determine the drug binding location on the biomolecule.

There are many research projects regarding toxic metals in biology that have yet to be investigated or even discovered. This is an area of research with an almost endless future because of the changing dynamics of biological systems. What is deemed safe today may show toxic effects in the future. Evolutionary changes in protein structures may render them more susceptible to toxic metal binding. As the understanding of toxicity evolves, so does

the demand for new toxic metal research. New instrumentation designs and software make it possible to perform research that could not be done in the past. What was undetectable yesterday will become routine tomorrow.

ACKNOWLEDGEMENTS

This work was performed at Ames Laboratory under Contract No. W-7405-Eng-82 with the U.S. Department of Energy. This work was funded by the Chemical and Biological Sciences Program, Office of Basic Energy Sciences, Division of Chemical Sciences. I would like to thank L. Huang and Bayer Company for donating the TSQ-7000 triple quadrupole instrument and Agilent Technologies for the loan of their instrument.

The research that led to the composition of this manuscript could have not been done without the guidance, knowledge and support of Professor R. S. Houk. It was truly a privilege and honor to work in the Houk group. I also enjoyed the fishing outings which often provided a much needed relief from the regular graduate school schedule. I enjoyed the camaraderie of past and present Houk group members, and look forward to staying in contact with all of you. I was honored to be awarded the Procter & Gamble Fellowship in Analytical Chemistry and an Iowa State University Teaching Excellence Award for the 2005-2006 academic year. I would to thank Procter & Gamble and Iowa State University for the awards, and their commitment to scientific research.

Last, but not least I would like to thank the people in my life that encouraged me to achieve a dream of mine. I would like to thank my parents for their lifelong support and allowing me to pursue my dreams and goals. I would like to thank my wife, Rebecca, for her encouragement and understanding of a graduate student's unpredictable schedule. I would also like to thank my wife's parents for their enthusiasm towards my research.